INTERPRETATION OF WELL TESTS IN ACUTE FRACTURE-WELLBORE SYSTEMS

ADNAN AYDIN

INFORMATION TO USERS

This manuscript has been reproduced from the microfilm master. UMI films the text directly from the original or copy submitted. Thus, some thesis and dissertation copies are in typewriter face, while others may be from any type of computer printer.

The quality of this reproduction is dependent upon the quality of the copy submitted. Broken or indistinct print, colored or poor quality illustrations and photographs, print bleedthrough, substandard margins, and improper alignment can adversely affect reproduction.

In the unlikely event that the author did not send UMI a complete manuscript and there are missing pages, these will be noted. Also, if unauthorized copyright material had to be removed, a note will indicate the deletion.

Oversize materials (e.g., maps, drawings, charts) are reproduced by sectioning the original, beginning at the upper left-hand corner and continuing from left to right in equal sections with small overlaps. Each original is also photographed in one exposure and is included in reduced form at the back of the book.

Photographs included in the original manuscript have been reproduced xerographically in this copy. Higher quality 6" x 9" black and white photographic prints are available for any photographs or illustrations appearing in this copy for an additional charge. Contact UMI directly to order.

UMI

A Bell & Howell Information Company
300 North Zeeb Road, Ann Arbor MI 48106-1346 USA
313/761-4700 800/521-0600

INTERPRETATION OF WELL TESTS IN ACUTE FRACTURE-WELLBORE SYSTEMS

by

©Adnan Aydın, B.Sc., M.Sc.

A thesis submitted to the
School of Graduate Studies
in partial fulfilment of the
requirements for the degree of
Doctor of Philosophy

Department of Earth Sciences
Memorial University of Newfoundland

August 1994

St John's Newfoundland

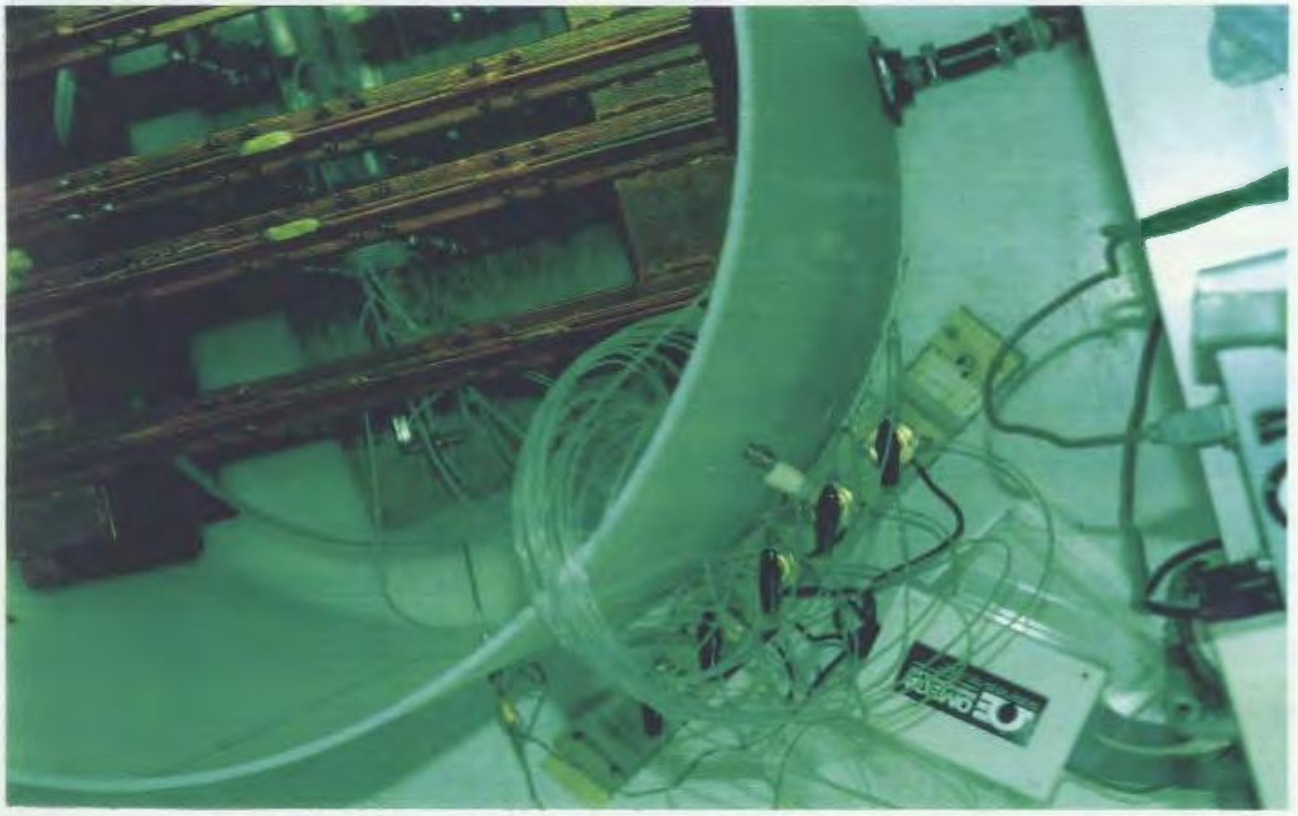

FRONTISPIECE: Views of the model installed in the box frame (top) and the experimental set-up (bottom).

ABSTRACT

The problem of well test interpretation in acute systems has been investigated both theoretically and experimentally. This investigation : a) establishes a basic understanding of the near wellbore flow mechanism in acute systems; b) formalizes the intersection angle-dependent variations in the streamline pattern and hence in pressure distribution and observed response; and c) provides mathematical tools to predict these variations.

The theoretical component of this study involves: a) the derivation, for acute systems, of the governing differential equation of flow in fractures; b) the introduction of analytical models for constant-flux tests under transient and steady-state conditions; c) the formulation of the streamline-equipotential network created by injection/pumping through acute systems under initially non-uniform heads; and d) the development of a general, semi-analytical model accounting for the roughness, turbulence and intersection effects in interpreting single-well, constant-flux tests.

The experimental investigation is intended: a) to verify the formation of the idealized streamline pattern and examine the effects of likely interactions at the acute intersections, particularly during injection tests; and b) to quantify the exit/entry loss coefficients as a function of the intersection angle. The experimental set-up designed to carry out this investigation includes three distinct fracture-wellbore system models with 90°, 20° and 10° intersection angles. The laboratory

programme involved testing these models for three different apertures under steady, constant-flux, injection and pumping conditions. The overall experimental set-up successfully simulated the conceptual testing environment which the mathematical model is expected to reproduce.

The pumping pressure distribution observed in the acute system model tests is in good agreement with the predictions whereas the injection pressure distribution at large intersection angles proves to be directionally variable. Although the latter poses a theoretical limitation, the mathematical models, in practice, are equally capable of interpreting single-well, injection as well as pumping test data, and are valid for the design of the wellbore activities.

ACKNOWLEDGEMENTS

I would like to thank Dr. J. Malpas for providing me a shelter under which I experienced the joy of academic independence and the pain of self-supervision. Without his positive attitude, I would have little reason to celebrate. I would like to express sincere appreciation to Drs. G. Quinlan, J. Malpas and W. Jamison for reading the manuscript and helpful comments.

I gratefully acknowledge the financial support by the School of Graduate Studies, the Department of Earth Sciences, the Faculty of Science, and the NSERC grant to Dr. J. Malpas.

Tony Randell of the NRC Institute of Marine Dynamics kindly provided free time and technical assistance for the use of the computerized lathe. Doug Boulger of Engineering Technical Services of the Memorial University ably assisted during the preparation of the experimental set-up.

I would like to thank my wife, Nurdan Aydın, for consistently sharing the excitements and troubles of our student lives at home and abroad.

This thesis is dedicated to my dear parents, Münevver and Necmettin Aydın.

TABLE OF CONTENTS

LIST OF FIGURES AND TABLES

Table

LIST OF SYMBOLS

$2b$	parallel plate aperture; aquifer thickness	L
A	cross-sectional area of conduit	L^2
B	linear formation loss constant	---
C	well loss constant	---
d	characteristic length of void structure	L
D_h	hydraulic diameter	L
D_i	fracture scanline vector	L
f	conductivity modification factor	---
F	pulsed-head well function	---
F_s	skin factor	---
g	gravitational acceleration	L/T^2
G	constant-head well function	---
h	hydraulic head	L
h_0	initial hydraulic head	L
H	total head	L
H^*	head in tubing or test interval	L
H_0^*	initial head in tubing	L
I_j	components of overall head gradient	---
I_0	(zero order) modified Bessel function	---
J_0	(zero order) Bessel function	---

J_1	(first order) Bessel function	---
k^*	permeability	L^2
k^*_{ij}	permeability tensor	L^2
k	mean absolute height of protrusions	L
K	hydraulic conductivity	L/T
K_0	(zero order) modified Bessel function	---
K_1	(first order) modified Bessel function	---
l	distance from and normal to wellbore face	L
l_c	critical distance	L
l_{OB}	distance to outer boundary	L
L	distance to observation well; entry length	L
n_i, n_j	direction cosines	---
N	permeability shape factor for void geometry	---
P	hydrostatic pressure	M/LT^2
q	flow rate per unit width of parallel plate conduit	L^2/T
Q	flow rate	L^3/T
r_b	distance to boundary	L
r_c	critical radius; radius of open tubing	L
r_i	radius of influence	L
r_s	radius of wellbore in test interval	L
r_w	wellbore radius	L
R	radial distance to observation well	L

Re	Reynolds number	---
s	drawdown/rise in hydraulic or total head	L
s_e	exit/entry head loss	L
s_l	linear head loss	L
s_n	nonlinear head loss	L
s_w	wellbore head loss	L
s'	residual head	L
$\tilde{s}$	Laplace transform variable	---
S	storativity	---
S_s	specific storativity	1/L
t	time	T
t_b	time at which boundary is felt	T
t'	shut-in time	T
T	transmissivity	L^2/T
$\vec{u}$	unit vector in mean flow direction	L
v	(microscopic) velocity	L/T
$\bar{v}$	average (macroscopic) velocity	L/T
$\bar{v}_l$	average velocity normal to equipotential surfaces	L/T
v_p	velocity of passing stream; wellbore velocity	L/T
v_x	exit velocity	L/T
V_0	initial fluid volume in test interval	L^3
w	width of conduit	L

Y_0	(zero order) Bessel function	---
Y_1	(first order) Bessel function	---
W	constant-flux well function	---
z	elevation head	L
α	kinetic energy corr. factor; complementary position angle	---
$\overline{\alpha}$	fracture inclination from horizontal	---
β	fracture-wellbore intersection angle	---
γ	Euler's constant	---
Γ	wetted perimeter; perimeter of equipotential surfaces	L
δ_{ij}	Kronecker delta	---
ϵ	perimeter of ellipse divided by 2π	L
Z	acute intersection well function	---
η	hydraulic conductivity under turbulent flow conditions	T^2/L^2
θ	position angle of a point on an elliptical curve	---
λ	friction factor	---
ν	kinematic viscosity	L^2/T
ξ_e	exit/entry loss coefficient	---
ξ_n	entry loss coefficient	---
ξ_w	wellbore loss coefficient	---
ξ_x	exit loss coefficient	---
ρ	density of fluid	M/L^3
σ_l	compressibility of fluid	LT^2/M
σ_m	compressibility of solid matrix	LT^2/M
φ	porosity	---

GLOSSARY OF SELECTED TERMS

Active well: a well in which the pressure disturbance is induced.

Entry loss: head loss associated with entry of fluid into the fracture.

Exit loss: head loss associated with exit of fluid from the fracture.

Fabrication aperture: distance adjusted between the model plates during the model fabrication.

Fracture: natural and man-induced rock mass discontinuities whose third dimension (i.e. aperture) is much smaller than their areal dimensions. The natural discontinuities range from faults and joints to bedding and schistosity. As their mode of occurrence varies, their dimensions, volumetric density, orientation distribution, aperture and roughness characteristics exhibit great diversity.

Fully established flow: part of flow in which velocity profile is independent of the entry effects.

Head: mechanical energy per unit weight of fluid.

Hydraulically smooth: flow behaviour of a fracture whose asperities do not disturb the boundary layer structure at a given Reynolds number.

Linear flow: laminar convergent/divergent flow characterized by linear total head distribution along streamlines.

One-dimensional flow: laminar/turbulent flow parallel to an axis of local cartesian coordinates. Also called rectilinear, parallel or unidirectional flow.

Single-well tests: well tests where the response of the subsurface medium is observed in the active well.

1 INTRODUCTION

Wells provide access to the subsurface for purposes such as: a) resource exploration, exploitation and management; b) geotechnical site assessment, remediation and monitoring; and c) waste disposal and containment. Depending on the nature and operating environment of these projects, well testing is needed at various stages to assess such parameters as: a) the extent and producibility of the reserve; b) the cost of production, drainage or artificial recharge; and c) the stability and tightness of the ground.

Well testing is based on the principle of: a) inducing a pressure disturbance; b) monitoring the flow/pressure response of the perturbed medium; and c) drawing inferences about the hydraulic properties of the medium. The corresponding procedure is: a) to remove/add fluid or stop production; b) to record transient/steady pressure (and flow rate); and c) to select an appropriate mathematical model that can reproduce the observed response. This way of identifying the properties of an unknown/incompletely defined system (i.e. inverse problem) inevitably results in non-unique answers. Being based on various simplifications, none of the models may be assured of reproducing the behaviour of the medium under different levels and/or periods of disturbances. The better the subsurface control and wider the range of tests, the more evolved and reliable the selected model is for designing planning strategies.

1.1 Statement of the problem

In the evaluation of well tests the observed relationship between

the disturbance and the response is attributed to the nature of the system as conceptualized. In other words the accuracy of the model predictions remain unknown since the influence of any overlooked system parameter on the response is implicitly absorbed by the lumped model parameters such as hydraulic conductivity. In this respect, fundamental investigations toward a better understanding of the role of every identifiable system parameter are essential for the progress of well test evaluation. The investigation of the influence of the fracture-wellbore intersection angle is therefore a step forward in this direction. A particular gain of this is in refining various predictions made through single-well tests.

The probability that a wellbore intersects natural fractures at acute angles is close to certainty. To a lesser extent, this is also true for hydraulic fractures since the least principal stress may not be aligned exactly parallel or normal to a plane including the wellbore axis. However, because of the absence of relevant models for well-test evaluation, intersections of fracture-wellbore systems are usually approximated as being parallel or normal to such a plane. How much error is involved in this and which approximation is best for a given acute intersection cannot be answered definitively.

In some cases, the system intersection angle required by the employed model is produced via oriented drilling. In geotechnical applications, for example, it is an established practice to drill normal to the fracture (set) whose permeability is to be determined (Louis and Maini, 1970; Rissler, 1978). The possibility of making positive permeability determinations in acute systems so that the investigated rock

volume can be sampled more homogeneously with a given number of wellbores is worthwhile to pursue. Again for interpretation purposes, Hot Dry Rock (HDR) geothermal recovery wells (deviated at the production levels) are assumed to orthogonally intersect the hydraulic fractures created in the injection wells (Murphy, 1979). For fluid recovery wells, in general, the impact of producing such an intersection on the well losses and hence on the production cost cannot be assessed accurately.

1.2 Purpose and scope

The objectives of this study are therefore: a) to establish an understanding of the influence of the (fracture-wellbore) system intersection angle on the near well flow mechanism; and b) to develop mathematical models which can reproduce the responses of acute systems to various forms of disturbances under different conditions. The pursuit of these interlacing objectives involves, as a base: a) a synthesis of the present knowledge of flow in fractures and fracture-wellbore systems; and b) derivation of a basic differential equation governing flow in conceptualized acute systems. Thereafter, the study focuses on: a) seeking analytical solutions to this equation for transient and steady-state constant-flux test conditions; b) investigating the extent and geometry of the zone influenced by the induced disturbances; c) extending the steady-state solution to a semi-analytical model accounting for the effects of fracture roughness, flow turbulence and system intersection on single-well test results; and d) devising physical models to conduct an experimental study of actual flow processes in acute systems as conceptualized.

It is evident that the influence of the system intersection angle on the well test response can be investigated in a general sense only if the system components can be idealized to some common forms, e.g. a hollow cylinder for the wellbore and a parallel plate conduit for the fracture. It is then essential to understand the mechanics of flow through such forms and the theoretical concerns behind such idealizations. Because the results of well tests are often extrapolated to a larger scale, it is also important to analyze the nature of the rock-mass scale heterogeneities and modelling methods. These fundamental points are reviewed in a critical and comprehensive manner in the following sections.

2.1 Introduction

The Navier-Stokes equation, the general equation of Newtonian fluid motion, can be derived from simultaneous consideration of forces acting on an infinitesimal fluid element (Rouse, 1961). For isothermal flow of an incompressible fluid, considering that the body forces usually consist only of the weight forces, the Navier-Stokes equation may be written, in local cartesian coordinates, as

$$\frac{\partial v_i}{\partial t} + v_j \frac{\partial v_i}{\partial x_j} = -\frac{1}{\rho} \frac{\partial (P+\rho g z)}{\partial x_i} + \nu \frac{\partial^2 v_i}{\partial x_j^2} \qquad \{ i, j = 1, 2, 3 \quad (2.1)$$

where v: (microscopic) velocity,

t: time,

ρ: density,

g: gravitational acceleration,

P: hydrostatic pressure,

z: elevation from a datum, and

ν: kinematic viscosity.

The fundamental flow laws that constitute the core of the fracture flow theory are based on this equation. Integrating Equation 2.1 over a macroscopic (representative) volume of granular porous media, Hubbert (1956) showed that the empirical Darcy law of laminar flow is of a universal nature at a proper scale. Accordingly, the Darcy law for any porous medium,

$$\overline{v}_i = -K\frac{\partial h}{\partial x_i} \tag{2.2}$$

where $\overline{v}$: average (macroscopic) velocity,

K: (homogeneous and isotropic) hydraulic conductivity, and

h: hydraulic head, a combined expression of pressure and elevation heads, i.e. $\frac{P}{\rho g} + z$.

The hydraulic conductivity term in the Darcy law was shown to be a lumped, variable parameter (Hubbert, 1940;1956)

$$K = k^* \frac{g}{\nu} \tag{2.3}$$

where k^* represents the permeability of the medium and the role of fluid is expressed by its kinematic viscosity. The inherent difficulty of relating the permeability to some quantifiable property of the medium

resulted in theoretical approaches that employ different conceptual models and medium parameters (Bear, 1972) according to the type of effective porosity (i.e. granular, karstic or fracture). Section 2.2 describes the application of such an approach to single fractures using a parallel plate idealization.

Theoretically-derived permeability relations hold provided that the geometry of the real flow domain is well represented by the model and flow obeys the Darcy law. Cases where these conditions fail in fracture flow are discussed in Section 2.3 whereas Section 2.4 explains how these situations can be treated using empirical modification factors and completes the formulation at the scale of a single fracture. The basic concepts, problems and methodologies of the fracture flow studies at the rock-mass scale are reviewed in Section 2.5.

2.2 Theoretical basis of single-fracture models

Rock fractures have often been idealized as planar conduits (Figure 2.1.a) bounded by two parallel plates with smooth walls (Baker, 1955; Huitt, 1956; Snow, 1969; Louis, 1974; Iwai, 1976). This geometric simplification allows an exact analytical solution of the Navier-Stokes equation (Equation 2.1) subject to the following conditions (Schlichting, 1979):

$\frac{\partial v_1}{\partial t} = 0$: steady flow,

$v_2 = v_3 = 0$: one-dimensional flow, in the x_1 direction,

$\frac{\partial v_1}{\partial x_1} = 0$: continuity condition (in fully established flow through a constant cross-section), and

$\frac{\partial v_1}{\partial x_2} = 0$: constant cross-section along the width.

Substituting these, Equation 2.1 reduces to

$$0 = -\frac{1}{\rho}\frac{\partial (P + \rho g z)}{\partial x_1} + \nu \frac{\partial^2 v_1}{\partial x_3^2} \tag{2.4}$$

Writing this in terms of hydraulic head,

$$0 = -g\frac{\partial h}{\partial x_1} + \nu \frac{\partial^2 v_1}{\partial x_3^2} \tag{2.5}$$

and integrating twice with respect to x_3,

$$v_1 = \frac{g}{\nu}\frac{\partial h}{\partial x_1}\frac{x_3^2}{2} + C_1 x_3 + C_2 \tag{2.6}$$

where C_1 and C_2 are the integration constants.

The no-slip condition at the boundaries, i.e. $v_1 = 0$ at $x_3 = \pm b$, requires that

$$C_1 = 0 \; ; \; C_2 = -\frac{g}{\nu}\frac{\partial h}{\partial x_1}\frac{b^2}{2} \tag{2.7}$$

where b is the half-width of the parallel plate opening (Figure 1). Thus

$$v_1 = \frac{g}{\nu} \frac{\partial h}{\partial x_1} \frac{x_3^2 - b^2}{2} \tag{2.8}$$

which shows that the velocity profile is parabolic under the specified flow conditions.

Averaging the velocity across the flow section

$$\overline{v}_1 = \frac{1}{2b} \int_{-b}^{+b} v_1 \, dx_3 \tag{2.9}$$

yields a linear relationship known as the Poiseuille law

$$\overline{v}_1 = - \frac{g (2b)^2}{12 \nu} \frac{\partial h}{\partial x_1} \tag{2.10}$$

which is a specialized form of the Darcy law (Equation 2.2). The hydraulic conductivity of a fracture with smooth, parallel walls therefore is

$$K_f = \frac{g (2b)^2}{12 \nu} \tag{2.11}$$

It follows from Equation 2.3 that the permeability of this idealized fracture is given by

$$k_f^* = \frac{1}{12} (2b)^2 \tag{2.12}$$

which compares to the typical permeability expression suggested for granular porous media (Hubbert, 1940)

$$k^* = N d^2 \tag{2.13}$$

where N is a shape factor depending on certain properties describing the

void space geometry of the specific medium (e.g. angularity of grains) and d is a characteristic length of that medium (e.g. mean grain diameter). From a visual inspection of Equations 2.12 and 2.13, the shape factor for the parallel plate flow geometry appears to be

$$N_f = \frac{1}{12} \tag{2.14}$$

It is of both practical and academic interest to determine when Equation 2.14 becomes inadequate in describing flow geometry of rock fractures.

The Poiseuille law (Equation 2.10) can be expressed in terms of q, the flow rate per unit width of the fracture,

$$q = -\frac{g(2b)^3}{12\nu}\frac{\partial h}{\partial x_1} \tag{2.15}$$

which is the so-called cubic law. The Poiseuille (or cubic) law may be taken as approximately valid for parallel plate conduits having gradual variations in the local apertures and/or curved (undulating) surfaces, the radii of curvature of which are large compared with the local apertures (Lamb, 1945). In both forms (Equations 2.10 and 2.15) the summarized solution of the Navier-Stokes equation has been the basic model in the study of laminar flow through rock fractures.

2.3 Deviations from Poiseuille law

Fracture flows that can be fully characterized by the Poiseuille law (Equation 2.10) are rare occurrences in nature. The deviations stem from: a) oversimplifying the fracture void structure; and b) ignoring the inertial forces. Fractures generally are planar features with surfaces

that can be characterized by asperities superimposed on larger scale undulations. These surface elements often produce a highly complicated void structure surrounding and enclosed by areas in contact, and hence tortuous flow paths throughout the fracture plane (Sharp and Maini, 1972; Pyrak-Nolte et al. 1987). As the fracture void structure becomes increasingly different from a simple opening between parallel smooth walls, the theoretical permeability (Equation 2.12) cannot sustain the linearity between mean flow velocity and corresponding gradient, although flow may still be of laminar character.

Groundwater flow usually occurs under low hydraulic gradients (Bear, 1979). However, in many engineering environments, such as those near active wellbores and excavated faces, artificial disturbances frequently induce steep gradients. The consequent increase in inertial forces is accompanied by shifting of streamlines due to flow separation at the diverging and/or curved points of the void structure (Bear, 1972). This implies that the microscopic structure of the effective voids imposes an additional control on the initiation and intensity of flow separation. Increasing significance of inertial forces relative to shear forces results in a nonlinear relationship between mean velocity and hydraulic gradient, regardless of the void structure.

In summary, deviations from the Poiseuille law can be attributed to tortuosity and/or inertial forces. From a practical point of view, the deterministic approach is ideal for the treatment of these complications. The main concern in this approach is not in the details of the void structure (i.e. in geometric similarity between the model and fractures),

but in reproducing equivalent responses to given excitations. In selecting the model it is advantageous: a) to maintain the theoretical base gained by the Poiseuille law; and b) to use the parallel plate aperture as a parameter providing physical continuity for the entire formulation.

In accordance with the above rationale, major experiments designed to investigate hydraulic behaviour of fractures (Baker, 1955; Huitt, 1956; Parrish, 1963; Louis, 1974, Rissler, 1978; Cornwell and Murphy, 1985) have consistently used physical models consisting of parallel plate conduits of varying roughness (Figure 2.1.b). Although introducing roughness as an additional parameter improves void structure characterization, it does not entirely prevent some loss of control over the phenomenon being investigated. Owing to the large number of and complex relations between the (unknown) system parameters involved in well test evaluations and rock-mass scale characterization, present practice relies heavily on developments based on the parallel plate idealization. The next section explains the procedure that enables the use of the parallel plate concept in establishing flow expressions for rough fractures and/or nonlinear conditions for which the Poiseuille law fails.

2.4 Hydraulics of parallel plate conduits

For fully established flow through straight, uniform conduits, the difference in the hydraulic head between any two points arises from the energy dissipation due to both: a) viscous shear and/or turbulent mixing within the fluid body; and b) frictional and/or pressure drag on the conduit walls and protrusions. The resulting head gradient, regardless of

the causes, can be predicted from the Darcy-Weisbach equation, originally derived for pipes of circular section (Vennard and Street, 1982). Dropping indicial and partial derivative notations, this empirical equation has the general form

$$\frac{dh}{dx} = \lambda \frac{1}{D_h} \frac{\overline{v}^2}{2g} \tag{2.16}$$

where λ: friction factor, and

D_h: hydraulic diameter.

The conduit geometry in Equation 2.16 is specified through the hydraulic diameter term defined as

$$D_h = 4 \frac{A}{\Gamma} \tag{2.17}$$

where A: cross-sectional area, and

Γ: perimeter (i.e. length of contact between fluid and boundary).

Hence, for an opening between two parallel plates,

$$D_h = 4 \frac{(2b)\, w}{w + w} = 2\,(2b) \tag{2.18}$$

where w is the width of the opening.

The Darcy-Weisbach equation (Equation 2.16) does not explicitly account for the influences of roughness, flow regime and fluid viscosity. The friction factor can, however, be effectively scaled by means of two dimensionless parameters (Vennard and Street, 1982): a) relative roughness, the ratio of mean absolute height of the protrusions, k (Figure

2.1.b) to the hydraulic diameter, D_h (Equation 2.18); and b) Reynolds number, the ratio of inertial to viscous forces, and therefore an index of the flow regime,

$$Re = \frac{\bar{v} D_h}{\nu} \tag{2.19}$$

On the basis of the hydraulic approach outlined above, several investigators including Huitt (1956) and Louis (1974) have attempted to empirically determine friction factor expressions from rough model fractures under a wide range of flow conditions. The friction factor expressions adopted in this study are listed in Table 2.1. The domains of each expression are delineated in Figure 2.2. Before explaining the integration of the expressions into flow laws for these domains, the following properties of Table 2.1 and Figure 2.2 need emphasis and clarification:

a) the transitions from; (i) laminar to fully turbulent flow, (ii) hydraulically smooth to completely rough behaviour, and (iii) parallel ($k/D_h \leq 0.033$) to non-parallel ($k/D_h > 0.033$) wall geometry are all assumed to be abrupt, resulting in discontinuous boundaries between the flow domains,

b) above the boundary value of $k/D_h = 0.033$, the friction factor corresponding to the Poiseuille law is no longer valid due to additional energy dissipation in the process of viscous damping of increased wall disturbances,

c) below $k/D_h = 0.033$, the critical Reynolds number, marking the

persistence limit of laminar flow, is constant at $Re_c=2300$,

d) below $k/D_h=0.033$, the friction factors of classical hydraulics are valid, and

e) below $k/D_h=0.033$, in the turbulent domain, as the viscous sublayer gets thinner and/or disrupted with increasing Reynolds number, the resulting exposure of protrusions changes hydraulic behaviour of the model fracture from smooth to rough.

Laminar domains

The friction factor denoted as Poiseuille (Table 2.1) can be derived from equating hydraulic gradient terms in the Darcy-Weisbach (Equation 2.16) and Poiseuille (Equation 2.10) equations and making use of Equations 2.18 and 2.19. Comparing this with the friction factor of Louis L (laminar), the modification factor, f, necessary in the laminar domain with $k/D_h>0.033$ appears to be

$$f=[1+8.8\,(k/D_h)^{1.5}] \tag{2.20}$$

Introducing this as an external parameter into the Poiseuille law (Equation 2.10) reveals that the shape factor (Equation 2.14) is a function of surface roughness in this domain

$$N_f=\frac{1}{12\,f} \tag{2.21}$$

Turbulent domains

Two distinct forms of flow relationships are widely used to

formulate the observed nonlinearity between the velocity and hydraulic gradient (Basak, 1978; Hannoura and Barends, 1981): a) the series form of the Forchheimer equation

$$\frac{dh}{dx} = a\bar{v} + c\bar{v}^2 \qquad (2.22)$$

and b) the exponential form of the Missbach equation

$$\frac{dh}{dx} = \eta\,\bar{v}^n \qquad \{\ 1<n<2 \qquad (2.23)$$

where a, c, and η are empirical proportionality coefficients. The symbol η denotes the hydraulic conductivity of a fracture under turbulent flow conditions. The Forchheimer equation provides a better alternative in cases where the transitional turbulent flow persists over a considerable spatial extent for a wide range of flow rates, such as in granular porous media (Bear, 1972). However, for (particularly convergent/divergent) flow through fractures, transition to fully turbulent flow is more abrupt. Therefore, it is appropriate to apply the Missbach equation in the turbulent flow domains shown in Figure 2.2 (Louis and Maini, 1970; Louis, 1974; Zeigler, 1976; Rissler, 1978).

In accordance with the assumption of abrupt transition to fully turbulent flow (Figure 2.2), the Missbach equation (Equation 2.23) is taken to be quadratic, i.e. $n=2$. Equating the Missbach and Darcy-Weisbach (Equation 2.16) equations yields the turbulent domain hydraulic conductivity, η, in terms of the empirical friction factors and the parallel plate aperture

$$\eta = \lambda \frac{1}{4\,(2b)\,g} \tag{2.24}$$

Critical Reynolds number

Any observed relationship between the mean velocity and hydraulic gradient can now be formulated by selecting the appropriate flow law (Equation 2.10 or 2.23) and then adjusting its proportionality constant (i.e. hydraulic conductivity) adopting an appropriate friction factor expression (Table 2.1). For this purpose, the values of the relative roughness of the fracture and the Reynolds number of flow can be directly compared to the flow boundary domains depicted in Figure 2.2 and Table 2.1. The critical Reynolds numbers defining the boundaries of these domains are calculated in the following manner:

a) for $k/D_h \leq 0.033$: the critical Reynolds number, Re_c, is essentially constant (Figure 2.2)

$$Re_c = 2300 \tag{2.25}$$

b) for $k/D_h > 0.033$: Re_c can be obtained by the simultaneous solution of the friction factor expressions of Louis L (laminar) and Louis T (turbulent) (Table 2.1)

$$Re_c = 384\left[1 + 8.8\,(k/D_h)^{1.5}\right]\left(\log\frac{1.9}{k/D_h}\right)^2 \tag{2.26}$$

c) for $k/D_h \leq 0.033$ and $Re > 2300$: the boundary between hydraulically smooth and completely rough flow domains satisfies the

friction factor expressions of both Blasius and Nikuradse

$$Re_c = 2.553\left(\log\frac{3.7}{k/D_h}\right)^8 \qquad (2.27)$$

Any formulation derived by the procedure as outlined includes two unknowns, namely, the aperture and hydraulic gradient. In practice, hydraulic gradient is measured in order to determine the equivalent parallel plate aperture of fractures.

2.5 Flow in rock masses

Assessment of the seepage, production or contaminant transport potential in fractured media ideally requires knowledge of: a) the spatial distribution of active fractures; and b) the geometric, hydraulic and mechanical properties of these fractures. Obviously such a thorough description of the flow network is practically an impossible notion. Therefore studies on flow through fractured rock masses have adopted indirect approaches assuming the existence of: a) an equivalent (granular) porous medium (EPM) behaviour (Snow, 1969; Castillo, 1972; Louis, 1974); and b) statistically equivalent networks of discrete fractures (Long and Witherspoon, 1985; Schwartz and Smith, 1985; Rouleau, 1988; Nordqvist et al., 1992).

2.5.1 Directional permeability of equivalent continua

Fractures impart anisotropy and heterogeneity to the permeability of rock masses. In anisotropic media, the Darcy law (Equation 2.2) becomes (Bear, 1972)

$$\overline{v}_i = k^*_{ij} \frac{g}{\nu} I_j \tag{2.28}$$

where k^*_{ij} is a second order tensor defining the permeability at a point and I_j denotes the components of the overall head gradient. This equation implies a fictitious continuum replacing the multiphase (solid and pore) medium. Therefore the tensor represents the average permeability of a certain volume of the actual medium centred at that point. If the permeability is insensitive to slight changes in this volume, it is specified as the representative elementary volume (REV) (Hubbert, 1956; Bear, 1972). In order that the same REV can be defined at all points of the flow domain (Bear, 1979), heterogeneities should have a high volumetric density (relative to the REV) which can be uniform or vary smoothly across the flow domain. Consequently a fractured medium is said to behave like an EPM (or a continuum) if the REV exists at a scale smaller than that of the measurement and also of the detail required in the studied flow problem (Neuman, 1987).

A method to calculate the directional permeability tensor in fractured media was developed by Snow (1969) who implicitly assumed the existence of the REV with uniform heterogeneity density. Incorporating the cubic law modification factor to the equivalent parallel plate permeability, the tensor for a single fracture is (Snow, 1969; Rissler, 1978)

$$k^*_{ij} = \left[\frac{(2b)^2}{12f}\right] \frac{(2b)}{|n_i D_i|} (\delta_{ij} - n_i n_j) \tag{2.29}$$

where δ_{ij}: Kronecker delta,

n_i, n_j: direction cosines of the normal to the fracture, and

D_i: scanline vector of length D.

The underlying assumptions of the method are that: a) all fractures traversed repeat for every scanline length D so that the orthogonal distance (or spacing) between each fracture and its image is $|n_i D_i|$; b) fractures are continuous (or extend to a specified boundary); and c) there is no flow interference at the fracture intersections.

The first assumption implies that the rock is homogeneous at the scale of the scanline length since identical heterogeneities can be sampled along every such length. The average permeability calculated from such a representative elementary length (REL) equals the REV (Bear, 1972). The summation of all single-fracture tensors for each scanline station yields the permeability tensor for the REV. As the number of stations increases, the tensor is refined by averaging, hence reducing the sampling bias. Also the more extensive the fracture is, the higher its chance of being traversed by multiple scanlines and being weighted more heavily. Therefore, for the multiple scanline surveys the REL contains an imaginary but more representative sample of fractures.

The second assumption indicates that contribution of a fracture to the overall permeability is not affected by its network connectivity. Each fracture encountered along a scanline contributes to the permeability of the REV independently and proportionally to its equivalent aperture, roughness and orientation with respect to the overall gradient vector.

Fractures oblique to the scanline are weighted more heavily to eliminate the orientation bias.

Flow rate reduction and pressure loss at the fracture intersections due to cross flow (i.e. flow interference) are negligible in laboratory model experiments in the laminar flow range (Wilson and Witherspoon, 1976) verifying the third assumption. However, Neuman (1987) suggested, referring to a field case study in the literature, that intersections may exert a greater influence on the overall hydraulic conductivity than do fracture planes.

The magnitude and directions of the principal permeabilities are obtained from the eigenvalues and eigenvectors, respectively, of the final permeability tensor. Velocity and gradient vectors in an anisotropic medium do not coincide except in the principal directions of permeability. The polar plot of the inverse square root of the permeability in the direction of the overall gradient yields an ellipsoid whose axes are the principal directions of permeability (Bear, 1972). The degree of elipticity reflects the degree of deviation from a continuum behaviour.

The influence of various network parameters on continuum behaviour was investigated by several two dimensional network models. These include the conceptual (square and triangular) grid models for the aperture variations (Parsons, 1966), the resistivity analogs of a square grid model for the finite size of fracture sets (Caldwell, 1972), and the statistical networks for the degree of interconnection (Long and Witherspoon, 1985). The maximum permeability calculated by the outlined method of Snow (1969) was found to be a reasonable approximation in homogeneous media given that

the length of fractures exceeds a certain limit (Long and Witherspoon, 1985).

2.5.2 Heterogeneity in fractured rocks

The type of medium determines the scale at which the REV may exist. Fractured rock masses usually exhibit several episodes of fracturing, each resulting in a higher level of heterogeneity at a given site (Chernyshev and Dearman, 1991). These levels display differences not only in fracture density but also in connectivity and ability to form a global flow network. Networks formed by dense but isolated, or sparse but active fractures are natural probabilities. Accordingly there may be more than one volumetric scale at which the REV behaviour exists at a given point (Wilson et al., 1983; de Marsily, 1985; Smith and Schwartz, 1985). Only the largest of these might be the true REV scale for the flow domain.

A number of field observations imply that geometrically and hydraulically defined fracture frequencies can be very different. From measurements of injection pressures at which pre-existing fractures start opening, Cornet (1992) concluded that stress heterogeneities are associated with active zones, and the regional stress field is not perturbed by most of the fractures. Similarly, Tsang et al. (1990), using a time sequence of electrical conductivity logs, detected merely nine active fractures scattered along a 900 m wellbore interval. The preceding observations also indicate that, although there is a general decline in the well yield with increasing depth at shallow depths of hydrogeological interest (Wooley, 1982), this is not a rule for long intervals

particularly when away from the zone of surface weathering and percolation.

A parametric study using two dimensional synthetic networks of randomly distributed and oriented fractures (i.e. homogeneous and isotropic at the REV scale) demonstrated that the existence and scale of the REV are strongly dependent on the length of the fractures (Long and Witherspoon, 1985). The occurrence of fractures in clusters is, however, a common phenomenon inconsistent with the assumption of randomness (Snow, 1970; de Marsily, 1985; Schwartz and Smith, 1985). To form a global flow network, fractures in such cases may have to be extremely long for the REV to exist if local networks are not connected by several pervasive fractures.

These results emphasize the importance of improving in situ detection, testing and evaluation methods to obtain more refined estimates of network parameters and to identify the most significant fractures at a given scale (Wilson et al. 1983). Particularly, single-hole packer testing to obtain hydraulically derived geometrical information or direct local permeability is an essential method (Wilson et al. 1983; Neuman, 1987). Techniques to determine fracture connectivity include, in accordance with the nature of the problem, cross-hole tests involving multi-level measurements of pressure signals (Hsieh, 1987), temperature (Silliman and Robinson, 1989) and gamma ray (Marine, 1980) variations in response to injection or pumping.

Hydraulic characterization of fractured rock masses generally requires the use of multiple sources of information to assess

heterogeneity variation at different scales (Hsieh, 1987). In planning to acquire such information, geological and mechanical controls of fracturing intensity such as lithology, thickness, structural association and depth (Stearns and Friedman, 1972) should be considered first. Geophysical and hydrological testing should follow this guide in delineating areas of uniform heterogeneity where the permeability tensor can be determined and in extrapolating the available data to the whole flow domain. The extent of testing to be undertaken depends on the quality, quantity and variety of the data needed, which in turn is determined by whether there is REV behaviour. Statistical models incorporating the available geometrical fracture data might be useful in answering these questions.

2.5.3 Statistical models

The EPM approach assumes a priori that REV exists, while studies with discrete fracture networks test whether and under what conditions the REV might exist. Discrete fracture network models need statistical information about the geometry and spatial distribution of fractures. Density, length, location, orientation, aperture, etc. of fractures are considered random entities from a probability distribution function (Long and Witherspoon, 1985; Rouleau, 1988). Distribution parameters are estimated from sample observations. These distributions are then randomly sampled to generate statistically equivalent networks.

Different levels of heterogeneity can be modelled by including major fractures separately (Wilson et al., 1983) or by superimposing independently generated fracture assemblages (Long and Witherspoon, 1985).

Single fractures are idealized as, for example, parallel plate discs, rectangles, etc. whose aperture may be constant (Rouleau, 1988) or variable (Nordqvist et al., 1992). Distribution of apertures (Bianchi and Snow, 1969) as well as lengths (Long and Witherspoon, 1985) of fractures in a sampled rock volume might obey a lognormal distribution function.

Since flow network parameters such as connectivity and areal extent cannot be directly measured, statistical network models are designed to predict them using other parameters such as frequency and trace length. More significantly there may be a few fractures controlling network connectivity in which case their apertures cannot be simply estimated. An alternative to avoid these shortcomings is a method which treats the conductivity values determined by single-hole packer tests as random variables generated by a stochastic process defined over a continuum (Neuman, 1987).

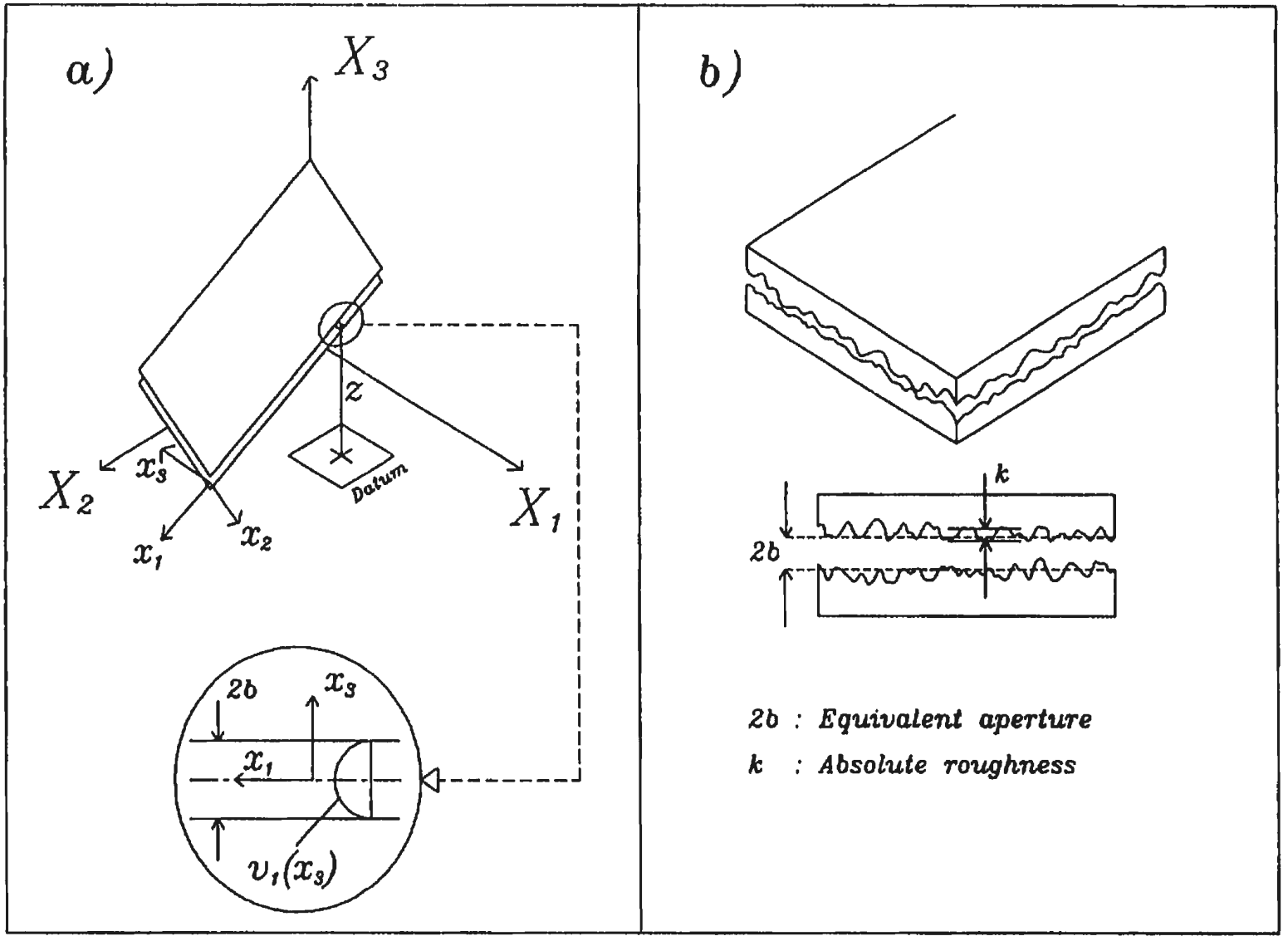

Figure 2.1.a) An arbitrarily oriented parallel plate conduit and the flow velocity profile in local coordinates, b) parameters characterizing the geometry of rough parallel plate conduits.

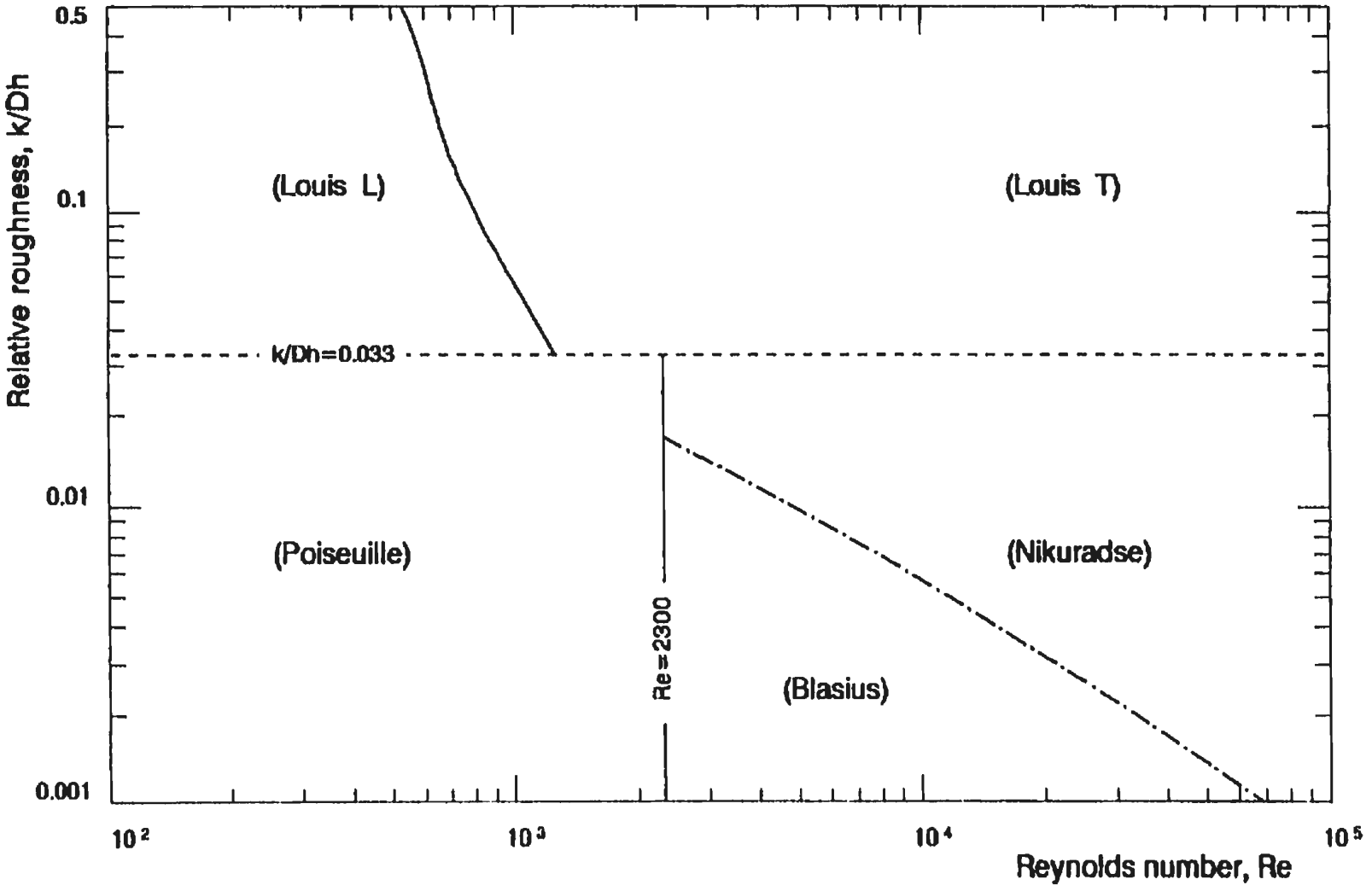

Figure 2.2. Fracture flow domains and corresponding friction factors (Table 2.1).

Table 2.1. Friction factors governing fracture flow in the domains delineated in Figure 2.1 (after Louis, 1974).

FLOW REGIME	*L A M I N A R*		
RELATIVE ROUGHNESS	$k/Dh \leq 0.033$		$k/Dh > 0.033$
HYDRAULIC BEHAVIOR	*SMOOTH*		
FRICTION FACTOR (λ)	$\frac{96}{Re}$ (Poiseuille)		$\frac{96}{Re}\left[1+8.8(k/Dh)^{1.5}\right]$ (Louis L)
FLOW REGIME	*T U R B U L E N T*		
RELATIVE ROUGHNESS	$k/Dh \leq 0.033$		$k/Dh > 0.033$
HYDRAULIC BEHAVIOR	*SMOOTH*	*COMPLETELY ROUGH*	
FRICTION FACTOR (λ)	$0.316\ Re^{-0.25}$ (Blasius)	$\left[2\ \log\frac{3.7}{(k/Dh)}\right]^{-2}$ (Nikuradse)	$\left[2\ \log\frac{1.9}{(k/Dh)}\right]^{-2}$ (Louis T)

3 THEORY AND PROBLEMS OF SINGLE-WELL TESTS IN FRACTURED MEDIA

The intersection angle which determines the shape of the inner boundary of the fracture flow domain is merely one of the system parameters that may influence the response observed in the active well. It is therefore necessary to examine the test situations in which various parameters become influential and dominate deviations from the ideal response. This analysis, in turn, allows the identification of specific conditions and test methods for which intersection angle can be isolated as the main parameter for the purposes of the present investigation. These concerns, relating to the theory and problems of the single-well tests, are dealt with in this chapter.

3.1 Introduction

The law of conservation of mass requires that the net inward flux through any arbitrary volume be equal to the rate of accumulation. For fluid flow within porous media, this balance (per unit volume and time) can be expressed as

$$-\frac{\partial(\rho \bar{v}_i)}{\partial x_i} = \frac{\partial(\rho \varphi)}{\partial t} \tag{3.1}$$

where φ is the porosity (defined over the REV) and ρ is the fluid density. The rate of accumulation of the fluid mass under confined conditions is related to the elasticity of the solid-fluid system occupying the concerned volume (Jacob, 1940; Bear, 1972)

$$\frac{\partial(\rho \varphi)}{\partial t} = \rho \left[\rho g (\varphi \sigma_1 + \sigma_m)\right] \frac{\partial h}{\partial t} = \rho \left[S_s\right] \frac{\partial h}{\partial t} \tag{3.2}$$

where σ_l and σ_m are the compressibility of the fluid and the (moving) solid matrix, respectively, and S_s is the specific storativity of the system.

Since the spatial density variations can be assumed negligible in most problems (Hantush, 1964), Equation 3.1 when combined with Equation 3.2 reduces to

$$-\frac{\partial \overline{v}_i}{\partial x_i} = S_s \frac{\partial h}{\partial t} \tag{3.3}$$

Assuming laminar flow conditions, and hence substituting the average velocity as determined from the Darcy law for homogeneous isotropic media (Equation 2.2) yields the fundamental equation of diffusion in porous media

$$\frac{\partial^2 h}{\partial x_i^2} = \frac{S_s}{K} \frac{\partial h}{\partial t} \tag{3.4}$$

Here both specific storativity and conductivity are referenced to the initial values of the system properties. Integrating through the entire thickness, $2b$, of the saturated zone

$$\frac{\partial^2 h}{\partial x_i^2} = \frac{S}{T} \frac{\partial h}{\partial t} \tag{3.5}$$

where S and T are the storativity and transmissivity of the zone, respectively,

$$\begin{aligned} S &= S_s (2b) \\ T &= K (2b) \end{aligned} \tag{3.6}$$

Note that Equation 3.5 applies only to isotropic, non-leaky, confined aquifer conditions. Variations in this equation address other possibilities such as anisotropy in permeability, leakage to/from confining layers, unconfined (gravity) drainage and/or steady-state behaviour (Hantush, 1964; Kruseman and de Ridder, 1970; Lohman, 1972).

The solution of Equation 3.5 or its various equivalent forms for given initial/boundary conditions and flow domain geometry allows one: a) to estimate the subsurface hydraulic properties from field measurements; and subsequently b) to predict the pressure behaviour upon changes in boundary conditions or upon natural/artificial disturbances. The former is referred to as the inverse problem whereas the latter is the forecasting problem (Bear, 1979).

The essential aim and usage of well testing is to solve the inverse problem. Section 3.2 briefly outlines the constitution of the well test models from this general perspective. The underlying assumptions and the derivation of the basic constant-flux test solutions are reviewed in detail in Section 3.3. This review constitutes the core of the evaluation models for single-well, constant-flux tests (Section 3.5) and sets a comparative basis for the mathematical developments presented in Chapter 4. While maintaining the generality in the variety of test methods, this chapter thereafter focuses on the basic evaluation models for single-well tests in confined media. This is to highlight the influence of individual fracture characteristics on the near well flow phenomena and consequently on the observed response. First the inherent problems of the observations in an active well are thoroughly discussed in Section 3.4. The subsequent

sections (Sections 3.5 and 3.6) include brief descriptions of the application, testing and evaluation procedures for single-well tests and a critical appraisal of their results with reference to Section 3.4.

3.2 Well test evaluation models

The mathematical models used in the analyses of well tests consist of (analytical) solutions of Equation 3.5 and its variations for different conceptual models and inner boundary conditions. These conditions vary according to the test technique (e.g. constant-flux/head, slug, pulse) and other considerations such as wellbore storage, skin effect, finite well radius, intersecting fracture, wellbore penetration (Gringarten, 1982; Karasaki, 1987). The conceptual models are built upon idealizations about the medium (e.g. confined, multilayered, composite, double-porosity), the flow domain geometry (e.g. the outer boundary, thickness, orientation) and consequently the flow pattern (e.g. parallel, radial, polar). Detailed general reviews of the analytical models of well test evaluation are available both for granular porous media (Hantush, 1964; Matthews and Russell, 1967; Kruseman and de Ridder, 1970; Lohman, 1972) and fractured media (Zeigler, 1976; Streltsova, 1978; Gringarten, 1982; Karasaki, 1987).

3.3 Basic models of constant-flux tests

The most common well tests involve measurements of changes in hydraulic head (or pressure) in the observation (and active) wells in response to fluid suction/injection at a constant rate from/into the tested medium. Data obtained during such tests conducted in confined media

may be evaluated by one of the two fundamental analytical models assuming that:

a) the medium is homogenous and isotropic, of infinite extent (i.e. boundary effects are not felt during testing), horizontal and of constant thickness,

b) the zones immediately overlying and underlying the medium do not leak under induced vertical pressure differentials,

c) the well fully and vertically penetrates, and uniformly communicates with the medium,

d) the hydraulic head distribution prior to testing is uniform,

e) flow is radially symmetric (as conditioned by a-d),

f) water is instantaneously released from/enters into the storage as the hydraulic head descends/rises, respectively, and

g) the wellbore radius is infinitely small, i.e. the well acts as a line sink/source with no self-storage.

The last two assumptions are necessary only when the head response is time-dependent (i.e. transient).

3.3.1 Transient head

Distribution of transient hydraulic head in a radial flow field can be expressed in one dimensional form by writing Equation 3.5 in plane polar coordinates

$$\frac{\partial^2 h}{\partial r^2} + \frac{1}{r}\frac{\partial h}{\partial r} = \frac{S}{T}\frac{\partial h}{\partial t} \qquad (3.7)$$

The initial and boundary conditions posed by the assumptions are

formulated as

$$\begin{aligned} h(r,0) &= h_0 \\ h(\infty,t) &= h_0 \\ \lim_{r=r_w \to 0} \left[2\pi r T \frac{\partial h}{\partial r}\right] &= Q \end{aligned} \tag{3.8}$$

where h_0: initial hydraulic head,

r_w: wellbore radius, and

Q: flow rate.

Re-writing Equation 3.7 in terms of net drawdown/rise in the initial hydraulic head, i.e. $s = h_0 - h(r,t)$, and applying the Laplace transform method (Hantush, 1964) yields

$$s(r,t) = \frac{Q}{4\pi T}\int_u^\infty \frac{e^{-x}}{x}dx = \frac{Q}{4\pi T}W(u) \qquad \left\{ u = \frac{Sr^2}{4Tt} \right. \tag{3.9}$$

where x: integration variable, and

W: constant-flux well function.

This solution, first introduced by Theis (1935) by analogy to the equivalent heat conduction problem, is now known as the Theis equation. The numerical values of the function W are obtained from the series expansion of the exponential integral (Jacob, 1940; Tuma, 1987)

$$W(u) = -\gamma - \ln u + u - \frac{1}{2}\frac{u^2}{2!} + \frac{1}{3}\frac{u^3}{3!} - \cdots \tag{3.10}$$

where $\gamma = 0.5772$ (Euler's constant).

The Theis equation is extensively used in practice despite being an oversimplification. The computation of the two unknowns (S and T) in Equation 3.9 is accomplished by means of graphical procedures such as type-curve matching (Theis, 1935) or straight-line plotting through the so-called logarithmic approximation (Cooper and Jacob, 1946). The latter is based on the fact that for a long testing period

$$W(u) \approx -\gamma - \ln u \tag{3.11}$$

and hence

$$s(r,t) = \frac{Q}{4\pi T} \ln \frac{2.25\,Tt}{r^2 S} \tag{3.12}$$

the semi-logarithmic plots of which form straight lines, regardless of the choice of the independent variable. Among these, the drawdown-time graph enables the determination of the transmissivity from the measurements in active wells.

3.3.2 Steady head

Steady-state implies that subsurface pressures have assumed a new state of equilibrium in response to the induced disturbance. As the drawdown is a continuous function of time (Equation 3.9), equilibrium is theoretically impossible. However, when the hydraulic gradient stabilizes (i.e. $\left.\frac{\partial h}{\partial t}\right|_1 - \left.\frac{\partial h}{\partial t}\right|_2 = 0$) and/or transients are negligible (i.e. $\partial h/\partial t \approx 0$) after some period of pumping/injection, it is justifiable to assume that steady-state is attained (Lohman, 1972).

For $\partial h/\partial t=0$, Equation 3.7 reduces to the Laplace equation

$$\frac{\partial^2 h}{\partial r^2}+\frac{1}{r}\frac{\partial h}{\partial r}=0 \tag{3.13}$$

When integrated using the underlying boundary conditions

$$\begin{aligned} &h(R)=h_R \\ &\lim_{r=r_w\to 0}\left[2\pi r T\frac{\partial h}{\partial r}\right]=Q \end{aligned} \tag{3.14}$$

the result is known as the Thiem equation (Lohman, 1972)

$$s(r)=\frac{Q}{2\pi T}\ln\frac{r}{R} \tag{3.15}$$

where R is the radial distance to the observation well. In the case of single-well data the initial hydraulic head is utilized as an estimate of the undisturbed head at a point outside the zone of influence.

3.4 Nature of measurements in active wells and well losses

Pumping from porous media, under the assumptions of the Theis/Thiem equations (Equations 3.9 and 3.15), results in an axisymmetric cone of depression representing the hydraulic head distribution within the zone of disturbance (Figure 3.1). According to Equation 3.15 the hydraulic heads measured simultaneously at any two points along a radial section in this zone should vary linearly as a function of the logarithmic distance between these points. In practice, however, the heads measured in and around the vicinity of active wells are substantially lower than theoretically predicted (Figure 3.1).

As the fluid under the induced gradient moves from the radius of influence, through the porous medium, into the wellbore and up to the pump (or tubing) intake, part of its mechanical energy is lost to maintain motion. This loss manifests itself as the difference in hydraulic heads measured in the active well before and during pumping, i.e. the total drawdown (Jacob, 1947). It is recognized that the total drawdown consists of four distinct components (Rorabough, 1953; Bruin and Hudson, 1955) which in the spatial order of their contribution are (Figure 3.1)

$$s = s_l + s_n + s_e + s_w \tag{3.16}$$

where s_l and s_n: linear and nonlinear head losses due to flow resistance of the medium under laminar and turbulent conditions, respectively,

s_e: exit head loss due to sudden enlargement of section and change in flow direction, and

s_w: wellbore head loss due to the wall friction within the well.

The preceding discussion equally applies to injection for which: a) the sequence of the head losses are reversed due to upconing; and b) the symbol s_e represents the entry head loss due to sudden contraction and directional change of flow section.

The first operational relationship between the total drawdown and pumping rate was introduced by Jacob (1947),

$$s = BQ + CQ^2 \qquad \begin{cases} BQ = s_l \big|_{r_i}^{r_w} \\ CQ^2 = s_e + s_w \end{cases} \tag{3.17}$$

where B and C: linear formation loss and well loss constants,

respectively, and

r_i: radius of influence.

The quadratic exponent in the well loss component originates from the fluid mechanics approximations of the exit/entry and frictional losses in pipes (Vennard and Street, 1982). The linear formation loss is as given by the Theis/Thiem equations (Equations 3.9 and 3.15).

Rorabough (1953) recognized that above a critical pumping rate, turbulent conditions dominate flow from a critical radius, r_c, to the well face (Figure 3.1). As the rate increases the critical radius extends further away implying increasing contribution of the nonlinear formation loss. Consequently B and C are not constants in practice. However, to enable the graphical determination of these, Rorabough (1953) modified Equation 3.17 as

$$s = BQ + CQ^n \qquad \begin{cases} BQ = s_l \Big|_{r_i}^{r_c} \\ CQ^n = s_n \Big|_{r_c}^{r_w} + s_e + s_w \end{cases} \tag{3.18}$$

where the exponent n accounts for variations from reference values of B and C. These expressions (Equations 3.17 and 3.18) constitute the basis for the analysis of step-drawdown tests.

Measurements in an active well are also influenced by the zone of altered permeability immediately surrounding the wellbore. In the case of enhanced permeability (such as by gravel packing around water wells), the resulting head recovery is accounted for by adopting an effective well radius (Jacob, 1947). On the contrary, a zone of reduced permeability,

known as skin (van Everdingen, 1953; Matthews and Russell, 1967) around oil wells, increases flow resistance. The corresponding head loss is included in the well loss component of the total drawdown as (Ramey, 1982)

$$CQ^n = \frac{1}{2\pi T}(F_s + D_n Q)\, Q \qquad (3.19)$$

where F_s is the skin factor and D_n is the constant reflecting a combined influence of the nonlinear formation and exit losses.

Flow rate efficiency of a fracture (or fractures of a set) under the same gradient can vary significantly depending on the distribution of the effective flow area relative to the active wellbore intersection (Sharp and Maini, 1972). This argument was verified by an electrical analog study (Sundaram and Frink, 1983) and numerical simulations (Smith et al. 1987) of radial fracture flow. Such pronounced influence of the near well fracture geometry occurs because a large percentage of the pumping/injection head is lost within a short distance of the wellbore. Therefore analyses of active well data assuming homogeneity at the scale of the narrow sampling window of the wellbore intersection may produce highly biased estimates of hydraulic properties. Observation wells offer the advantage of avoiding this bias as well as well losses, and of studying the inter-well connectivity. Aquifer/reservoir scale hydraulic characterization based on multiple observation wells is more dependable in strongly heterogeneous media in which the flow pattern may substantially differ from the assumed one.

3.5 Single-well constant-flux tests

As explained in Section 3.4, head measurements in active wells during constant-flux tests are altered by an additional, constant amount. The slope of the data plot (s vs. log t) from the late (infinite-acting) period therefore yields a transmissivity estimate using Equation 3.12. This estimate, although free of the effects of well losses and near-the-well heterogeneities, pertains to the part of the reservoir controlling the rate of head changes during the late period. This part corresponds to: a) the matrix domain for the equivalent homogeneous porous medium models (EHM) in which overall fracture anisotropy is represented by a single, high-permeability, vertical/horizontal fracture intersecting the active well (Gringarten, 1982); b) the outer continuum domain for the composite models (CM) in which inner (concentric) domain consists of discrete (vertical/horizontal/inclined) fractures intersecting the active well (Karasaki, 1987); and c) the entire domain within the zone of influence for the double-porosity models (DPM) of uniformly fractured porous media (Streltsova, 1978).

On the other hand, constant-flux test solutions based on the conceptual models such as EHM and CM predict that the early period is dominated by the fractures intersecting the active well (if wellbore storage and skin is negligible). This period, however, lasts only a few minutes in fractured water wells whereas in oil wells it usually is in the range of a few hours (Gringarten, 1982). Therefore it may not always be possible to capture data during this informative period.

In summary, apart from determining the magnitude of well losses and

of near-the-well bias in head measurements in active wells, the hydraulic characteristics and attitude of these fractures also modify the response patterns during the early period of testing. Recognition of these relations enables the assessment and improvement of the quality of the inferences made particularly through single-well testing. The constant-flux test methods usually conducted by means of a single well are examined below from this standpoint.

3.5.1 Pressure build-up or recovery tests

In producing oil fields, build-up tests are frequently used in place of constant-flux pumping tests, the analyses of which require uniform initial head distribution in the reservoir (Matthews and Russell, 1967). It is also a common practice in water well testing to record the head recovery in the wellbore after a constant-flux pumping/injection period. Analysis of the recovery data produces a check value for the transmissivity (Lohman, 1972).

The recovery upon stopping production is mathematically expressed by superposing the temporal variations in head as a result of hypothetical injection and continuing production at the same point and rate (Theis, 1935). Assuming no change in the transmissivity and storativity at the start of pumping and recovery, and utilizing the logarithmic approximation (Equation 3.12),

$$s'(t') = \frac{Q}{4\pi T} \ln \frac{t}{t'} \tag{3.20}$$

where s' is the residual head (i.e. difference in head at the start of the

actual pumping period and any time during recovery), and t' is the time elapsed since the pump was shut-off. The transmissivity value is calculated from the slope of the data plot (s' vs. log t/t'). It should be noted that the influence of well losses developed during the actual pumping period propagates into the recovery period in the form of a delay (in the actual process) during which formation pressure at the wellbore face equilibrates with the pressure in the packer-isolated interval and reaches the theoretical level predicted by the Theis equation (Equation 3.9).

3.5.2 Step-drawdown tests

The optimum well yield, the total drawdown at a desired pumping rate, and changes in the efficiency of a well after being used or developed are the essential information needed in the design of production and drainage wells and well fields. The necessary information can be extracted from a step-drawdown test, originally suggested by Jacob (1947) to quantify the well loss. The standard procedure to conduct this test is to record the total drawdown while increasing the pumping rate in stepwise manner. The well loss constant (and the exponent) are calculated from the slope of the data plotted in the following formats by rearranging: a) Equation 3.17 as

$$\frac{s}{Q} = B + CQ \tag{3.21}$$

and b) Equation 3.18 as

$$\log\left(\frac{s}{Q}-B\right)=\log C+(n-1)\log Q \qquad (3.22)$$

With the latter method the linear formation loss constant is repeatedly estimated until a straight line of slope $(n-1)$ is obtained.

The actual extent and pumping rate dependence of the head loss domains of Equation 3.16 are not considered in the graphical solutions. This is probably the main reason that tests in water wells yield values of the exponent as high as $n\approx 2.5$ (Rorabough, 1953) and even upto $n=3.5$ (Lennox, 1966). Theoretically the value of this exponent should equal 2 for exclusively linear flow as well as for linear flow with an abrupt transition to fully turbulent nonlinear flow within the medium. The existence of a long transitional nonlinear flow domain should reduce the value to less than 2. Any changes between the test steps such as stress-induced permeability reduction around wells, particularly in unconsolidated media, may substantially contribute to the deviations cited in the literature.

Well efficiency

Since the linear formation loss is an inevitable consequence of fluid movement through porous media, well efficiency is referenced to this loss as (Rorabough, 1953)

$$E_w=\frac{BQ}{s} \qquad \left\{ BQ=s_1\Big|_{r_1}^{r_w} \right. \qquad (3.23)$$

According to this definition, the efficiency of a well can be improved by reducing the well loss and especially the nonlinear formation loss. This

can be achieved by applying methods such as gravel packing and improving screen design in water wells (Kruseman and de Ridder, 1970), acidization, sand propping and hydraulic fracturing in oil wells (Baker, 1955; Matthews and Russell, 1967) and enlarging well radius in general.

3.5.3 Geotechnical permeability tests

The need for in-situ determination of permeability arises from the presence of heterogeneities in rock masses that cannot be tested in the laboratory at the scale/complexity with which they contribute to the bulk permeability. From the geotechnical point of view, in-situ information is crucial to delineate the distribution of seepage forces around engineering structures (Cedergren, 1988). In this context, field permeability values are obtained through well testing, generally based on steady-state approximation. This is adequate in engineering design, especially at shallow depths of investigation where the well head stabilizes relatively fast due to high permeability of fractures (Maini et al. 1972).

Constant-flux pumping/injection permeability tests are usually conducted in packer-isolated intervals in order to profile vertical conductivity and/or concentrate on the depths/features of interest along the fractured wells. The pumping tests require expensive large wellbores and are limited to saturated zones. Therefore the injection tests (also known as water pressure or lugeon tests), although prone to the clogging effect for there may be impurities in the test water (Cedergren, 1988), are routinely applied in site investigations.

Because of cost concerns and the desire to obtain a representative

sample of local permeabilities, much effort is focused on single-well tests. The permeability derived from the single-well injection tests is a local value (Louis and Maini, 1970), even for a single fracture, and only the fracture(s) directly intersecting the wellbore influence the results (Zeigler, 1976; Rissler, 1978). Considering the latter and assuming that fractures occur in orthogonal sets, wellbores are recommended to be drilled normal to each set in order to derive permeability independently (Louis and Maini, 1970; Maini et al. 1972). The permeability values can then be used either in a discrete (statistical) fracture network or in an anisotropic continuum model to study seepage and the alternative remedies.

Problems and method of analysis

The flow rate response of a packer-isolated fracture under high injection pressures may be significantly altered, in addition to well losses, by (Louis and Maini, 1970; Maini et al. 1972; Zeigler, 1976; Cedergren, 1988): a) the enlargement of fracture aperture; b) leakage of packers; and c) redistribution and/or washing out of filling materials. Assuming the confining blocks and the fracture to be extensive, aperture changes are limited to the elastic deformation of the matrix if injection pressures are below the overburden pressure. Low pressures also help control the leakage problem and the nonlinear formation loss. In general practice the causes altering the flow rate response to pressure increment are recognized from various nonlinear signatures on the flow rate-pressure graphs drawn from multistage injection test data. The graphic format of Equation 3.21 is more appropriate when used as for the step-drawdown

tests.

In the range where the nonlinearity is due solely to well losses, the analysis of single-well permeability tests can be based on the formulation of the head loss components (Equation 3.16). For a steady, radial, two-regime flow (i.e. one in which linear and nonlinear domains co-exist as specified for Equation 3.18) through a rough fracture, the relationship between the net head change in the active well and flow rate is approximated by (Rissler, 1978)

$$s = \frac{Q}{2\pi (2b) K} \ln \frac{r_i}{r_c} + \frac{\lambda Q^2}{16 \pi^2 (2b)^3} \left(\frac{1}{r_w} - \frac{1}{r_c} \right) + CQ^2 \qquad \{ CQ^2 = s_e + s_w \quad (3.24)$$

Similar forms of this equation were also derived by Rorabough (1953), Baker (1955) and Bruin and Hudson (1955). The expressions for the conductivity and friction factor in the linear and nonlinear formation loss components (Equation 3.24), respectively, are selected from Table 2.1 according to the relative roughness of the fracture. Details of the derivation in a fully explicit form of Equation 3.24 and the selection of the roughness-dependent parameters can be found in Section 4.5 for the generalized formulation of flow through arbitrarily oriented fractures.

3.6 Low-permeability media tests

It is contemplated that hazardous wastes might be disposed in low-permeability (crystalline, fractured) media at great depths. The high risks associated with the containment of these wastes in the repositories demand different well testing procedures and analysis methods for hydraulic characterization of such unusual media. A thorough description

of the groundwater system (under probable field gradients) and therefore of the effective fracture network is essential for an accurate portrayal of the migration patterns for the released contaminants. Well testing in this context is focused on defining the network mainly at the scale of a constituent fracture (Wilson et al., 1979; Doe et al., 1982).

Transient single-well test methods (i.e. constant-head injection, slug and pulse tests) are best suited for estimating the aperture, extent and connectivity of the packer-isolated fracture(s) in low-permeability media (Wilson et al., 1979; Doe and Remer, 1980; Doe and Osnes, 1985). These parameters are combined with other geometrical observations such as orientation and spacing to form statistically equivalent networks (Doe et al., 1982).

3.6.1 Constant-head injection tests

These tests can be rapidly applied over a wide range of permeabilities and are free of wellbore storage effects (Doe and Remer, 1980). The test procedure involves injecting fluid into a packer-isolated section under constant-head and recording the flow rate decline. Employing the analogy between a single fracture and a confined aquifer (Doe et al., 1982), the basic solution becomes the same as that of constant drawdown tests in extensive confined aquifers (Jacob and Lohman, 1952)

$$Q(t) = 2\pi T s G\left(\frac{Tt}{Sr_w^2}\right) \tag{3.25}$$

where G is the constant-head well function and s is the induced head change in the active well. The definition and the numerical values of the

function G and the associated type curve (log G vs. log Tt/Sr_w^2) are given by Lohman (1972).

A data plot (log Q vs. log t) from a single fracture test may reveal up to three temporal phases: a) an initial infinite response period; b) a steep decline signalling a (partly) closed or low permeability boundary; and c) stabilization indicating induced leakage or network connection (Doe et al., 1982; Doe and Osnes, 1985). The transmissivity and storativity of the fracture are obtained using curve matching of the first section of the data plot. The distance to the (closed or constant-head) boundary can be determined from an empirical relation such as that of Uraiet and Raghavan (1980)

$$r_b \approx \left(\frac{T t_b}{S} \frac{1}{0.1\pi} + r_w \right)^{1/2} \tag{3.26}$$

where r_b is the distance to the equivalent circular boundary and t_b is the time at which the boundary is felt.

The main limitation of this test methodology is the difficulty of obtaining early time data in rigid and/or finite fractures (Doe and Osnes, 1985). Additionally, flow rate dependence of the well losses and time dependence of fracture opening complicate data analysis from the early response period.

3.6.2 Slug and pulse tests

Both tests consist of instantaneous elevation or lowering of the head in the test interval and monitoring the decay or recovery,

respectively. Slug tests are conducted by addition or removal of a known volume into the test section through the open tubing whereas pulse tests involve, pressurizing or de-pressurizing a packer-isolated interval. This difference in producing the head change translates into different boundary condition expressions. Accordingly the flow rate, for example, into the fracture equals (Bredehoeft and Papadopulos, 1980): a) the rate of fluid volume decrease in the open tubing during slug tests, i.e.

$$2\pi r_s T \frac{\partial h(r_s, t)}{\partial r} = \pi r_c^2 \frac{\partial H^*(t)}{\partial t} \tag{3.27}$$

and b) the rate of volumetric expansion of fluid in the pressurized section during pulse tests, i.e.

$$2\pi r_s T \frac{\partial h(r_s, t)}{\partial r} = V_0 \sigma_1 \rho g \frac{\partial H^*(t)}{\partial t} \tag{3.28}$$

where r_s: radius of the wellbore in the test interval,

r_c: radius of the open tubing,

V_0: initial fluid volume in the test interval, and

H^*: head in the tubing or test interval.

The analytical solution simulating the head transient during a slug test in a finite diameter well in a confined aquifer is of the form

$$\frac{H^*(t)}{H_0^*} = F\left(\frac{r_s^2 S}{r_c^2}, \frac{Tt}{r_c^2}\right) \tag{3.29}$$

where H_0^* is the initial head in the tubing and F is the pulsed-head well

function the definition and numerical values of which were first introduced by Cooper et al. (1967). This solution is also valid for pulse test response when, from Equations 3.27 and 3.28, the following substitution is made

$$r_c^2 = \frac{V_0 \sigma_1 \rho g}{\pi} \tag{3.30}$$

Successful applications of this solution for both tests require limiting the head increments to the lowest possible level to prevent fracture opening and to minimize well losses during the early period.

The field observations can be evaluated by matching the data plot (H^*/H_0^* vs. log t) to one of the type curves (H^*/H_0^* vs. log Tt/r_c^2). Data collected during the 50 to 80 % decay period is sufficient for this purpose (Bredehoeft and Papadopulos, 1980). However, type curves for large variations of the group parameter, $r_s^2 S/r_c^2$ (Equation 3.29) are very similar in shape and therefore transmissivity is the only reliable estimate from these tests (Cooper et al., 1967).

The fracture volume influenced by these tests at the end of the full decay of a given head increment is a function of the radius of the tubing/wellbore and storativity of the fracture. On the other hand the length of time required for percent decay is solely determined by the transmissivity for a given head increment, tubing/wellbore radius and storativity. The range of transmissivity over which these tests apply is determined by this length of time which should be short to be practically observed, but not too short to obtain sufficient data free of wellbore and

instrumental effects. In this sense Pulse tests are adequate for very tight fractures (e.g. $2b < 20\mu m$) and are therefore complementary to constant-head injection tests (Wilson et al., 1979).

The closed boundary is felt as stabilization of head at an incomplete decay whereas a constant-head boundary should accelerate full decay. The distance to the equivalent circular boundary of a single fracture can be estimated from the total volume change at the time the boundary is felt.

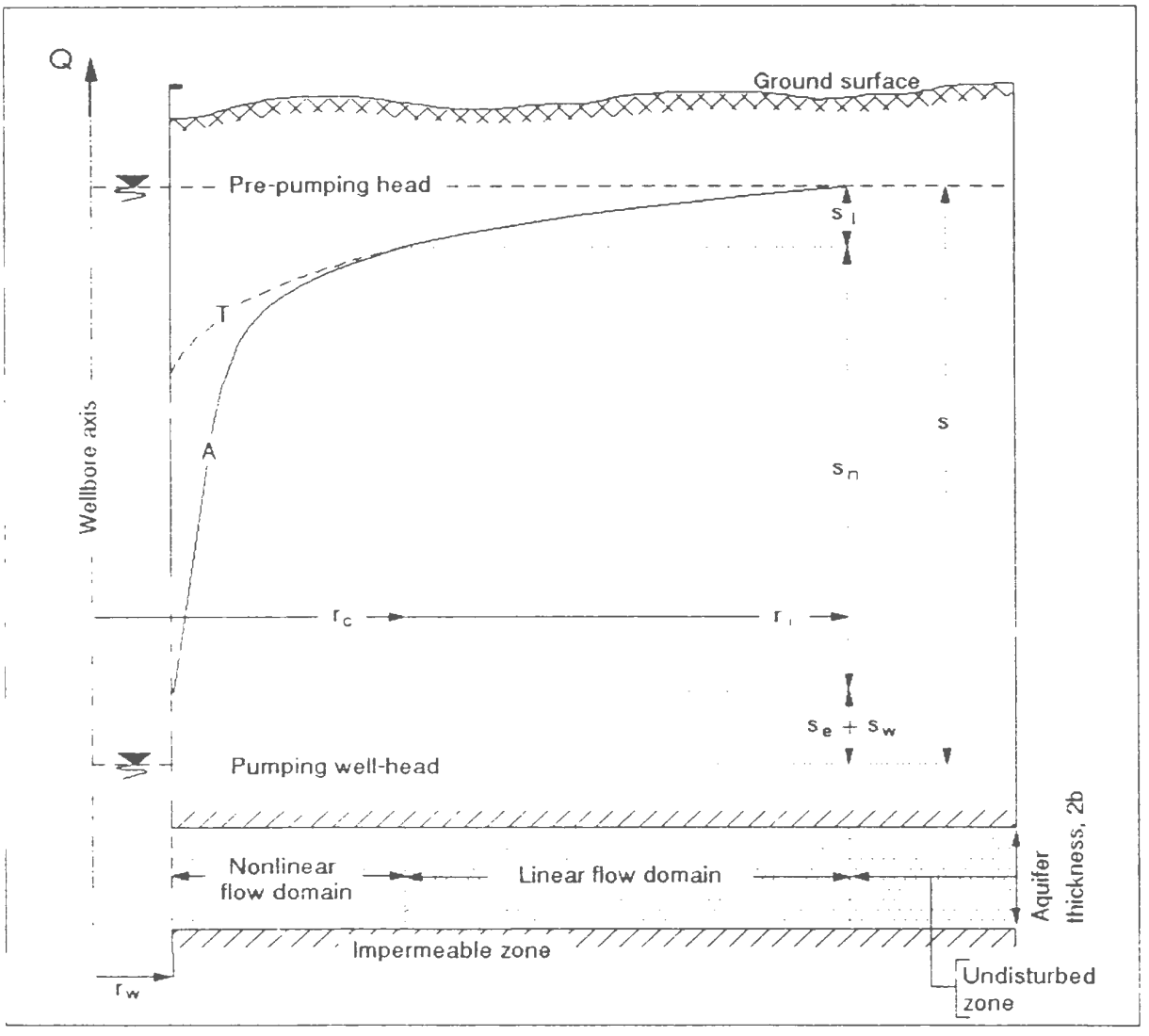

Figure 3.1. Radial half-section through the cone of depression developed upon pumping from a confined aquifer/fracture under the Theis/Thiem assumptions. Note the actual (A) and theoretical (T) head profiles, the components of the total head loss, and the corresponding flow domains.

4 MATHEMATICAL MODELS FOR WELL TESTS IN ACUTE FRACTURE-WELLBORE SYSTEMS

4.1 Introduction

The review in Chapter 3 demonstrates that the attitude as well as hydraulic properties of the fractures intersecting an active well may become important system parameters when the data being evaluated is from the active well (and the early test period, if the response is transient). The main purpose of this chapter is to develop analytical well test models for evaluating such data. A brief account of the most relevant literature is given in Section 4.2. The methodology of the model development described in Section 4.3 provides a firm ground on which the problem is formulated. The analytical solutions to the general diffusion equation developed in Section 4.3 are presented in Section 4.4 for transient and steady constant-flux tests. At the end of Section 4.4, potential theory is utilized to delineate the flow network and the zone of influence in acute systems during tests under initially non-uniform head conditions. The likelihood of nonlinear flow regime and its influence on the observed head changes and hence the aperture (or transmissivity) predictions are addressed in Section 4.5 where a general formulation is introduced. Section 4.6 provides an overall discussion for various models proposed and also includes a subsection addressing the natural extension of the basic concepts to refine estimates of other well test models.

4.2 Previous studies relating to acute systems

No well-test models that consider the system intersection angle as a variable that controls the intersection area and alters the flow pattern

and head distribution in the fracture were encountered during the course of this study. The models based on a horizontal or vertical fracture intersecting a wellbore (such as outlined in Zeigler (1976) and Gringarten (1982)) form the end members of a general system model in which both fractures and wellbores can change attitude. Another end member was conceived by Louis and Maini (1970) assuming the wellbore to be orthogonal to an inclined fracture.

Cinco-Ley (1974) developed a unique model simulating the transient response to a constant-rate production of a slab reservoir as a function of the fracture-wellbore intersection angle. Since the fracture in this model was considered to be a plane sink, the intersection angle merely changed the reservoir volume to be drained. Through a numerical simulation of the steady injection tests in unsaturated zones, Rissler (1978) evaluated the influence of fracture inclination in acute systems composed of a vertical wellbore intersected by an inclined fracture as well as in orthogonal systems with inclined fractures. In order to account for the dominance of the intersecting fractures on the near wellbore flow, Karasaki (1987) conceptualized the fractured medium as two concentric zones: the inner zone composed of a vertical, horizontal or inclined intersecting fracture (or fractures with identical hydraulic properties and attitude) and the outer zone of a three-dimensional, well-interconnected fracture network. For the case of an inclined fracture, the inclination was assumed to produce a three-dimensional connectivity between the two zones leading to a spherical flow field in the outside zone reducing to radial flow in the inner zone (or vice versa).

4.2 Methodology

Theoretical basis

The Darcy law (Equation 2.2) in vectorial form can be written as

$$\vec{v} = -K\, grad(h) \qquad \left\{ grad = \frac{\partial}{\partial x_i} \vec{u}_i \right. \qquad (4.1)$$

where $\vec{u}$ is a unit vector. The velocity and gradient vectors at any point are co-linear in isotropic media (i.e. where conductivity is a scalar). With regard to their definition, the gradient vectors are normal to the equipotential surfaces (delineated by $h = const.$) and the streamlines are tangent to the velocity vectors. Therefore, all equipotential surfaces and (instantaneous) streamlines intersect each other at right angles (Rouse, 1961). This deduction also holds for turbulent two-dimensional flow in homogeneous, isotropic media (Bear, 1972). Furthermore, in such media, the streamline pattern in an induced flow field is solely controlled by the geometry of the flow domain for an initial head distribution. These theoretical considerations underlie the assumptions necessary to validate specific flow patterns conceptualized to form during well tests.

The inner boundary of a convergent/divergent flow field in a fracture is the intake/outlet section at the fracture-wellbore intersection. This section coincides with the innermost equipotential surface to which streamlines will be normal. Provided that the fracture void space is homogeneous, isotropic and extensive and that the head distribution before flow is induced is uniform, streamlines will remain normal and hence straight. Since the induced head distribution along all

these streamlines will be identical, equipotential surfaces pass through points of equal distance from the wellbore face. Again for this reason, most analytical models of well tests are formulated in plane-polar coordinates which is best suited to describe the head distribution along straight radial streamlines.

Description of the conceptual model

It is clear from the preceding discussion that the geometry of the inner boundary determines the streamline pattern and subsequently the head distribution. The boundary geometry is, in turn, determined by the angle of intersection between a fracture and the wellbore. Here, the fracture is thought of as a parallel plate conduit, an idealization theoretical aspects of which are extensively discussed in Chapter 2. For parallel and orthogonal intersections (Figure 4.1.a), the inner boundary outline are of linear and circular forms, and the resulting streamlines are parallel and radial, respectively (Figure 4.1.b). For acute intersections, models based on assumptions constraining streamlines to these forms provide approximate estimates, the accuracy of which could not be quantified previously.

Acute fracture-wellbore intersections (Figure 4.1.a) produce intake/outlet sections that are elliptical in plan view (Figure 4.1.b). For a given wellbore radius, as the ratio of the axes of the ellipse varies with the intersection angle, the streamline pattern is not of a fixed form but a general one (Figure 4.1.b). The streamline pattern, given that the head distribution is initially uniform, is independent of the inclination of the fracture-wellbore system with respect to datum.

Justification for single fracture system models

Fluid exchange between fractured rock masses and wellbores generally takes place via a limited number of fractures (Sharp and Maini, 1972). These fractures contribute to the total flow rate in varying proportions and form fracture-wellbore subsystems. The contribution of each subsystem is determined by the attitude and hydraulic properties of its fracture component. For example, the fracture with the largest aperture in the test section dominates the flow rate (Rissler, 1978; Doe and Remer, 1980) given that all the fractures are parallel and identically connected to the flow network.

In well testing practice, it is equally essential to understand the interactions at the subsystem level. For example, oil wells are often terminated at the interval where the first significant mud loss occurs generally because of the presence of a single dominant fracture (Baker, 1955). Hydraulic fracturing for the stimulation of fluid recovery wells typically creates a single fracture dominated flow condition. Another common case is where a single fracture is packer-isolated in the test section.

Significance of total head in convergent/divergent flows

For viscous, incompressible, established flows through uniform conduits, the (weighted-mean) total head across a flow section is given by the modified Bernoulli equation (Rouse, 1961)

$$H = h + \alpha \frac{\overline{v}^2}{2g} \tag{4.2}$$

where H: total head (or total mechanical energy per unit weight),

$\bar{v}^2/2g$: velocity (or kinetic) head,

α: kinetic energy correction factor for non-uniform velocity profiles, and

$\bar{v}$: average velocity calculated from the continuity condition.

In such conduits, the difference in the total head between two sections is

$$\Delta H = \Delta h \tag{4.3}$$

which verifies that the driving force of the fluid movement, i.e. the gradient, can be conveniently expressed in terms of the hydraulic head rather than the total head. However, when the area of flow at each of these sections is different, both the magnitude and the profile of the velocity varies,

$$\Delta H = \Delta h + \alpha_2 \frac{\bar{v}_2^2}{2g} - \alpha_1 \frac{\bar{v}_1^2}{2g} \tag{4.4}$$

In convergent/divergent flows, velocity variations occur regardless of the conduit geometry. For example, fluid particles flowing toward a well through a uniform parallel plate accelerates in response to narrowing flow area to maintain the continuity in volumetric flow rate. This phenomenon is accommodated by the continuous transformation between hydraulic and velocity heads. Subsequently, the irrecoverable losses in the energy of fluid can be directly depicted only in terms of the total head (Figure 4.1.c). In conclusion, the Darcy law (Equation 2.2 or 4.1) and other flow equations discussed in Chapter 2 must be re-written in terms of the total head in order to be adapted to the formulation of well

flow problems, especially wherever the velocity head differences are expected to be significant.

4.3 Mathematical formulation of the problem

The first step in the development of analytical models to simulate well tests (and any subsurface flow problem) is to write the diffusion equation (e.g. Equation 3.5) in appropriate coordinates. The purpose of this section is therefore to introduce the derivation of this fundamental differential equation, for the present problem, for which analytical solutions will be sought.

In a (convergent) flow field displaying the general streamline pattern, the net accumulation of fluid mass during a finite period within an elemental volume bounded by (concentric) equipotential surfaces may be expressed by

$$\Delta t\left(\Gamma|_{l+\Delta l}\,(2b)\,(\rho\,\overline{v}_l)-\Gamma|_l\,(2b)\,[(\rho\,\overline{v}_l)+\Delta(\rho\,\overline{v}_l)]\right)=\Gamma|_l\,(2b)\,\Delta l\,(\varphi\,\rho)\,|_t^{t+\Delta t} \tag{4.5}$$

where Γ is the perimeter of the equipotential surfaces passing through points at distances l and $l+\Delta l$ from the wellbore face, and $\overline{v}_l$ is the average velocity normal to these surfaces. Obviously, it is not possible to proceed from Equation 4.5 unless the perimeter of the equipotential surfaces can be formulated as a function of the distance from the wellbore face. The derivation of the perimeter expression for the general streamline pattern is presented in Appendix A. The resulting functional

relationship is (Equation A.15)

$$\Gamma|_l = 2\pi\,(e+l) \tag{4.6}$$

where e is the perimeter of the ellipse divided by 2π. Substituting Equation 4.6 in Equation 4.5 and dividing both sides by the elemental volume, $\Gamma|_l\,(2b)\,\Delta l$,

$$\frac{\Delta(\rho\,\overline{v}_l)}{\Delta l} - \frac{1}{(e+l)}\,(\rho\,\overline{v}_l) = \frac{\Delta(\varphi\,\rho)}{\Delta t} \tag{4.7}$$

Passing to the differentials (and remembering that $\overline{v}_l|_l > \overline{v}_l|_{l+\Delta l}$),

$$\frac{\partial(\rho\,\overline{v}_l)}{\partial l} + \frac{1}{(e+l)}\,(\rho\,\overline{v}_l) = -\frac{\partial(\varphi\,\rho)}{\partial t} \tag{4.8}$$

Neglecting the density variations along streamlines (i.e. $\frac{\partial\rho}{\partial l} \to 0$), and substituting the velocity term with the Darcy law (Equation 2.2) and the right hand side with Equation 3.2 (both re-written in terms of the total head)

$$\frac{\partial^2 H}{\partial l^2} + \frac{1}{(e+l)}\,\frac{\partial H}{\partial l} = \frac{S_s}{K}\,\frac{\partial H}{\partial t} \tag{4.9}$$

which is the desired diffusion equation. By taking $\partial h/\partial t = \partial H/\partial t$, it is also assumed that the velocity field is steady. Since, by the definition, the velocity term in Equation 4.2 represents an average of the flow section, Equation 4.9 can also be written as

$$\frac{\partial^2 H}{\partial l^2} + \frac{1}{(e+l)}\,\frac{\partial H}{\partial l} = \frac{S}{T}\,\frac{\partial H}{\partial t} \tag{4.10}$$

which is the counterpart of Equation 3.7. However it should be noted that the solution domain in Equation 4.10 starts from the wellbore face whereas in Equation 3.7 from the wellbore axis.

4.4 Analytical models of constant-flux tests

In this section, solutions of Equation 4.10 corresponding to the Theis and Thiem equations (Equations 3.9 and 3.15) are presented. The assumptions underlying these solutions are specified in the following (using the same order as in Section 3.3):

a) the fracture is homogenous and isotropic in aperture and roughness (i.e. parallel plate idealization is valid), of infinite extent (i.e. boundary effects are not felt during testing), and of arbitrary inclination,

b) the matrix of the confining blocks behave as impermeable (under induced vertical pressure differentials),

c) the well intersects the fracture at an arbitrary angle,

d) the hydraulic head distribution prior to testing is uniform,

e) the streamline pattern is not axisymmetric but of a general type (as conditioned by a-d), and

if the head response is transient,

f) water is instantaneously released from/enters into the storage as the hydraulic head descends/rises, respectively, and

g) the test section is a short, packer-isolated interval so that the wellbore storage is negligible, but the wellbore has a finite diameter.

Attention needs to be drawn particularly to the assumption (e) which provides originality to the following solutions. As the equipotential surfaces approximate circular rings (i.e. $e+1 \approx 1$) at some distance from the wellbore face (Figure 4.1.b), it may be allowed to assume more reasonably that the fracture is of finite extent and connected to a laterally extensive fracture flow network (Karasaki, 1987). Naturally, any differences between the hydraulic properties of the network and the fracture should be reflected in the observed response pattern.

4.4.1 Transient head

The preceding assumptions lead to the initial and boundary conditions,

$$\begin{aligned} &H(l,0) = h_0 \\ &H(\infty, t) = h_0 \\ &\lim_{l \to 0} \left[2\pi\,(e+1)\,T \frac{\partial H}{\partial l} \right] = Q \end{aligned} \tag{4.11}$$

where the initial head level is chosen as datum (i.e. $h_0 = 0$). Employing the Laplace transform method and the initial condition, the diffusion equation (Equation 4.10) can be reduced to the (zero order) modified Bessel equation

$$(e+1)^2 \frac{d^2\overline{H}}{dl^2} + (e+1) \frac{d\overline{H}}{dl} - \overline{k}^2 (e+1)^2 \overline{H} = 0 \qquad \left\{ \overline{k} = \sqrt{\frac{S}{T}\,\overline{s}} \right. \tag{4.12}$$

where $\overline{H}(l,\overline{s}) = \mathcal{L}[H(l,t)]$ and $\overline{s}$ is the transform variable. The general solution of Equation 4.12 is (Tuma, 1987)

$$\overline{H} = A_1 I_0[\overline{k}(e+1)] + A_2 K_0[\overline{k}(e+1)] \tag{4.13}$$

where I_0 and K_0 are the (zero order) modified Bessel functions, and A_1 and A_2 are constants. From the first boundary condition, $\overline{H}(\infty,\overline{s}) = h_0/\overline{s} = 0$ and since $K_0(\infty) = 0$ and $I_0(\infty) = \infty$, $A_1 = 0$. Hence

$$\overline{H} = A_2 K_0[\overline{k}(e+1)] \tag{4.14}$$

Applying the second boundary condition and taking the derivative of Equation 4.14 with respect to l

$$A_2 = -\frac{Q/2\pi T}{\overline{s}} \frac{1}{e\overline{k}K_1[\overline{k}e]} \tag{4.15}$$

where K_1 is the (first order) modified Bessel function. Substituting A_2 (Equation 4.15) and $\overline{k}$ (defined in Equation 4.12) in Equation 4.14

$$\overline{H} = -\frac{Q}{2\pi T}\left[\frac{K_0[\tau\sqrt{s}]}{\overline{s}(\omega\sqrt{s})\,K_1[\omega\sqrt{s}]}\right] \qquad \begin{cases}\tau = \sqrt{S/T}(e+1)\\ \omega = \sqrt{S/T}e\end{cases} \tag{4.16}$$

Employing the inverse transform of the function in the main brackets given by Carslaw and Jaeger (1959) results in the desired solution

$$H(l,t) = -\frac{Q}{4\pi T}\mathbf{Z}\left(\frac{t}{\omega^2},\frac{\tau}{\omega}\right) \qquad \begin{cases} t/\omega^2 = tT/Se^2\\ \tau/\omega = (e+1)/e\end{cases} \tag{4.17}$$

where

$$Z\left(\frac{t}{\omega^2}, \frac{\tau}{\omega}\right) = \frac{4}{\pi}\int_0^{\infty}\left[1 - e^{(-t/\omega^2 \cdot x^2)}\right] R\, dx$$

$$\left\{R = \frac{J_1(x)\, Y_0(\tau/\omega\ x) - Y_1(x)\, J_0(\tau/\omega\ x)}{x^2\left[J_1^2(x) + Y_1^2(x)\right]}\right. \qquad (4.18)$$

and Z is the acute intersection well function, x is the integration variable, J_0, J_1, Y_0 and Y_1 are the Bessel functions of zero and first order. A solution of the same form as Equation 4.17 was previously applied to the radial flow in orthogonal wellbore-aquifer systems with finite diameter wells by Hantush (1964). A short table of values for a function that equals $(1/4\pi)\,Z$ was presented by Ingersoll et al. (1950). Thus, the transmissivity of a fracture forming an acute intersection with the active well can be predicted by matching the well head (or drawdown) vs. time graph to the type curve (Figure 4.2), drawn from these values corresponding to $\tau/\omega = 1$ (i.e. the wellbore face). On Figure 4.2, the acute intersection type curve is compared with that of the line source solution of Theis (1935) in order to demonstrate another advantage of the present solution.

4.4.2 Steady head

The diffusion equation (Equation 4.10) reduces to the Laplace equation when it can be assumed that $\partial H/\partial t = 0$

$$\frac{\partial^2 H}{\partial l^2} + \frac{1}{(e+l)} \frac{\partial H}{\partial l} = 0 \qquad (4.19)$$

The boundary conditions for steady constant-flux tests in acute systems are

$$\begin{aligned} H(L) &= H_L \\ \lim_{l \to 0} \left[2\pi (e+l)\, T \frac{\partial H}{\partial l} \right] &= Q \end{aligned} \qquad (4.20)$$

where L is the distance to the point of measurement. Following the standard integration procedure for these conditions (Equation 4.20),

$$s(l) = \frac{Q}{2\pi T} \ln\left(\frac{e+l}{e+L}\right) \qquad (4.21)$$

The zone of influence in unsaturated zones

In many cases, an acute system is created by a vertical wellbore cutting through an inclined fracture. When the initial heads are not uniformly distributed, the pattern of streamlines will deviate from that of the uniform heads (Figure 4.1.b). This situation is frequently encountered during injection tests for foundation permeability determination in unsaturated zones. It is therefore of interest to delineate the modified network of streamlines and equipotentials to assess the compounded (asymmetric) bias in the fracture surface coverage in such test settings.

The influence of fracture inclination can be simulated by the (fictitious) gravity flow (Louis and Maini, 1970). Utilizing the linearity

of the Laplace equation (Equation 4.19), the resultant head distribution is obtained from the superposition of the solutions for the source (Equation 4.21) and gravity flows

$$H(l,\theta) - H(L,\theta) = \frac{Q}{2\pi T} \ln\left(\frac{e+l}{e+L}\right) + x(l,\theta) \sin\bar{\alpha} \qquad (4.22)$$

where $x(l,\theta)$ and θ are as defined in Appendix A (Equation A.8 and Figure A.1, respectively), and $\bar{\alpha}$ is the inclination of the fracture from the horizontal. Similarly, the stream function for the superposed source and gravity flows is

$$\psi(l,\theta) = \frac{Q}{2\pi (e+l)} \Gamma(l,\theta) - y(l,\theta)\, K \sin\bar{\alpha}\, (2b) \qquad (4.23)$$

where

$$\Gamma(l,\theta) = \frac{r_w}{\sin\beta} E(\kappa,\alpha) + l \tan^{-1}\left(\frac{\tan\theta}{\sin\beta}\right) \qquad (4.24)$$

$y(l,\theta)$, κ and α can be obtained from Equations A.9, A.16 and A17, respectively, and $E(\kappa,\alpha)$ is the incomplete elliptical integral of the second kind. As the point of stagnation exists at $\theta=0$, the general equation defining the zone of influence in acute systems is found to be

$$\psi(l,\theta) = 0 \qquad (4.25)$$

An example of the zone of influence upon injection in acute and orthogonal systems is illustrated in Figure 4.3.

4.5 Total drawdown in steady-state, two-regime flows

The solutions (Equations 4.21 and 4.17) developed in Section 4.4 are

based on the assumption of laminar flow (i.e. validity of Darcy law). Therefore the drawdown predicted by these solutions represents the linear formation loss component of the total drawdown (Equation 3.16). Considering that the turbulent flow domain is generally limited to near wellbore region where the velocity is largest and that the onset of turbulence is facilitated during injection by the intersection geometry (Maini et al., 1972), it is desirable to pursue equivalent solutions for the turbulent flow conditions. This is particularly important for steady-state injection tests where focus is on the near wellbore environment.

The relationship between the total head gradient and the average velocity in a fully turbulent flow domain is given by the Missbach equation (Equation 2.23)

$$\frac{dH}{dl} = \eta \overline{v}^2 \qquad \left\{ \eta = \frac{\lambda}{4g(2b)} \right. \tag{4.26}$$

where η is as defined in Equation 2.27. Substituting this in the equation of continuity (Vennard and Street, 1982)

$$Q = \overline{v}A \qquad \{ A = 2\pi (e+l)(2b) \tag{4.27}$$

and integrating between any two points within the domain yields

$$s_n(l) = \frac{\lambda Q^2}{16 g \pi^2 (2b)^3} \left[\frac{1}{(e+l_1)} - \frac{1}{(e+l_2)} \right] \tag{4.28}$$

where s_n is the nonlinear formation loss component of the total drawdown (Equation 3.16).

With analogy to the pipe flow studies (Vennard and Street, 1982), exit and wellbore losses in fracture-wellbore systems can be modeled as

linear functions of the velocity heads at the inlet/outlet section and within the wellbore, respectively, as in Equation 3.24 (Rissler, 1978). Hence, introducing the concept of the critical distance and writing the conductivity in terms of the aperture, the expression of total drawdown for the entire flow system results

$$s=\frac{6\nu f Q}{g\pi(2b)^3}\left[\ln(e+l_{OB})-\ln(e+l_c)\right]+ \frac{\lambda Q^2}{16 g\pi^2(2b)^3}\left(\frac{1}{e}-\frac{1}{e+l_c}\right)+\xi_e\frac{Q^2}{8g\pi^2e^2(2b)^2}+\xi_w\frac{Q^2}{2g\pi^2 r_w^4} \tag{4.29}$$

where f: conductivity modification factor (Equation 2.20),

l_{OB}: distance from the wellbore face to the outer boundary,

l_c: critical distance at which an abrupt transition between laminar and fully turbulent flow conditions is assumed to take place, and

ξ_e and ξ_w: empirical exit/entry and wellbore loss coefficients, respectively.

The critical distance can be estimated from

$$l_c=\frac{Q}{\nu\pi Re_c}-e \qquad \left\{\overline{v}=\frac{Q}{2\pi(e+l)(2b)}\right. \tag{4.30}$$

where Re_c, the critical Reynolds number, can be computed as explained in Section 2.4.2 for a given estimate of the relative roughness of the fracture. This estimate is also necessary to compute the friction factor

in the nonlinear flow domain (Table 2.1) and the conductivity modification factor in the linear domain (Equation 2.20). Therefore, the predictive ability of this semi-analytical model of steady, constant-flux tests (Equation 4.29), within the limitations of its assumptions, is primarily based on the estimate of the relative roughness.

The variations in the magnitude of the exit/entry loss coefficient (Equation 4.29) as a function of the intersection angle is investigated by the laboratory study described in the following Chapters 5 and 6. In the meantime, differences in aperture predictions at the same injection head for various intersection angles are presented in Figure 4.4 by assuming that the total head at the wellbore face is known.

4.6 Discussion

A conceptual study undertaken to understand how the intersection angle between a fracture and a wellbore modifies the response lead to both transient (Equation 4.17) and steady-state (Equation 4.21) solutions for constant-flux tests in acute systems. No further assumptions other than those of the Theis/Thiem equations (Equations 3.9 and 15) were introduced, whereas the vertical wellbore and horizontal aquifer/fracture assumptions were lifted. The test models can simulate the head response in the entire range of intersection angles. These models offer a better physical understanding of flow around the fractured wells and exemplify flow analysis where the streamline pattern is asymmetric with respect to the origin. However, the use of the acute intersection models are as easy as their radial equivalents. Various aspects and practical implications of

these models are discussed below.

The type curve depicted in Figure 4.2 indicates that, for all intersection angles, the transient response pattern is identical in the domain of the dimensionless time, t/ω^2. It is also shown on Figure 4.2 that for $t/\omega^2 \geq 25$, the acute system response coincides with that predicted from the Theis (line source) solution (Equation 3.9). However, the real time t at which this is realized are delayed with reference to the orthogonal system by a factor of $(e_\beta/e_{90})^2$ as the intersection angle decreases. In other words, the early period where the intersection angle dominates the response is longer for smaller angles. The delay factor $(e_\beta/e_{90})^2$ reaches an order of magnitude at $\beta \simeq 12°$.

The solution for steady response (Equation 4.21) predicts the linear formation loss, and therefore is directly incorporated in the model of total drawdown (Equation 4.29). The streamline-equipotential network that develops during tests under steady, laminar flow conditions in unsaturated zones can be analytically simulated using the formulation presented in Equations 4.22 to 4.25. Interestingly, the zone of influence is practically unchanged with the intersection angle (Figure 4.3). This observation is important in that individual permeability test results from acute systems with different intersection angles can be directly integrated in a rock mass model.

The development of a model (Equation 4.29) to evaluate the steady, constant-flux tests in acute systems with rough fractures is of utmost practical significance. Based on this model, Figure 4.4 illustrates that

the fracture aperture for an acute system is overestimated by the orthogonal system model (Equation 3.24). The magnitude of the error at any head level is constant for a given intersection angle, and varies only slightly for different combinations of test variables because of the remarkable sensitivity of the total head loss to the aperture. Obviously, this magnitude will be somewhat different if one references the predictions to the head inside the wellbore and includes the intake/exit loss for that intersection angle.

Looking at Figure 4.4 from a cost efficiency perspective, it becomes very clear that well losses can be significantly prevented by reducing the intersection angle using oriented drilling at the production levels. Similarly, efficiency of wells drilled by the identical procedures into the same medium may differ substantially if the fractures dominating the flow rate form different intersection angles in each wellbore. Furthermore, the necessity of multiple orthogonal drilling in determination of anisotropic permeability is unjustified as a single wellbore may be sufficient for this purpose.

Equivalent radius concept in the evaluation of single-well tests

Beside constant-flux tests, there are a variety of other single-well tests (Chapter 3) evaluation of which equally needs consideration of the fracture-wellbore intersection angle. Although specific models for each test type may be developed, at least through numerical inversion of the solution in Laplace space (Stehfest, 1970), this is beyond the scope of the present study. However, it is noteworthy that the equivalent radius

concept as defined in Equation A.15 may be used to refine the estimates of the available solutions of the single-well tests. According to this, an acute fracture-wellbore system is replaced with an orthogonal system which has proportionally larger wellbore radius. Thus the influence of the acute intersection is reduced to a simpler problem of changing the wellbore radius. This approach can be extended to other solutions based on more complicated conceptual systems such as the composite model (Karasaki, 1987) and the equivalent homogeneous medium model with wellbore storage and skin effects (Gringarten, 1982).

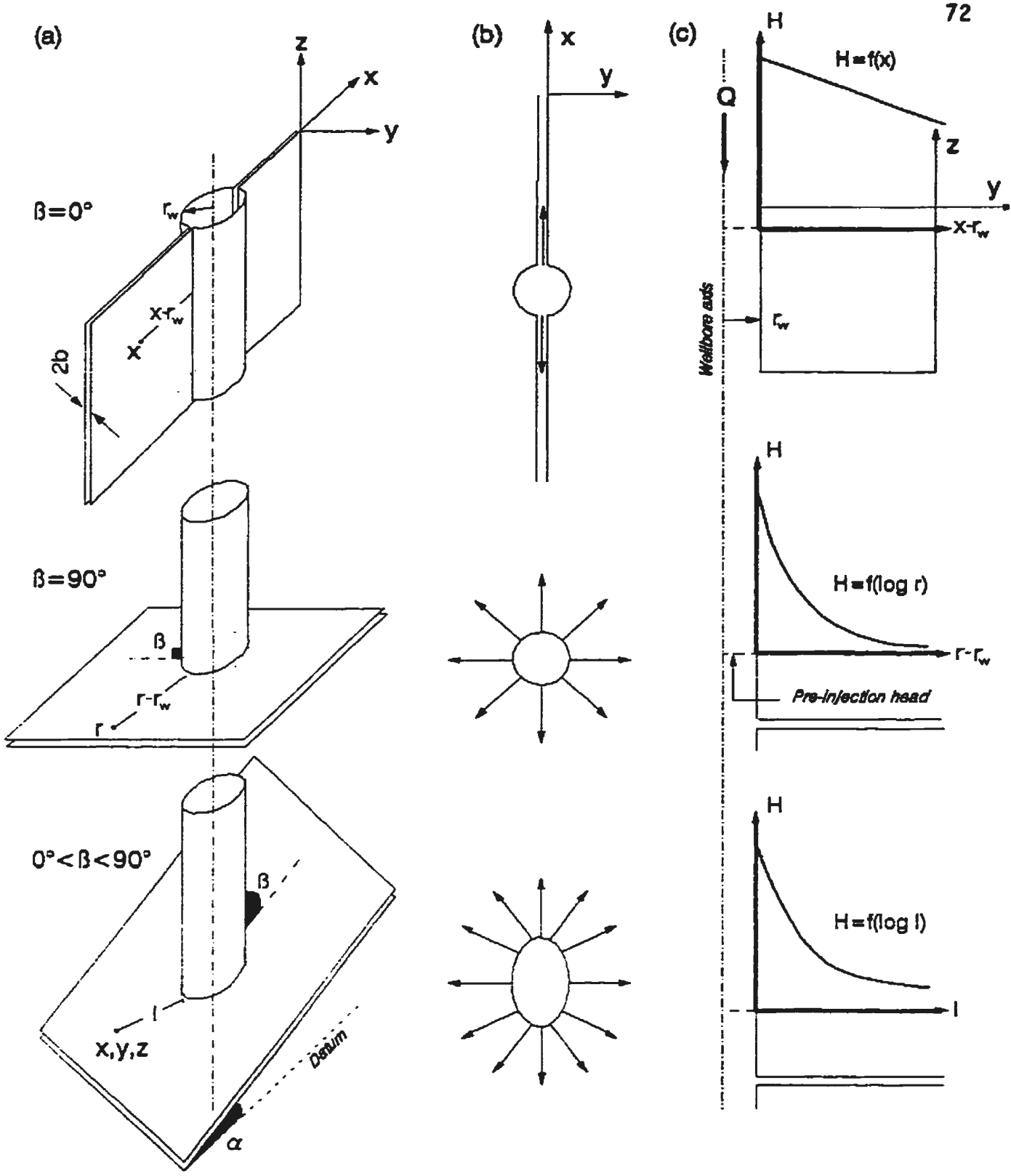

Figure 4.1.a) Parallel, orthogonal and acute fracture-wellbore intersections along a vertical wellbore; b) corresponding intersection outlines (linear, circular, elliptical) and streamline patterns (parallel, radial, general); and c) sketches of total head profiles upon injection under initially uniform head and laminar flow conditions.

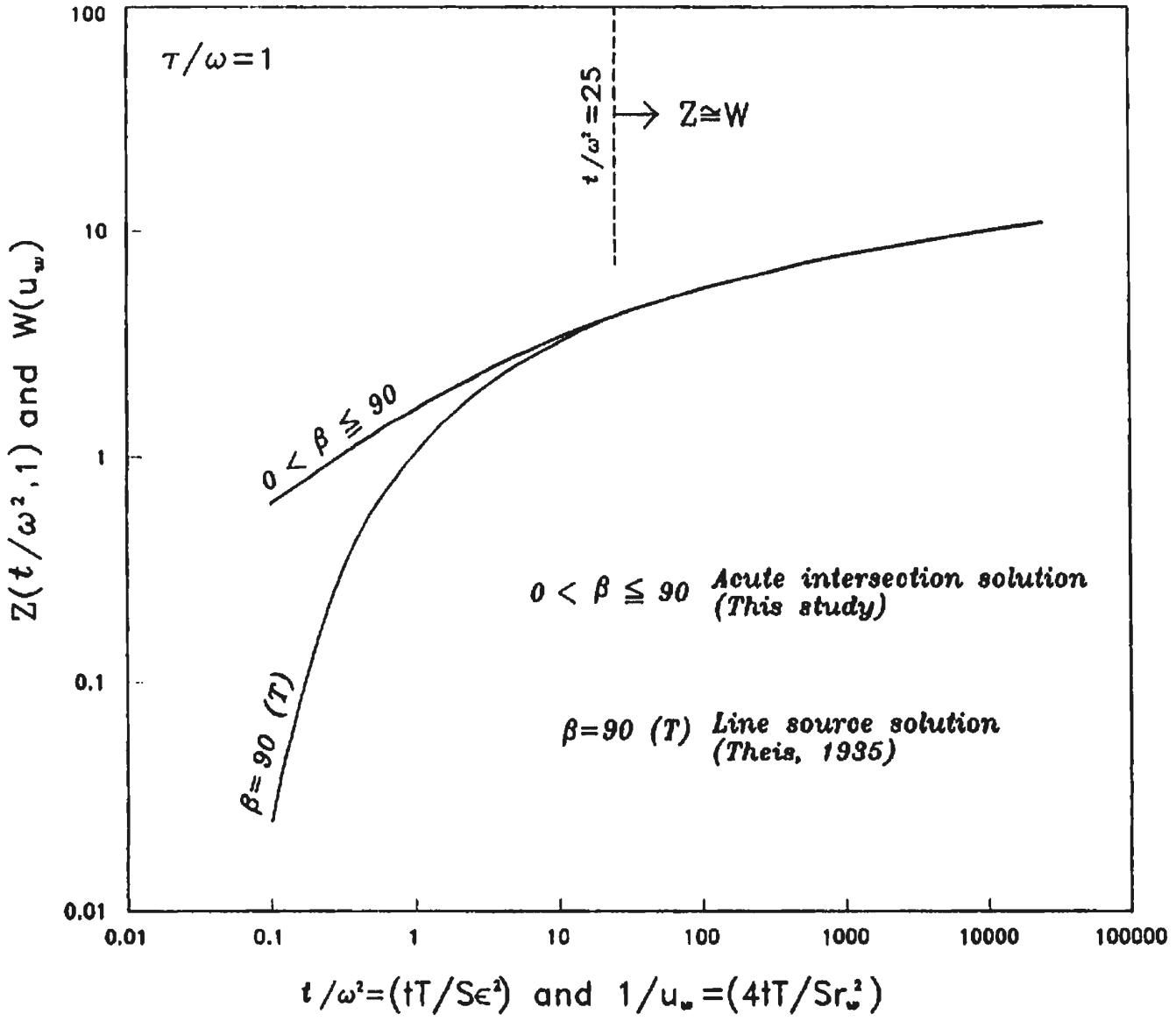

Figure 4.2. Acute intersection and the Theis type curves simulating the transient response at the active well.

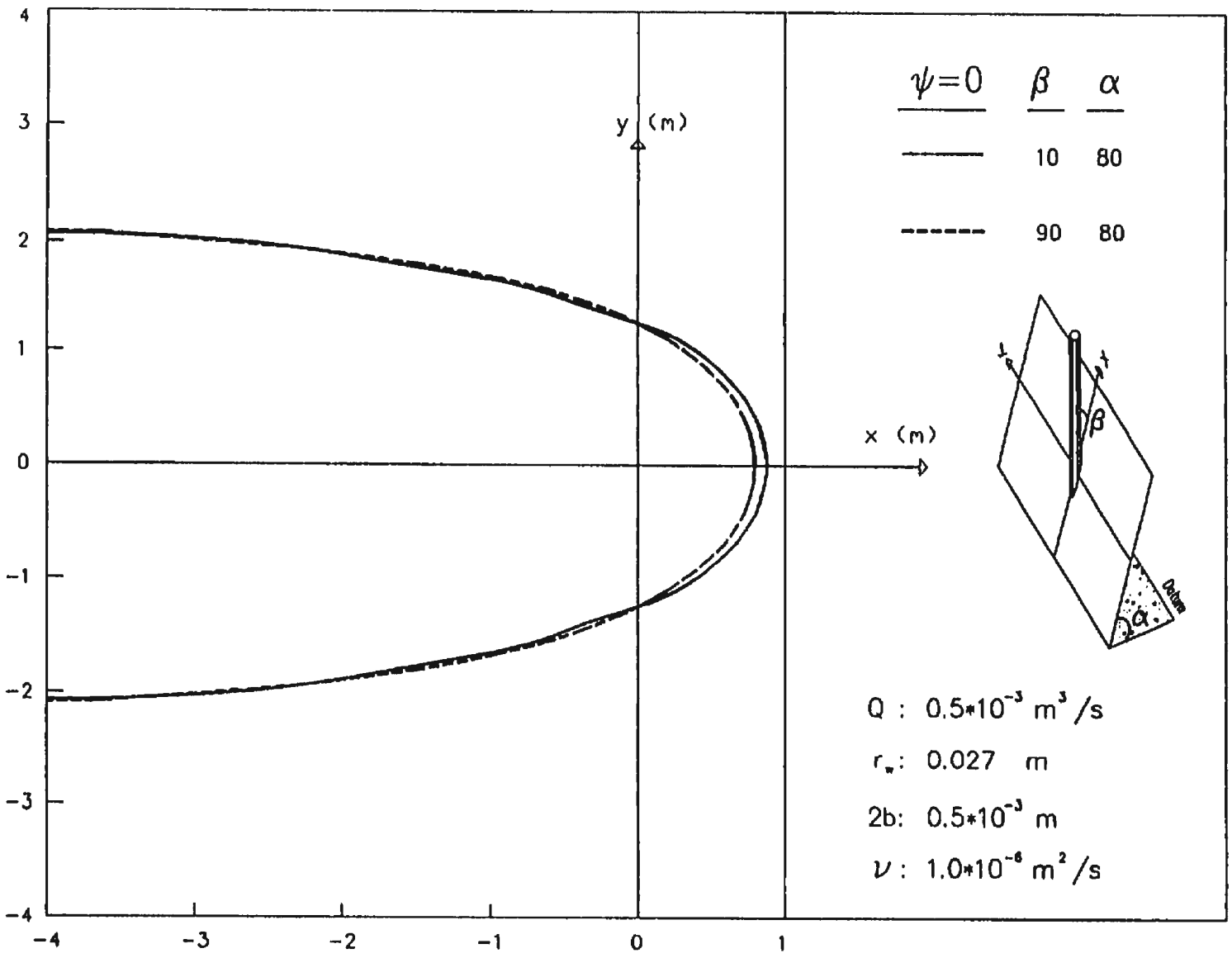

Figure 4.3. The zone of influence upon injection into acute and orthogonal systems with inclined fractures in unsaturated zones.

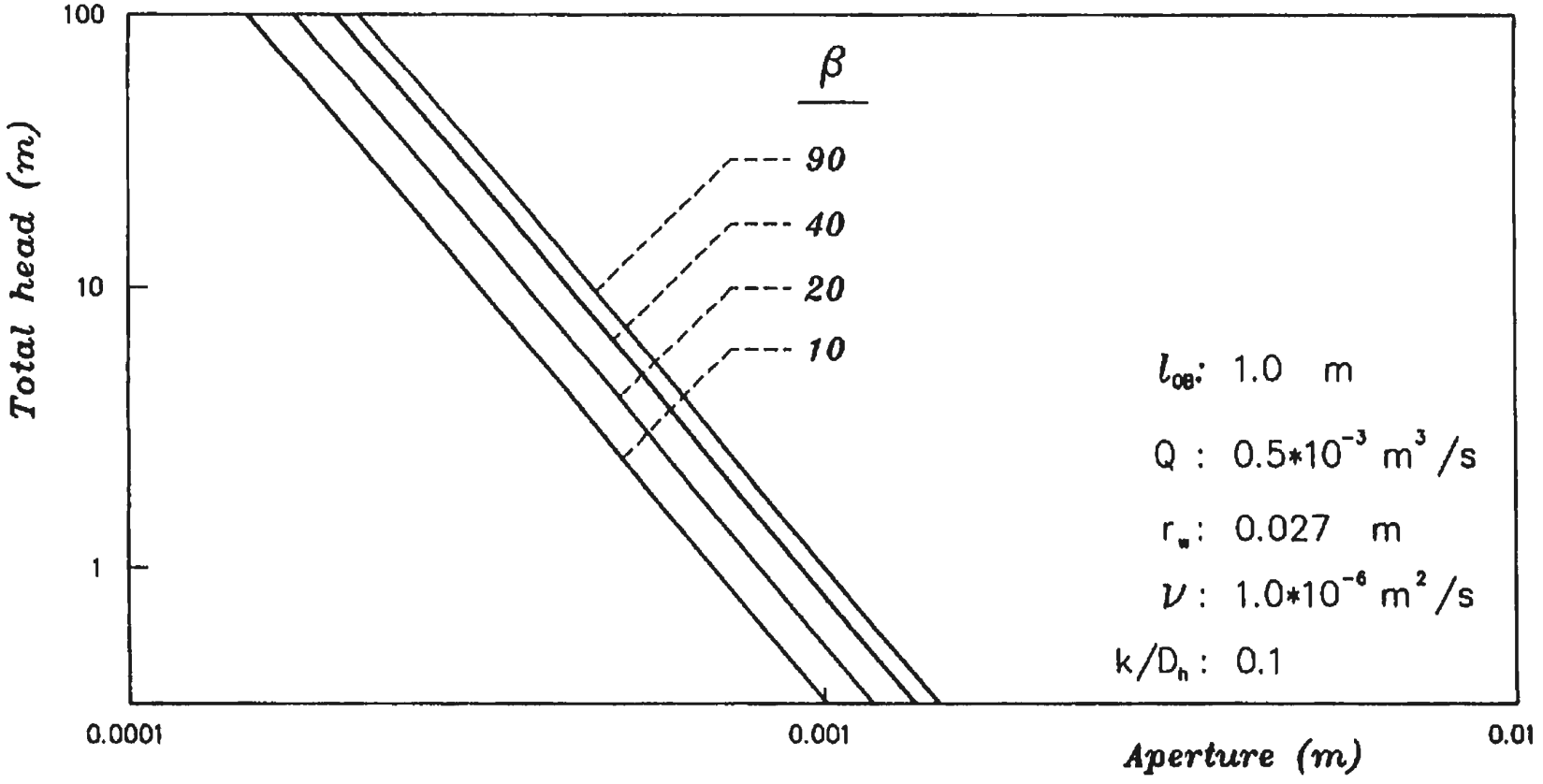

Figure 4.4. Comparison of aperture predictions for given total heads at the wellbore face: steady, two-regime flow through rough fractures.

5 LABORATORY STUDY OF FLOW THROUGH ACUTE FRACTURE-WELLBORE SYSTEMS

5.1 Introduction

The total head loss that occurs during single-well, constant-flux injection/pumping tests conducted through acute systems is formulated in Section 4.5 (Equation 4.29). As a semi-analytical equation, this:

a) provides a basis for a controlled laboratory design and systematic analysis intended to develop a better understanding of flow mechanics in acute systems; and

b) necessitates comprehensive testing to establish a fully functional expression.

Accordingly, the objectives of the laboratory study are defined:

a) to test the validity of the conceptual streamline pattern and study the flow interactions at the intersection under both pumping and injection conditions; and

b) to determine the empirical relationship between the intersection angle and exit/entry losses related to sudden changes in flow area and direction at the intersection.

Previous experimental work and the theoretical background are reviewed in Sections 5.2 and 5.3, respectively. Then the design features and fabrication procedure of the acute system models and the box frame are explained using detailed drawings (Section 5.4). Description of the experimental set-up also includes water circulation and instrumentation components. Finally, experimental design and test results are outlined (Section 5.5). Analysis and interpretation of experimental data are presented in Chapter 6.

5.2 Physical models of orthogonal systems

Experimental research on flow through fracture-wellbore systems is focused on identifying causes of head losses in order to improve predictive radial flow models and/or minimize the well losses, for a wide variety of industrial applications. The influence of turbulence and surface roughness in radial flow was first studied experimentally by Baker (1955). He devised a physical model made of concrete to specifically simulate fractures in limestone reservoirs. In his mathematical derivation of a two-regime radial flow expression, parallel plate conductivity was employed in the linear regime, and roughness was expressed as a coefficient in the turbulent regime. This coefficient and the critical Reynolds number were determined as empirical constants.

In an attempt to improve water pressure (lugeon) test analysis, Rissler (1978) tested the validity of theoretical and empirical one-dimensional flow expressions (reviewed in Chapter 2) in describing divergent, two-regime, radial flow. His physical model consisted of a rigid, open and rough (radially isotropic) fracture with apertures as small as 10^{-4} m. A satisfactory agreement between measured and calculated pressures was reported. Atkinson (1987) extended this to convergent radial flow in rough deformable fractures and addressed the problem of mine dewatering using vertical drainage wells.

An extensive experimental study was undertaken by Murphy (1979) mainly to explore the influence of acceleration on convergent laminar and turbulent flow predictions. Tests with laminar flow through a rigid, smooth, open fracture verified pressure profiles obtained from a numerical

solution of Navier-Stokes equation (Equation 2.1) in radial coordinates. The study by Murphy (1979) is specifically concerned with the flow mechanism near the outlet of a geothermal recovery well.

Experimental set-ups used in these earlier studies have been reviewed in detail to provide a viable, versatile and functional design in the current study.

5.3 Theoretical basis for model design

Model design is centred around the Reynolds number concept (Equation 2.19) which:

a) allows generalization of the results obtained from experiments with physical models designed for one set of variables, and from a limited number of test runs;

b) helps set an optimum range for flow rate and fluid temperature that will produce Reynolds numbers typical of field experiments; and

c) provides flexibility in determining model dimensions (effective flow length, well radius, aperture) and boundary pressures, that will produce the targeted Reynolds numbers.

Simulating the flow processes using the Reynolds number is reliable under hydraulically smooth conditions for which the friction factor is approximated as a function of only the Reynolds number for both (laminar and turbulent) flow regimes (Table 2.1). Otherwise, the friction factor, and therefore associated head losses, are partly or totally independent of the Reynolds number. The model testing should therefore be conducted under hydraulically smooth conditions (Table 2.1) unless the model fracture is

morphologically smooth (i.e. $k/D_h \approx 0$).

5.4 Description of experimental set-up

The overall experimental set-up (Figure 5.1) used in this work consists of a) three fracture-wellbore system models separately fastened to b) a steel box frame, c) scheme for water circulation, and d) instrumental components. It should be clear from the experimental objectives that the set-up is expected to simulate and control the conditions on which the mathematical model (Equation 4.29) is based. These can be stated as:

a) the fracture is rigid (i.e. insensitive to changes in fluid pressure), of infinite areal extent, isotropic and homogeneous in hydraulic conductivity;

b) hydraulic heads are temporally constant at the boundaries and initially uniform over the confined flow domain; and

c) flow is isothermal.

The fracture properties are intended to produce straight streamlines, and head distribution and flow temperatures are prescribed to ensure steady-state tests. The following section explains how the above parameters are satisfied and other design features are decided.

5.4.1 Design of acute system models

The intake/outlet flow area at fracture-wellbore intersections is the key factor causing differences in flow responses of parallel, orthogonal and acute fracture-wellbore systems (Figure 4.1.a). A plot of

normalized flow area vs. intersection angle (Figure 5.2) indicates that this difference should become significant for angles less than 40°. To capture these more pronounced effects of the intersection geometry, the design and fabrication of two models with 10° and 20° intersection angles were carried out for the laboratory study. An orthogonal model was used mainly to verify the performance of the experimental set-up as a whole. Figure 5.3 illustrates various design features of these models as discussed below.

The areal dimensions of the models were determined on the basis of: a) an optimum effective length along which flow would fully establish and significant pressure differentials would develop; and b) a wellbore diameter which enables high Reynolds numbers to be reached at low flow rates and boundary pressures. A flow length of 0.27 m (0.28 m for 10° model) and a wellbore diameter of 25 mm were found to be satisfactory. Similar dimensions have been used in earlier models (Rissler, 1978; Murphy, 1979), but in different combinations. The short flow length of the models, however, requires the outer boundary to conform to the propagation front of the straight streamline flow in order to satisfy the assumption of infinite fracture extent.

The acute angle between the wellbore axis and fracture plane, and the obliquity of the intake/outlet flow section produce directional variations in the streamline bending angle (i.e. in inertial loss) and in the geometry of the section (i.e. in flow resistance), respectively. Coupled with contraction/enlargement of the section during flow exchange between a wellbore and a fracture, directional dependence of injection

pressure profiles are likely very influential in preventing a straight streamline flow pattern. This demanded a detailed study of pressure profiles along typical arrays (Figure 5.3.a), coinciding with expected streamlines, at test Reynolds numbers, i.e. in addition to low rate tracer injection tests which confirmed streamline flow visually.

Pressure holes were located so as to capture logarithmic variation in pressure. A few holes in each model were located on symmetrical streamlines at the same flow lengths in order to check aperture uniformity. Wellbore pressures were measured at the well bottom parallel to the wellbore axis and at two upstream positions (for 10° and 20° models) to monitor flow structure and wellbore losses in inclined holes.

Such pressure holes would likely introduce a slight disturbance in flow: an array of pressure holes along a streamline will record an increased disturbance downstream. In this study any such effect when recorded fell within the uncertainty range of pressure measurements, since readings on two radial arrays (Figure 5.3.a-90°) were almost identical with those holes at the same radial distance.

Transparent acrylic (Plexiglass) sheeting was chosen as the model material on the basis of workability, flow visibility and cost. It was decided to use a sheet thickness of 25 mm to help maintain flexural rigidity and also provide adequate depth to support the pressure holes and adapters (Figure 5.3.c-Inset). This also allowed for two central 0.22 m diameter disks to be mounted in the same main plates in the design of the 20° and 90° models (Figure 5.3.c). This resulted in a more tedious model fabrication but enabled machine drilling of the 20° inclined wellbore and

reduced material cost and labour. The long span of the inclined drill section of the 10° system required the fabrication of a separate model (Figure 5.3.b).

The intake/outlet section becomes off-set for any aperture, $2b$, other than that for which the well is drilled through the fracture. Quantitative analysis of test results from each model is therefore limited to that fabrication aperture, $2b$. An aperture of 1 mm was decided upon as a compromise between possible flow rates, pressure heads and desired Reynolds numbers. The chosen aperture value is also within a range encountered in nature (Bianchi and Snow, 1968; Chernyshev and Dearman, 1991).

If any morphological roughness is to be designed into the model fracture, it should be isotropic and homogeneous, but these are technically difficult features to provide. A relative roughness of 0.01, for example, would limit tests to $Re<5000$ (Figure 2.2) if theoretical validity is to be maintained. The fracture surfaces were therefore left smooth ($k/D_h \approx 0$), in the models used here.

5.4.2 Steel box frame

Fluid pressure distribution and flow rate are extremely sensitive to aperture changes near the wellbore where pressure differentials are largest. Adjusting and maintaining aperture uniformity is therefore the most vital requirement for the reliability of the test results. A steel box frame (Figure 5.4.a) was designed to act as an internally rigid system under calculated test pressures. The resultant assembly, when the

plexiglass models were installed in the frame, simulated a fracture in a rigid rock mass cut through by a wellbore.

The box frame contains two identical halves each consisting of four tie-beams with high flexural rigidity welded in parallel to two H-beams, thereby providing fixed ends. Each fracture model plate was fastened to the frame with twelve steel shoes (Figure 5.4.a-Inset). These were distributed evenly and symmetrically and not to block pressure holes in any of the three models. The shoes allowed for alignment of boundaries and uniform adjustment of the aperture. The frame design permitted the maximum closure or opening of the fracture aperture to be calculated from measured linear strains. At maximum differential test pressures the frame allowed an aperture change of only 0.01 mm.

5.4.3 Fabrication procedure

The trial and error process of fabrication was eliminated by computer aided design of the models and box frame. Most of the fabrication was done by the Engineering Technical Services facilities of Memorial University. Similar procedures were followed during fabrication of all physical models. To extend the wellbore length and to accommodate the push-in PVC connection pipe, thick plexiglass pieces were first fused onto the external surfaces of the plates. To avoid off-centring of the drill hole and to obtain the desired aperture, the model plates were clamped together with the aperture laminae placed in between.

Whereas the 20° and 90° holes were machine produced, the 10° hole was manually drilled through a guide hole. In this model, a 400 mm

inclined section was completed at the prescribed 10° angle by successively enlarging a smaller guide hole. Some boundary irregularities at the intersection resulting from drill vibration were smoothed using plexiglass flakes dissolved in methyl chloride. No such problem was encountered during fabrication of other models.

The large plates were cut to the theoretical outer boundary geometry by a computerized lathe at the NRC Institute of Marine Dynamics. The pressure holes were drilled 1.5 mm in diameter with square edges at calculated coordinates for accurate measurements (Goldstein, 1983). The holes were widened and threaded halfway for the pressure adapters (Figure 5.3.c-Inset). Finally the threaded holes for bolting the frame shoes were drilled on external surfaces of the plates.

5.4.4 Water circulation system

The components of the water circulation system were designed such that steady-state, pumping and injection tests could be conducted with minimal change in the set-up (Figure 5.1). A polyethylene tank of 0.90 m diameter was used to accommodate the box frame and installed model. This tank has side-wall access for inclined wellbore sections, drainage and a thermocouple probe. The box frame, and hence the model fracture, was laid horizontally in the tank to provide mechanical stability, and minimize space and data analysis complications. The results, however, are applicable to systems of any orientation with uniform and constant boundary hydraulic heads.

Reduction of injection pressure below vapour pressure at test

temperatures seems inevitable unless downstream pressures are high enough to compensate for the largest pressure drop at the entry vena-contracta. Wellbore pressure under vacuum pumping is also below the vaporization limit. This problem might be avoided by using a model tank that can be sealed and pressurized. However the results of earlier experiments with similar injection (Rissler, 1978) and pumping (Murphy, 1979) set-ups suggested that such an expensive option was unjustified. In both injection and pumping tests the vapour pressure limit was exceeded but no bubble formation was observed even at the highest flow rates. Large amounts of bubble formation would cause expansion and higher flow rate readings in the pumping set-up, and would violate the applicability of the Bernoulli equation based on the assumption of incompressibility (Equation 4.2).

In steady injection experiments, a net maximum head of 2.2 m was reached by elevating the water tank. The required Reynolds numbers are easily produced by this natural hydraulic head. Water supplied to the tank was de-aired through air vents and stabilized by the constant head apparatus. A valve located about 20 pipe diameters downstream from the flow sensor was used to regulate the flow rate. Water level in the model tank was kept below the level of the fracture to produce constant and uniform atmospheric pressure at the outer boundary.

For steady pumping experiments the model tank was allowed to overflow to ensure constant water table level. A centrifugal (1/6 hp) pump was sufficient to withdraw water at the same flow rates as used in the injection tests. In both injection and pumping set-ups the upstream length of the pipe from the flow sensor was about 40 pipe diameters to allow flow

to be fully established. The wellbore itself was kept straight and consistent in section for more than 20 diameters to eliminate flow disturbances.

5.4.5 Instrumentation

Details of instrumentation and wiring are illustrated on Figure 5.1 in an overall experimental setting. The data acquisition unit consisted of a plug-in card interfacing with a personal computer through a customized software that acquired and stored data in the required format. All measuring devices were connected to the card by an external terminal panel. Fluid temperatures were measured by a subminiature thermocouple probe inserted into the water in the model tank through its side wall. The open circulation of cold tap water provided very stable temperatures with less than $\pm$ 0.25 $^{\circ}$C variation during a test run.

Five solid state piezoresistive pressure transducers were used for both gauge and vacuum pressure measurements at twenty locations. Each transducer was connected to four manometer tubes with a 5-way valve. Injection/withdrawal flow rates were measured by a paddlewheel flow sensor connected to a signal conditioner for computer interfacing. The pipe assembly housing the flow sensor was made portable for easy rearrangement between the injection and pump set-ups and for fast mounting alignment.

A full bridge circuit strain gauge measurement technique was used to monitor any deformation of the fracture that may have taken place. Two active gauges were fixed on central tie-beams to measure linear strain due to their flexure and two other "dummy" gauges on an H-beam for temperature

compensation. All were covered with the protective coatings for underwater operation. Strain gauge responses were calibrated by simultaneous direct LVDT measurements of deflection due to step loading at the mid-span.

5.5 Experimental design and test results

The main parts of the experimental work were injection and pumping tests of the model fractures at the fabrication aperture. In order to detect Reynolds number dependent variations, each test was conducted at several flow rates. A series of test runs were performed at arbitrarily chosen, and occasionally repeated, flow rates to prevent the development of any systematic error in the readings. Water temperatures during each series of runs was kept constant to allow direct correlations of pressure measurements.

Nonlinearities or unexpected changes in observations during step-drawdown and other multi-rate tests often result from a combined effect of hydraulic opening/closure and turbulence. The influence of opening/closure of the aperture can be evaluated by adjusting the aperture manually and comparing the results with those obtained for the fabrication aperture. Since the wellbore axis becomes offset in acute systems with any change in aperture, it is also important to determine sensitivity of flow mainly to aperture change and somewhat to geometric structure at the intersection. Therefore this has been made an integral part of the systematic testing programme.

Each model was mechanically adjusted to the fabrication aperture and the frame-model assembly then lowered into the model tank. Both injection

and pumping test runs were completed under identical settings. PARKER PRESTOLOK-type connecters (Figure 5.3.c-Inset) with polyethylene manometer tubing were ideal for fast mounting of the models, de-airing of the tubes and accessing background pressures. The model, while in the model tank (Figure 5.1), was then re-adjusted to the specific aperture value to be tested and the testing procedure was repeated.

A total of twelve test series, each with an average of six runs were completed. The variables recorded during each run and the parameters characterizing each series are presented on Table 5.1 in testing sequence and in a format reduced to consistent metric units. Analysis of the data is the subject of the following chapter.

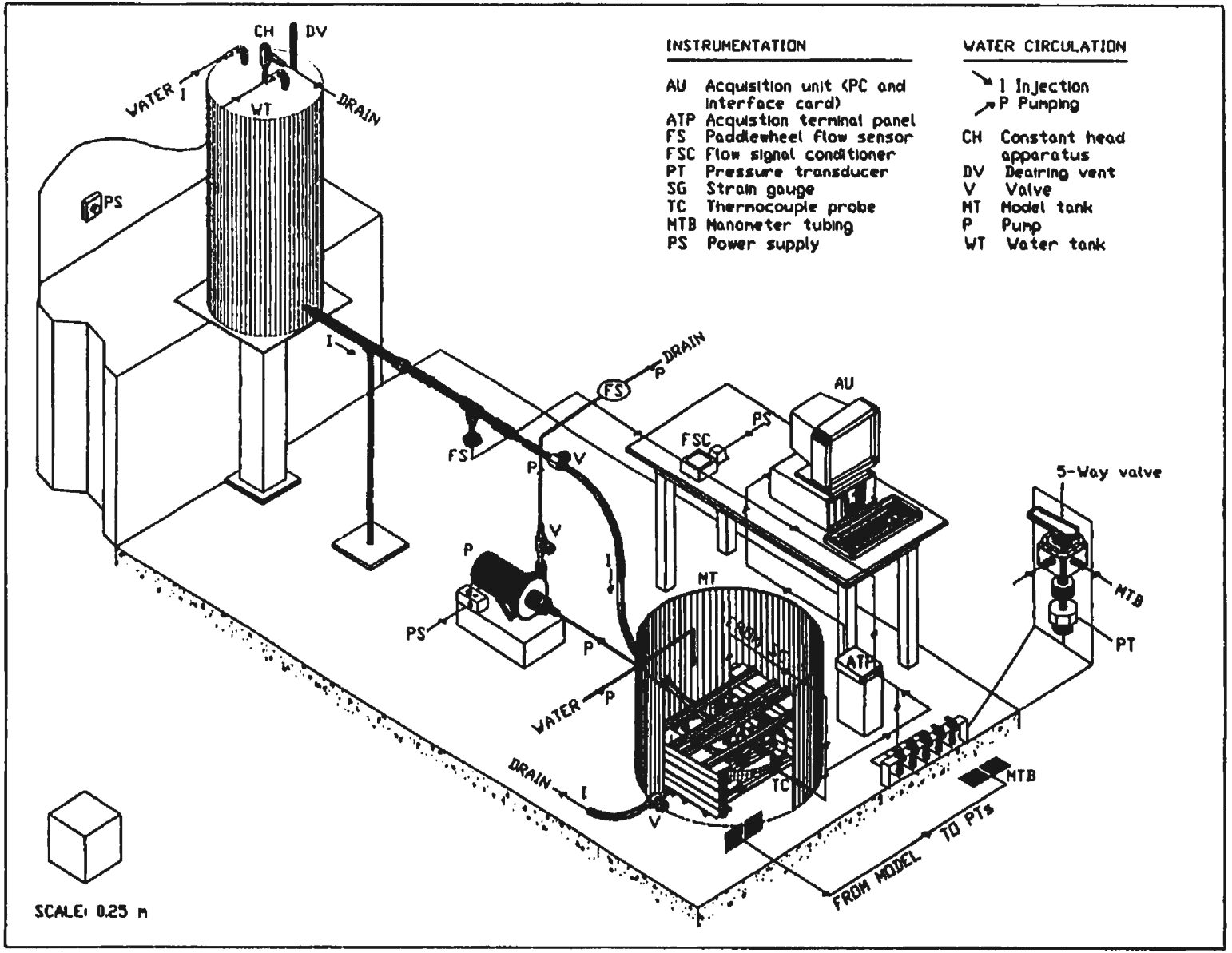

Figure 5.1. A generalized view of the experimental set-up with the frame-20° model assembly placed in the model tank. Water circulation in pumping tests is shown schematically.

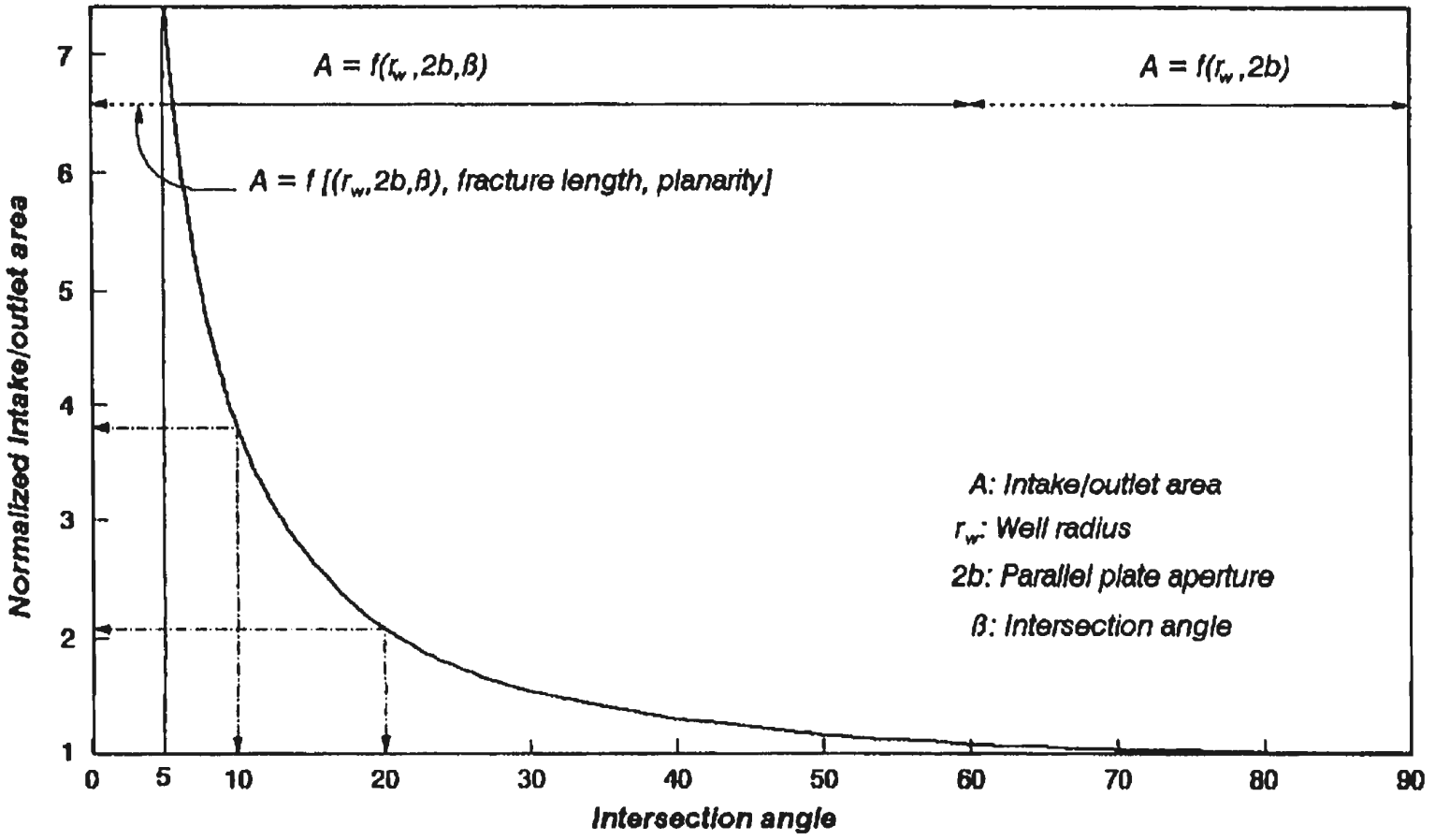

Figure 5.2. Rate of change of intake/outlet area as a function of the intersection angle. Figures are normalized with respect to the area of orthogonal intersections with equal diameter wellbores.

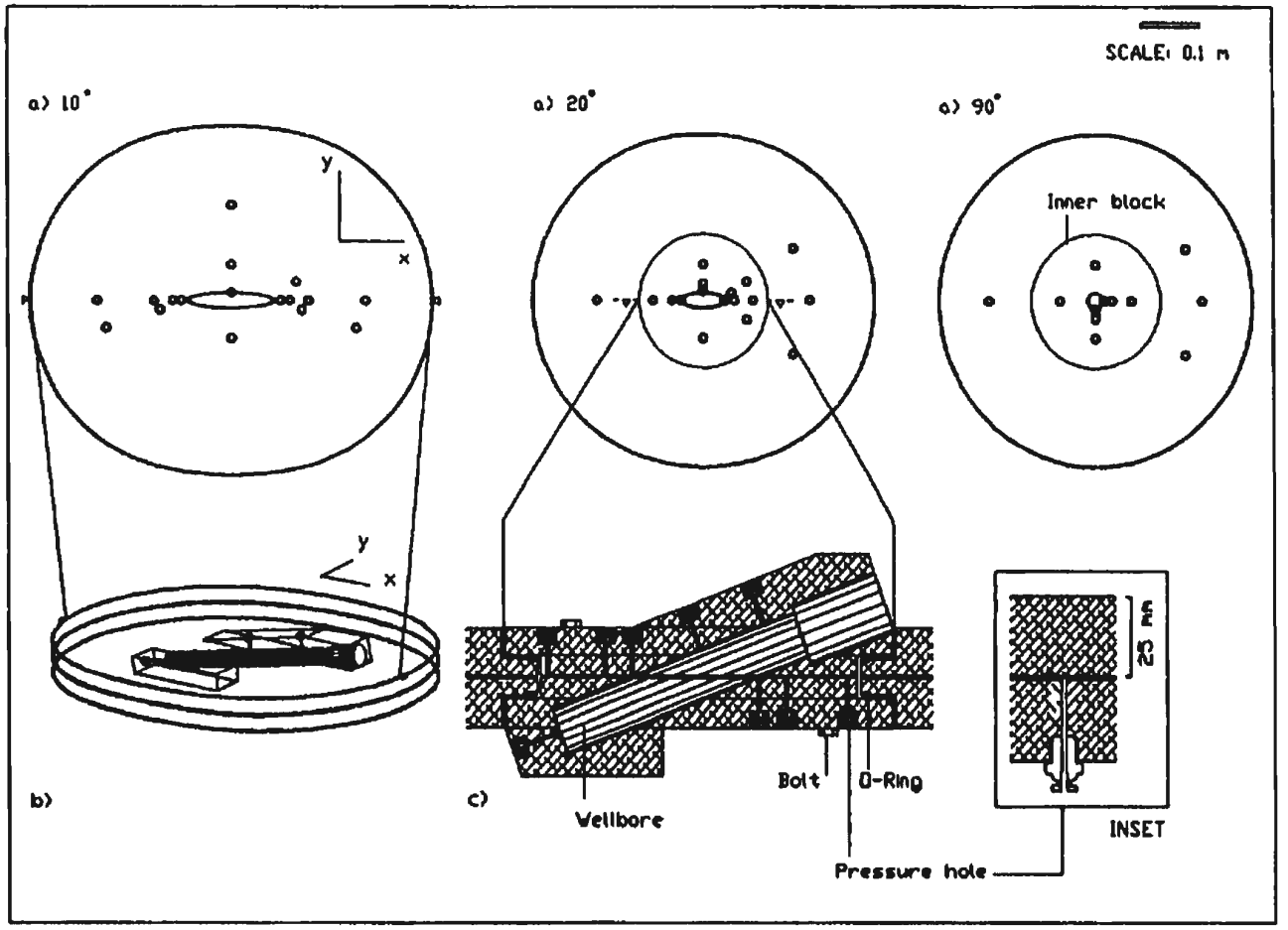

Figure 5.3.a) Pressure hole locations with respect to the fracture mid-planes; b) 3-D view of the 10° drill hole (only wellbore pressure holes are shown) and c) magnified cross-sections showing details of 20° model (x 3.0) and of pressure hole construction with tube adopter installed (x 5.0) (INSET). Note the enlargement of the wellbore sections to accommodate the PVC pipe extension.

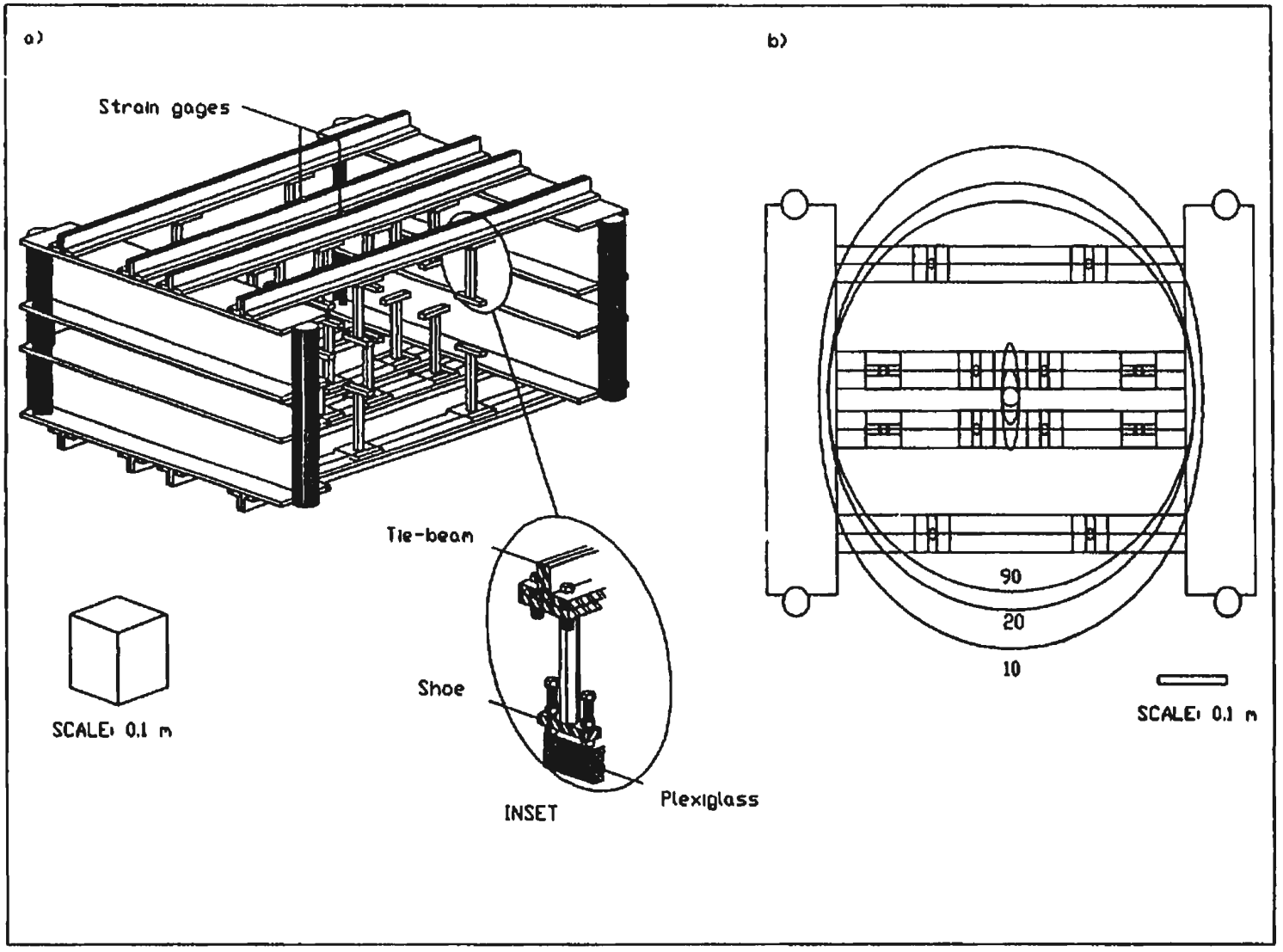

Figure 5.4.a) The steel box frame and details of frame-model connection (INSET); and b) plan view of the lower half frame with the model boundaries superimposed.

Table 5.1. Outline of experimental data from steady flow tests with common set-up parameters for each run series.

RUN NO.→	1	2	3	4	5	6	7	8	SET-UP
Q[1]:	0.423	0.281	0.215	0.170	0.515	0.758	0.639		ß : 20°
T:	11.47	11.47	11.54	11.57	11.54	11.35	11.35		2b: 1.1
h_w[2]:	0.417	0.229	0.154	0.111	0.564	1.075	0.803		h_{OB}: 0.00
Re_{IB}:	4056	2692	2067	1634	4945	7246	6105		
Re_{OB}:	382	254	195	154	466	683	576		INJECTION
Q:	0.810	0.757	0.681	0.182	0.288	0.443	0.202		ß : 20°
T:	14.58	14.35	14.59	13.57	12.84	13.68	14.10		2b: 1.1
h_w:	-0.931	-0.764	-0.541	0.397	0.269	0.012	0.377		h_{OB}: 0.52
Re_{IB}:	8395	7799	7062	1838	2858	4488	2070		
Re_{OB}:	791	735	666	173	269	423	195		PUMPING
Q:	0.363	0.229							ß : 20°
T:	11.91	11.78							2b: 0.6
h_w:	-1.226	-0.395							h_{OB}: 0.52
Re_{IB}:	3512	2213							
Re_{OB}:	331	209							PUMPING
Q:	0.610	0.777	0.408	0.287					ß : 20°
T:	11.33	11.29	11.32	11.34					2b: 1.6
h_w:	0.315	0.478	0.161	0.091					h_{OB}: 0.00
Re_{IB}:	5831	7411	3899	2739					
Re_{OB}:	550	699	368	258					INJECTION
Q:	0.175	0.279	0.343	0.433	0.473	0.524			ß : 90°
T:	16.21	15.69	15.65	15.80	15.59	15.61			2b: 1.1
h_w:	0.263	0.560	0.782	1.167	1.390	1.694			h_{OB}: 0.00
Re_{IB}:	3947	6207	7620	9643	10473	11614			
Re_{OB}:	188	296	363	459	499	553			INJECTION
Q:	0.292	0.183	0.395	0.454	0.481	0.391			ß : 90°
T:	15.67	15.63	15.61	15.60	15.59	15.57			2b: 1.1
h_w:	-0.322	0.151	-0.947	-1.382	-1.599	-0.918			h_{OB}: 0.52
Re_{IB}:	6478	4057	8753	10056	10649	8646			
Re_{OB}:	308	193	417	479	507	412			PUMPING
Q:	0.247	0.304	0.355	0.151	0.277	0.176			ß : 90°
T:	11.22	11.21	11.17	11.16	11.15	11.14			2b: 0.6
h_w:	-2.037	-3.077	-4.170	-0.650	-2.568	-0.966			h_{OB}: 0.52
Re_{IB}:	4907	6027	7038	2990	5491	3489			
Re_{OB}:	234	287	335	142	261	166			PUMPING

Table 5.1. cont.'d

RUN NO.→	1	2	3	4	5	6	7	8	SET-UP
Q:	0.383	0.498	0.600	0.661	0.346				β : 90°
T:	10.91	11.06	11.01	10.94	10.95				2b: 1.6
h_w:	0.439	0.701	1.004	1.192	0.369				h_{OB}: 0.00
Re_{IB}:	7548	9832	11842	13017	6817				
Re_{OB}:	359	468	564	620	325				INJECTION
Q:	0.371	0.583	0.676	0.497	0.175	0.220	0.298	0.392	β : 10°
T:	14.35	14.37	14.36	14.35	14.37	14.38	14.42	14.43	2b: 1.1
h_w:	0.183	0.327	0.401	0.262	0.072	0.091	0.134	0.196	h_{OB}: 0.00
Re_{IB}:	2086	3278	3804	2792	984	1235	1677	2211	
Re_{OB}:	321	504	585	429	151	190	258	340	INJECTION
Q:	0.193	0.312	0.366	0.537	0.601	0.664	0.375	0.451	β : 10°
T:	14.54	14.52	14.49	14.46	14.43	14.39	14.39	14.39	2b: 1.1
h_w:	0.409	0.342	0.306	0.171	0.111	0.049	0.300	0.242	h_{OB}: 0.486
Re_{IB}:	1089	1762	2068	3027	3385	3739	2108	2540	
Re_{OB}:	167	271	318	465	520	575	324	390	PUMPING
Q:	0.182	0.283	0.323						β : 10°
T:	15.11	15.02	14.92						2b: 0.6
h_w:	0.090	-0.190	-0.312						h_{OB}: 0.486
Re_{IB}:	1042	1618	1845						
Re_{OB}:	160	249	284						PUMPING
Q:	0.378	0.285	0.204	0.546	0.731	0.587			β : 10°
T:	15.29	15.12	15.13	15.14	15.10	15.06			2b: 1.6
h_w:	0.075	0.043	0.029	0.121	0.179	0.132			h_{OB}: 0.00
Re_{IB}:	2178	1637	1171	3133	4193	3362			
Re_{OB}:	335	252	180	481	644	517			INJECTION

[1]) Units: Q (lt/s) or ($10^{-3}\cdot m^3/s$); T (°C); h (m); 2b (mm) or ($10^{-3}\cdot m$)
[2]) Subscripts: w (wellbore); IB (inner boundary); OB (outer boundary)

6 ANALYSIS AND DISCUSSION OF TEST RESULTS

6.1 Introduction

The second phase of the laboratory study involves critical examination of the experimental data outlined in Table 5.1 and fully listed in Appendix B. In this phase the objectives are two-fold:

a) to assess the performance of the laboratory set-up; and

b) to fulfil the general objectives of the laboratory study, i.e. to determine the agreement between measured head profiles and those predicted by Equation 4.29, and the exit/entry loss coefficients in this equation as a function of the intersection angle.

The chapter begins with a background section (Section 6.2) reviewing available information relevant to analysis procedure and theory. The results are presented and interpreted in separate sections for pumping (Section 6.3) and injection (Section 6.4) tests. The results of the test series are illustrated graphically in each section. Verification of the laboratory set-up performance and the data quality is based on the pumping test results from the 90° model (Section 6.3). The chapter concludes with a brief summary of the significance of the laboratory study (Section 6.5).

6.2 Background

Knowledge of flow processes and resultant head losses associated with sudden changes in flow area and direction is essential to the interpretation of the data. Flow visualization experiments using contracting/enlarging sections (JSME, 1988) provide direct evidence for the scale and geometric variables of related processes. Numerous other

studies as compiled by, for example, Fried and Idelchik (1989) examine the resultant head losses in conduits of various shapes. These one-dimensional flow studies provide a basis for interpreting the data from accelerating/decelerating flows. The following is aimed to concisely introduce the relevant aspects of the present knowledge.

Fluid flowing through a sharp-edged entrance of an abruptly contracting conduit separates from the walls and forms a compressed jet (Figure 6.1.a). The acceleration of fluid mass, resulting from resistance to the sharp turn in flow direction, ends at the vena-contracta where effective flow area is minimum. After this point, the jet quickly expands to fill the conduit. Strong deceleration results in an adverse pressure gradient (i.e. increasing in the flow direction) which favours formation of unsteady eddies causing dissipation of mechanical flow energy (Vennard and Street, 1982). The entry process is completed as the eddies decay downstream and the velocity profile is fully established. The distance along which the whole process takes place is called the entry length (Figure 6.1.a).

The entry process in the case of acute intersections (Figure 6.1.b) is notably different than observed in orthogonal entry sections. The separation zone is asymmetric, irregularly enlarged and very unsteady, and the entry length is longer. These visual differences due to different intersection angles are also manifested in the magnitudes of head losses, usually modelled by a dimensionless loss coefficient (Fried and Idelchik, 1989)

$$\xi_e = \frac{\Delta P / \rho g}{\overline{v}^2 / 2g} \qquad (6.1)$$

where ΔP: static pressure change between end points of the entry length, and

$\bar{v}$: average velocity of fully established flow.

This expression is equally valid for the calculation of exit as well as entry loss coefficients. Variation of this coefficient with the intersection angle is summarized in Figure 6.2. for Reynolds numbers (Equation 2.19) greater than 10^4.

Ward-Smith (1980) reviewing the numerical solutions of the Navier-Stokes equation (Equation 2.1) of co-axial flow into infinite parallel plates recommended an entry loss coefficient of $\xi_n=0.662$, and an entry length, L, given by

$$L=0.022\,Re\,(2b) \tag{6.2}$$

for $Re>10^3$. Based on similar empirical expressions, Rissler (1978) derived loss coefficients of $\xi_n=0.711$ and $\xi_n=0.415$ for laminar and turbulent co-axial flows, respectively, into parallel plate contractions.

Flow adjustment to sudden co-axial enlargements involves similar processes: flow separation, eddy formation, expansion of jet and re-attachment (Figure 6.3.a). The resultant head losses are again related to incomplete pressure recovery. The exit loss coefficient, ξ_x, for uniform velocity profiles is usually given by the Borda-Carnot relation (Ward-Smith, 1980)

$$\xi_x=\left(1-\frac{A_1}{A_2}\right)^2 \tag{6.3}$$

where A_1 and A_2 are flow areas at the up- and down-stream faces of the enlargement, respectively. In accordance with this relation, Fried and Idelchik (1989) showed from the experimental literature that the exit loss coefficient is not sensitive to the intersection angle when the velocity of the passing stream, v_p, in the enlarged section is much less than the exit velocity, v_x (Figure 6.3.b). In fracture-wellbore systems, this condition likely often holds if one identifies A_1 and A_2 with the exit and wellbore areas, and v_x and v_p with the exit and wellbore velocities. For experimental analysis, however, the magnitude of exit losses will be investigated using Equation 6.1.

Accounting for the effects of variable flow section

The Poiseuille law (Equation 2.10) governs one-dimensional laminar flow through uniform parallel-plate conduits where the velocity profile is invariably parabolic. The kinetic energy correction factor (KECF) (Equation 4.2) for such flows has a constant value of 1.54 (Vennard and Street, 1982). In convergent/divergent flows, this value is relevant at some distance from the wellbore depending on the flow rate. Closer to the wellbore where the velocity becomes less parabolic (and more uniform), the KECF approaches unity. The knowledge of the KECF as a function of the distance from the wellbore face is therefore necessary in order to differentiate between the contributions of the frictional head loss and the variable velocity head to the observed hydraulic head changes (Equation 4.4).

Murphy (1979) compared a numerical solution of the Navier-Stokes equation (Equation 2.1) with its approximate analytical solutions which assume constant KECFs of 1.54 and 1.2 at all radii. Since the velocity head at large radii is negligible, the latter solution provides a better overall fit to the numerical predictions. Therefore the constant KECF of 1.2, which was also adopted by Baker (1955), Louis and Maini (1970) and Rissler (1978), will be used in the analyses of pressure data in the linear domain.

6.3 Pumping tests

Inspection of the experimental data (Appendix B) revealed that: a) exit losses are not Reynolds number dependent in the test range; and b) no systematic changes in percent discrepancy between measured and predicted pressure heads exists between the runs of any pumping test series. General characteristics of the data can therefore be exemplified by any one run from each series. The runs with most equal flow rates were selected for the graphical presentation of the data from corresponding series of each model (Figures 6.4 to 6.9). This selection allows the most direct comparison of the measured pressure profiles as a function of the intersection angle.

The graphs (Figures 6.4 to 6.9) consist of the direct pressure head measurements along all the pressure hole arrays (Figure 5.3.a) and the predicted pressure heads calculated from Equation 4.29 (with the total head loss term expressed by Equation 4.4). Equivalent radius (Equation A.15) adapted as abscissa is a useful concept which: a) allows a scaled

comparison between sizes of exit areas, and b) offers an alternative visualization of an equivalent radial pressure distribution as a function of wellbore radius.

Despite a fastidious fabrication and experimentation procedure, the development of uncertainty in the results is inevitable and can be attributed to interacting uncertainties associated with all the measured variables, dimensions and geometries (Kline and McClintock, 1953). The only measure of the extent of the resultant uncertainty can be obtained by comparing the 90° model data with the radial flow predictions established by earlier experiments (Rissler, 1978; Murphy, 1979). Measuring essentially the same pressure profiles along all pressure hole arrays of the 90° model and excellent agreement of these with the predicted profiles suggest that the laboratory set-up operated as designed. For a given run, discrepancy (between measured and predicted pressures) at any point tends to be proportional to the pressure gradient, clearly because of great sensitivity of pressure to aperture variations. Percent discrepancy over the full scale of the pressure difference is generally less than five percent for all runs.

Laminar flow predictions were proven valid despite high Reynolds number range attained particularly in 90° model tests (Table 5.1). As a result of convergent radial air flow experiments in a similar smooth model, Murphy (1979) also noted that measured profiles are consistent with the laminar predictions for Reynolds numbers ranging from 210 to 20700. Convergent, radial water flow through an open, rough fracture, however, reveals a considerably limited but still an extended range for laminar

flows up to Reynolds numbers of 4000 to 8000 (Baker, 1955). Murphy (1979) suggested that agreement at low Reynolds numbers establishes the validity of the experimental procedures and measurements. The agreement above the critical Reynolds number of 2300 (Figure 2.2), marking onset of the turbulence in one-dimensional flow, is attributed to the stabilizing role of positive pressure gradients on boundary layers in accelerated flow (Schlichting, 1979). Accordingly, during pumping tests, the laminar-turbulent transition in fractures characterized by $k/D_h \leq 0.033$ may be expected to occur at Reynolds numbers higher than 2300.

Variation in pumping pressure head as a function of the intersection angle is well predicted by the mathematical model. Minor entry losses from the model tank into the fracture are satisfactorily estimated using Equation 6.1 with $\xi_n = 0.662$. As can be found from Equation 6.2, flow is likely fully established before reaching the first pressure hole from the outer boundary. The percent discrepancy or the quality of predictions for the pumping test runs with the closure aperture (Figures 6.7 to 6.9) are not affected from the offset of the wellbore axis in the acute models.

The review in the preceding section indicates that exit losses are independent of the intersection angle in one-dimensional flow. The exit loss coefficient is substantiated to be approximately unity for accelerating flow. The fact that the wellbore axis is oblique to the fracture plane in the acute system models did not seem to affect the magnitude of the exit losses. This is probably because, although streamlines approaching the wellbore from different directions undergo bending in varying degrees, the overall loss is balanced out.

The pressures measured in the downstream section of the wellbore were slightly below that measured at the well bottom. Since the span of the monitored section was limited to two and four wellbore diameters for the 20° and 10° models, respectively, it was not possible to differentiate between entry effects and established flow losses in the wellbore. However, the data suggest no noticeable variation in wellbore losses due to changes in the intersection angle.

6.4 Injection tests

The injection pressure heads from the selected runs of each model are plotted on successive graphs (Figures 6.10 to 6.15) using different scales to emphasize variations along different pressure hole arrays. Similar discharge rates of the runs representing the group of test series for each aperture value facilitate direct comparison of the results as a function of the intersection angle. The distinct pressure patterns recognized for each of these runs are common characteristics of their series. Uncertainty in pressure head measurements stated in the previous section also applies to the injection tests.

The pressure head profiles predicted by Equation 4.29 and the entry loss coefficients are also illustrated on the graphs. The coefficients were calculated in terms of the entry velocity although associated losses vary continuously over the entry length. This calculation procedure causes the injection head to excessively drop at the entrance to the fracture to a level such that the total head at the outer boundary approximates zero. It was assumed here that the entry losses reach maximum within the model

boundary.

Pressure measurements near the wellbore boundary provide direct evidence for the vena-contracta formation and its magnitude (Figures 6.10 to 6.15). Note, however, that two of the holes in the 20° model which are located nearest to the boundary and along the major axis of the inlet section (hole no. 1 and 9 in Figure B.1) are largely exposed to the wellbore pressure regime due to the obliquity of the inlet section (Figures 6.11 and 6.14).

The pressure head profiles measured along different arrays are variable for the acute models. This is most distinguishable for the 10° model tests exhibiting two distinct grouping of the measurements: along the arrays parallel to the minor axis of the inlet (involving 90° bending of streamlines) and the other arrays (Figures 6.12 and 6.15). For the runs simulating opening of the fracture (Figures 6.13 to 6.15), the profiles follow similar patterns. Consequently, straight streamline visualization cannot be strictly true because of non-axisymmetric pressure distribution observed during injection tests in acute models.

The entry loss coefficients for all models form a tight cluster between ξ_n=0.65-0.71 and ξ_n=0.65-0.75 for the fabrication (2b=1.1 mm) and opening (2b=1.6 mm) aperture series, respectively. Note that, as the intersection angle decreases and/or aperture increases, the inlet area increases and hence the ratio of the velocity in the wellbore to that at the inlet increases. A slight increase in the coefficients from the 90° to 10° models and from the fabrication to opening apertures is therefore consistent with the results of one-dimensional flow experiments (Figure

6.2.Inset). It follows that the choice of the entry loss coefficients should be based on the ratio of the wellbore to inlet areas. The values of the coefficients calculated for Reynolds numbers up to 12000 span the range indicated by Rissler (1978) and Ward-Smith (1980) for one-dimensional flow between parallel plates. The coefficients of all test series appear to be independent of Reynolds number as in one-dimensional flow.

The mathematical model (Equation 4.29) incorporating the empirical entry loss coefficients is capable of reliably estimating one of the three basic test parameters (fracture aperture, injection head and flow rate) given the other two. Nevertheless, it hardly reproduces the in-fracture injection pressure distribution because of vena contracta formation and decay in all models, and small magnitude directional variations in the acute models. The results clearly demonstrate prevalence of the entry processes in determining pressure distribution around the wellbore where the turbulent regime is also most influential. This situation is treated in terms of an equivalent system of two superimposed independent processes. However, all these have little practical consequence because what needs to be measured/predicted is the total head at the boundaries rather than the actual energy transformation path within the fracture.

6.5 Summary

The Reynolds numbers calculated at the wellbore face (Table 5.1) suggest that the findings of this experimental study apply to a broad range of practical situations. With this incentive in mind, a better

understanding of the near well flow mechanisms taking place during pumping and injection tests has been established for the acute systems. The semi-analytical model (Equation 4.29) as a predictive tool has been verified and refined as a result of the laboratory study. The observations have been comprehensively discussed to provide a guidance for the deductions.

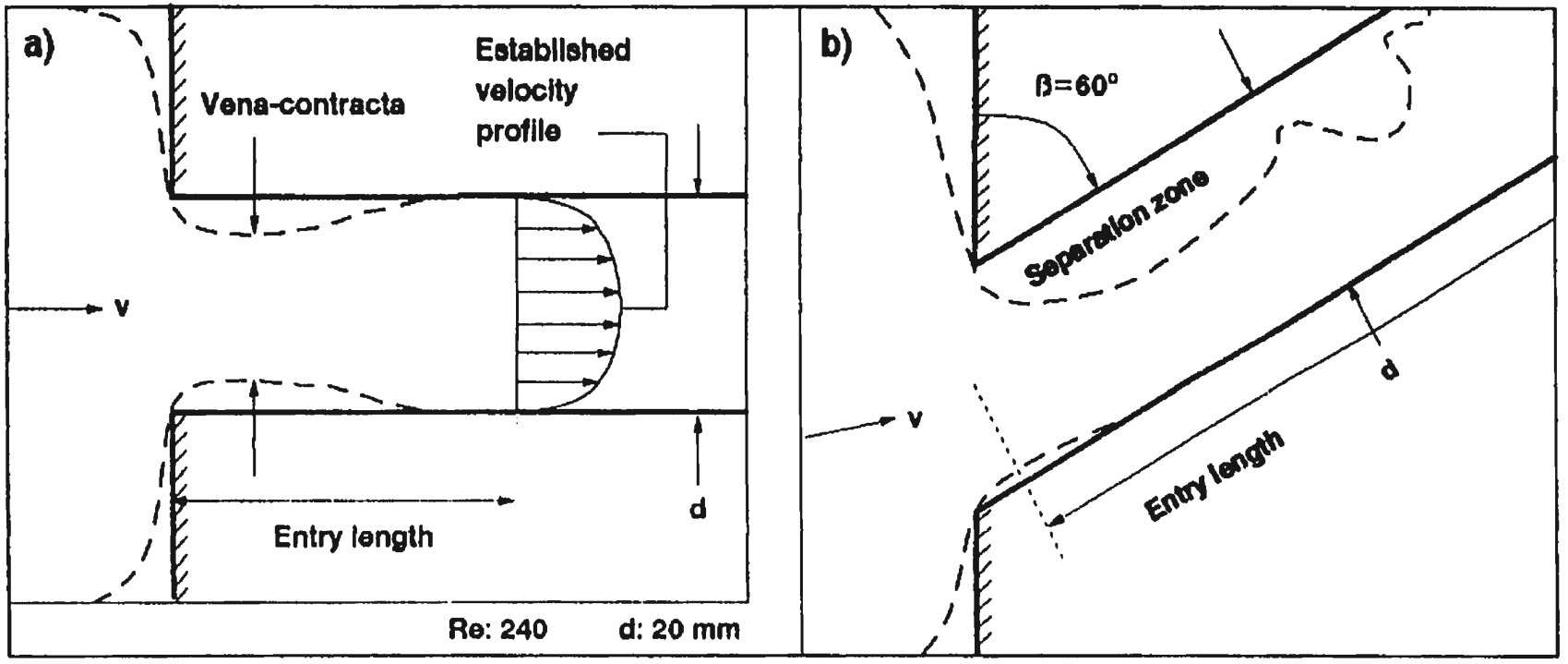

Figure 6.1. Profiles of bounding streamlines of flow from a large tank into a pipe mounted: a) normal; and b) oblique to the tank surface (schematized from JSME, 1988).

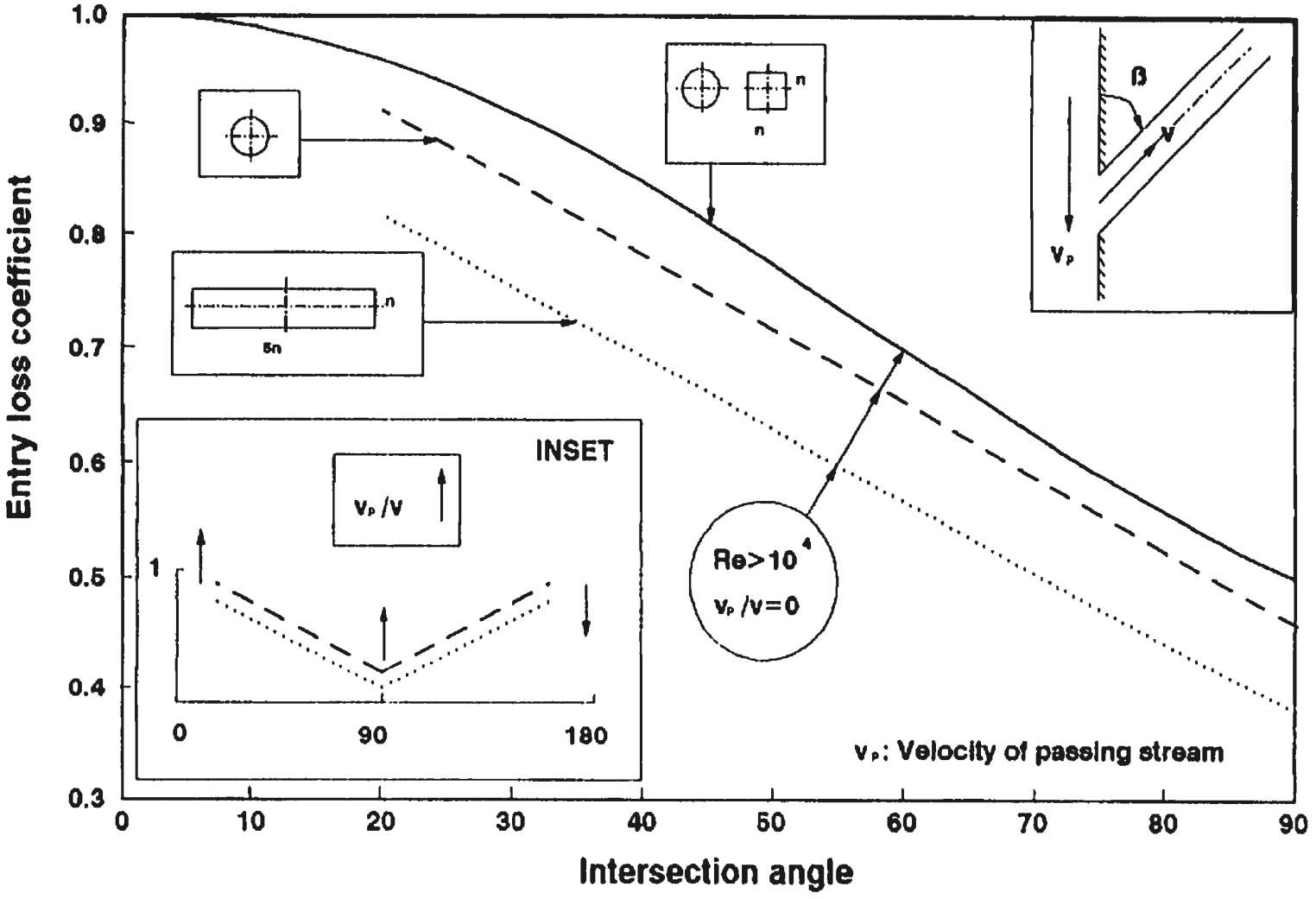

Figure 6.2. Entry loss coefficients of flow from an infinite space into conduits having different cross-sections and intersecting at different angles. Note the reverse trend in the variation of the loss coefficients as the ratio v_p/v increases (Inset). Prepared from an empirical expression (solid line) and data (dahsed lines) reported in Fried and Idelchik (1989).

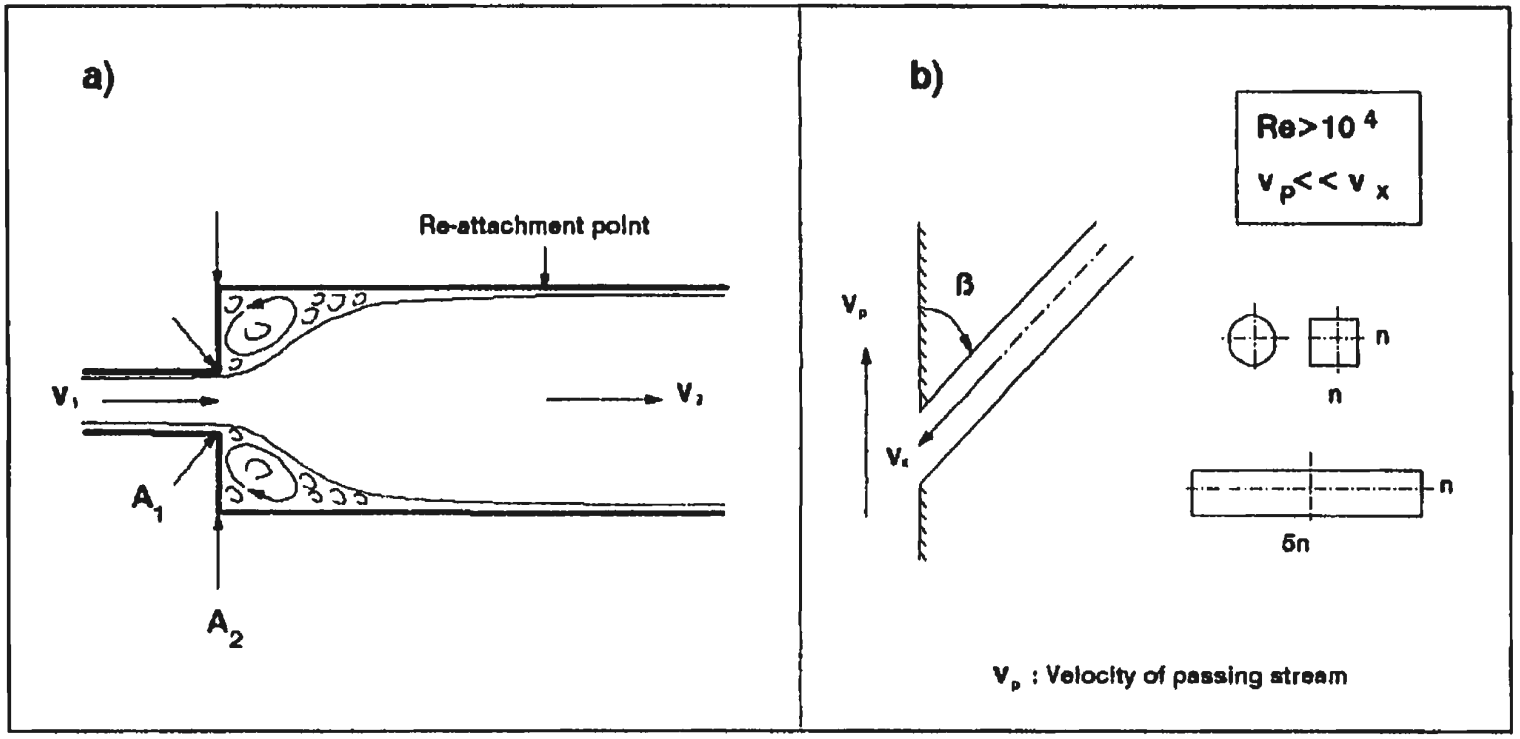

Figure 6.3.a) Idealized model of flow in a co-axial enlargement; and b) discharge from tubes of varying cross-sections mounted on a wall with passing stream (after Fried and Idelchik, 1989).

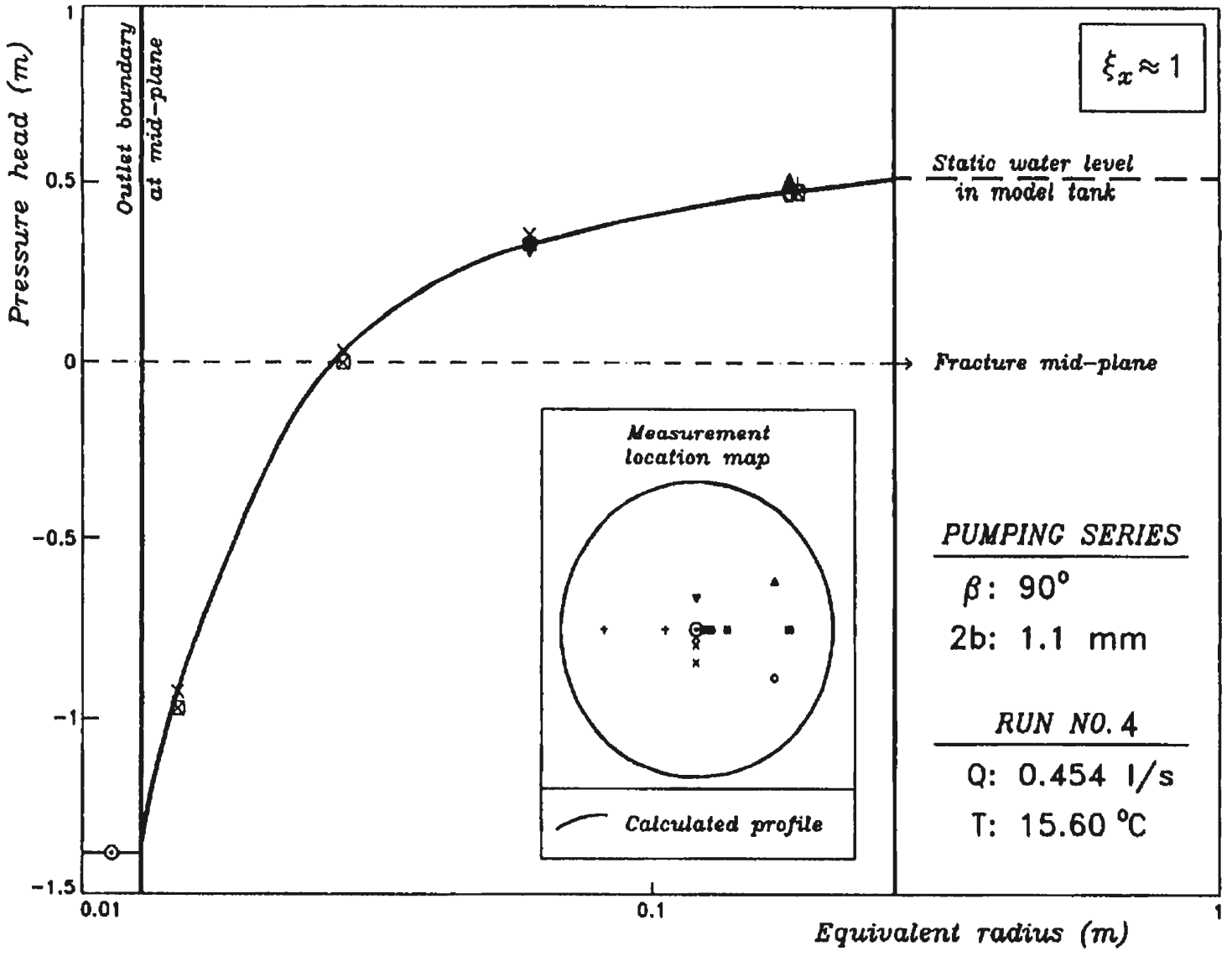

Figure 6.4. Pumping pressure head vs. logarithm of equivalent radius: β=90°; 2b=1.1 mm; Run no. 4 (Table 5.1).

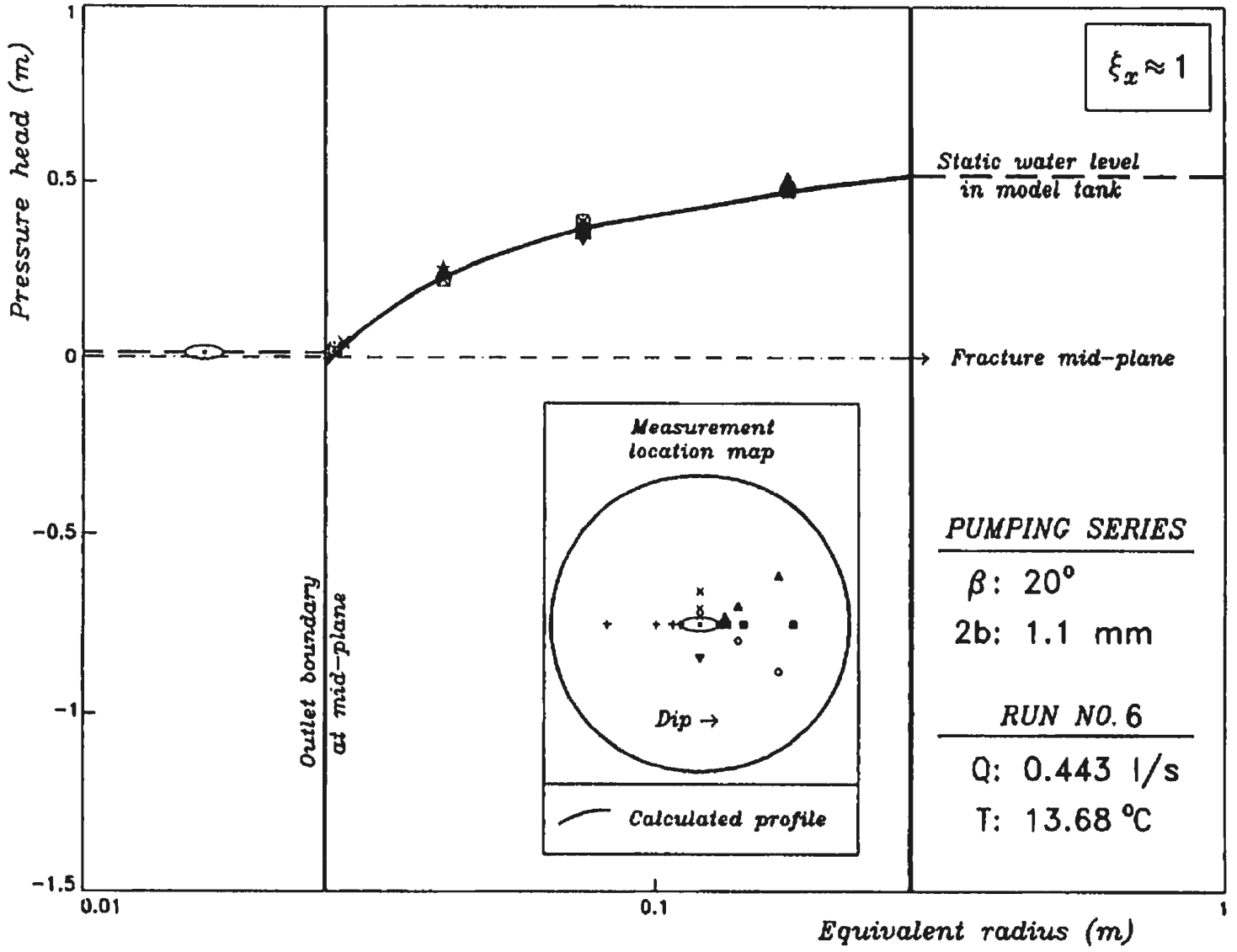

Figure 6.5. Pumping pressure head vs. logarithm of equivalent radius: ß=20°; 2b=1.1 mm; Run no. 6 (Table 5.1).

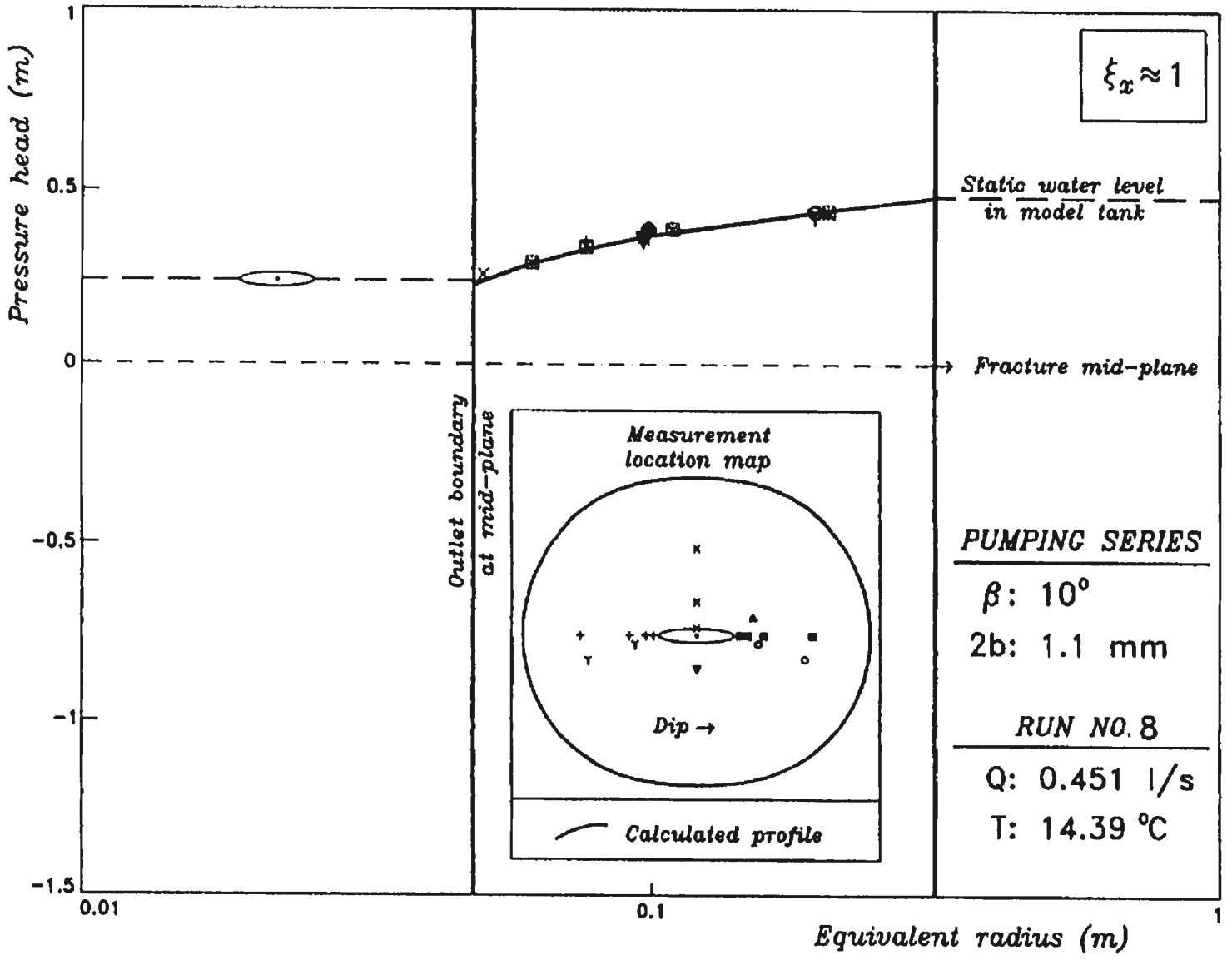

Figure 6.6. Pumping pressure head vs. logarithm of equivalent radius: ß=10°; 2b=1.1 mm; Run no. 8 (Table 5.1).

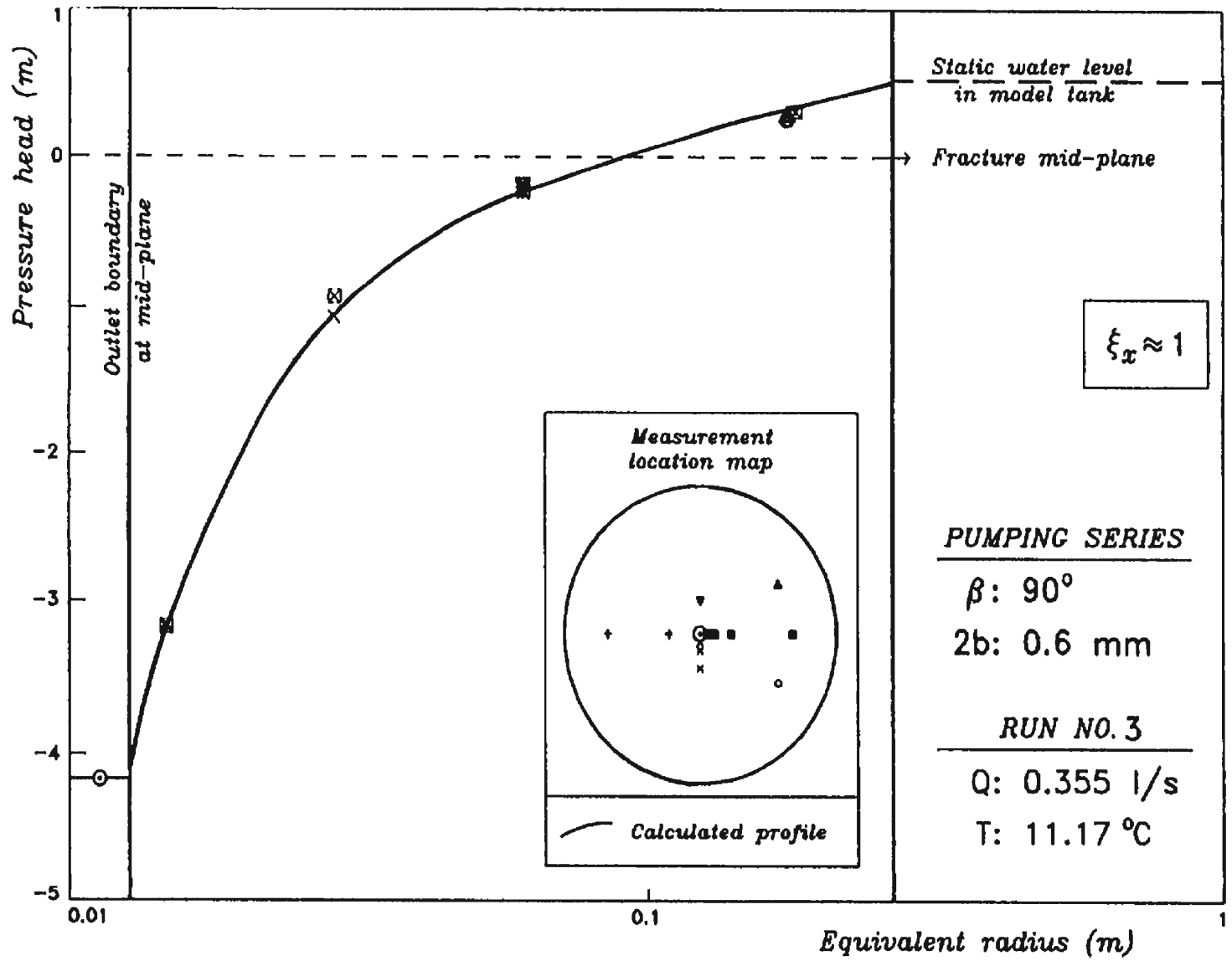

Figure 6.7. Pumping pressure head vs. logarithm of equivalent radius: ß=90°; 2b=0.6 mm; Run no. 3 (Table 5.1).

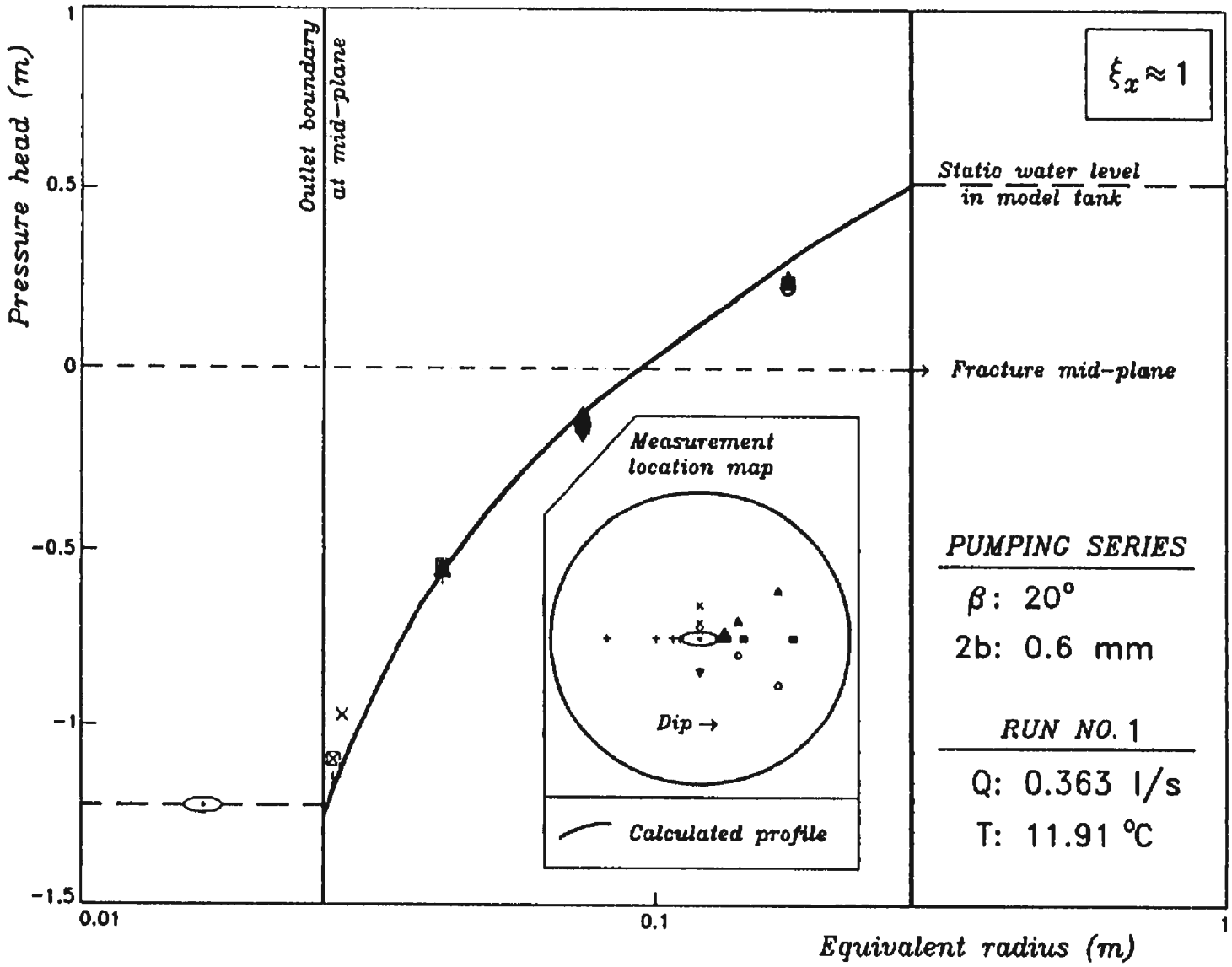

Figure 6.8. Pumping pressure head vs. logarithm of equivalent radius: β=20°; 2b=0.6 mm; Run no. 1 (Table 5.1).

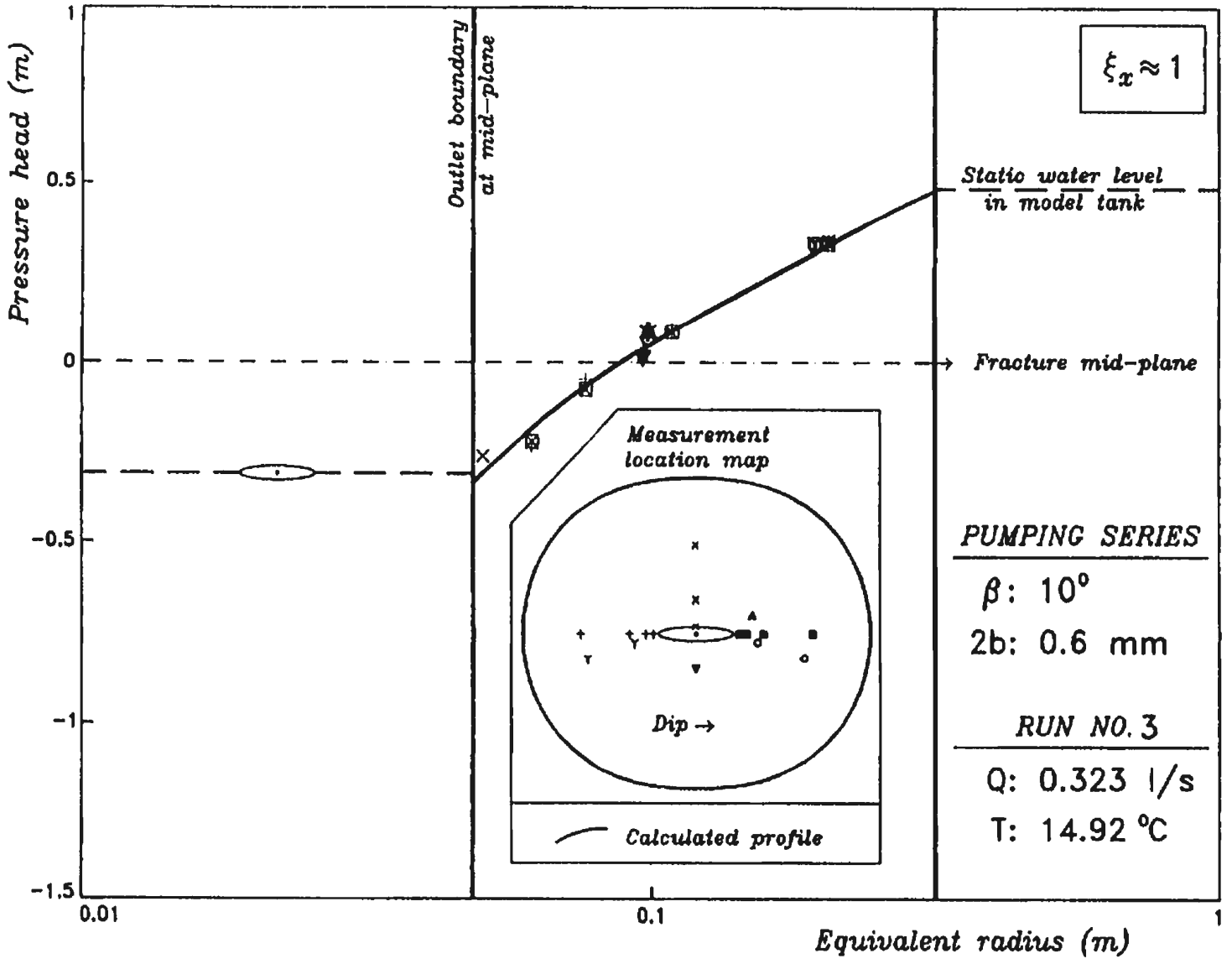

Figure 6.9. Pumping pressure head vs. logarithm of equivalent radius: β=10°; 2b=0.6 mm; Run no. 3 (Table 5.1).

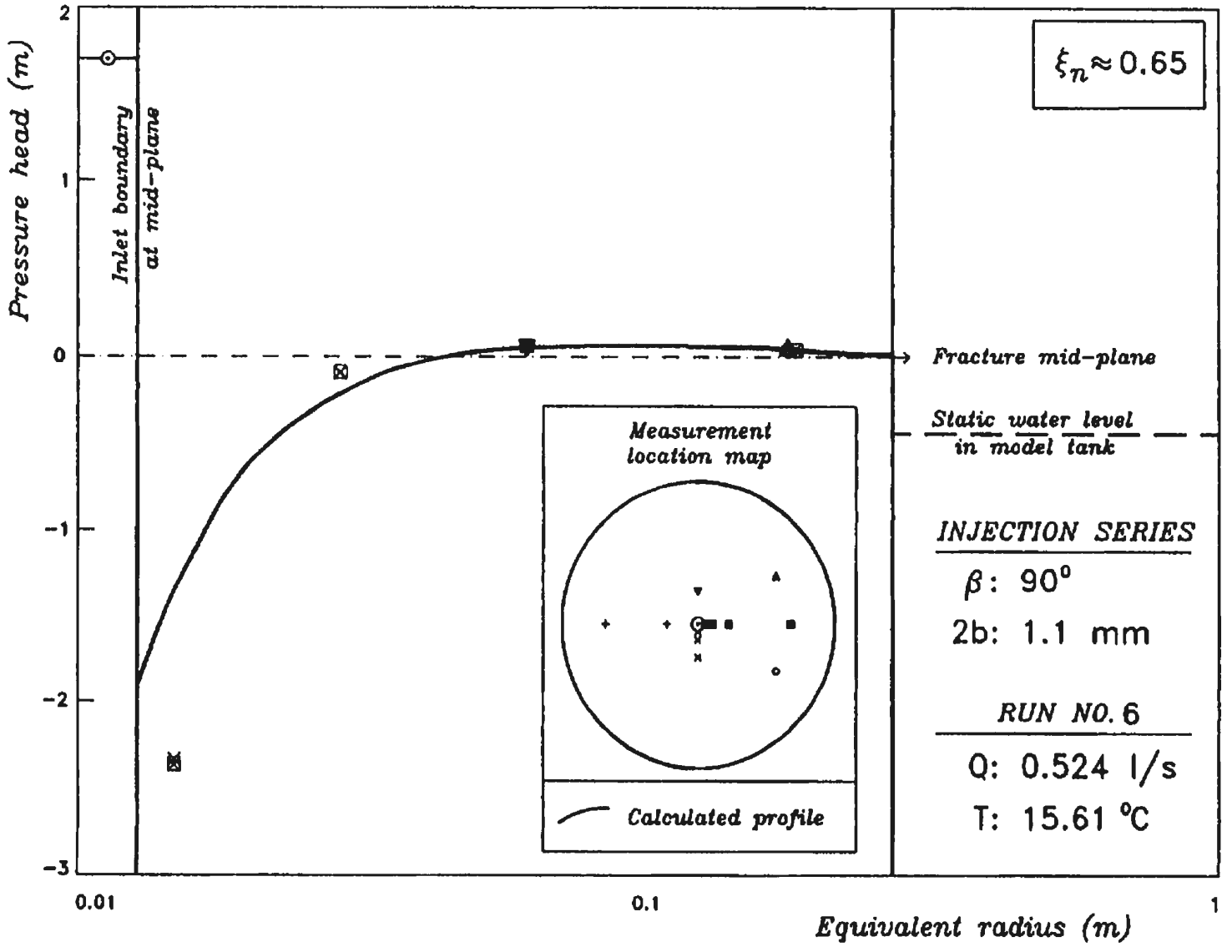

Figure 6.10. Injection pressure head vs. logarithm of equivalent radius: ß=90°; 2b=1.1 mm; Run no. 6 (Table 5.1).

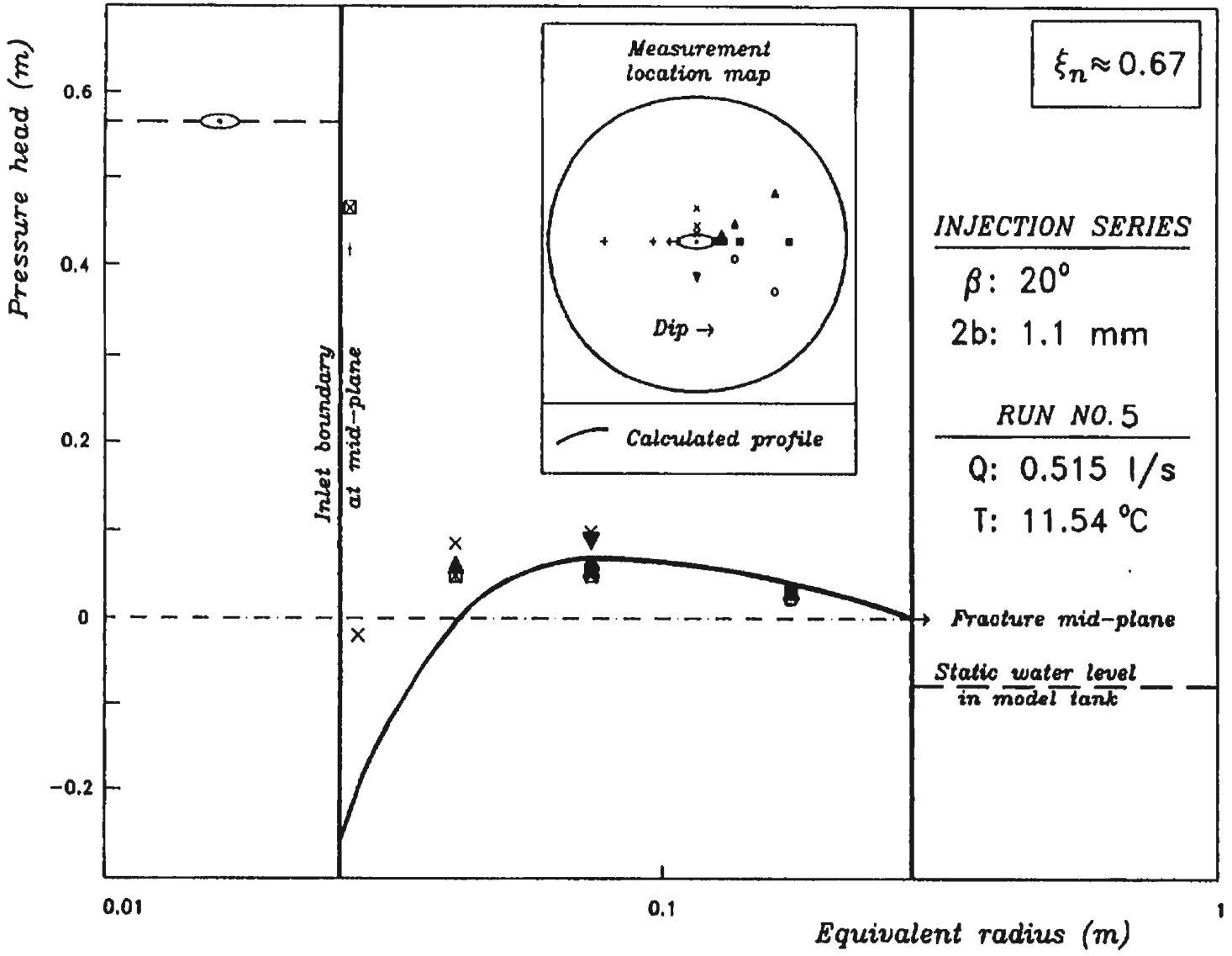

Figure 6.11. Injection pressure head vs. logarithm of equivalent radius: β=20°; 2b=1.1 mm; Run no. 5 (Table 5.1).

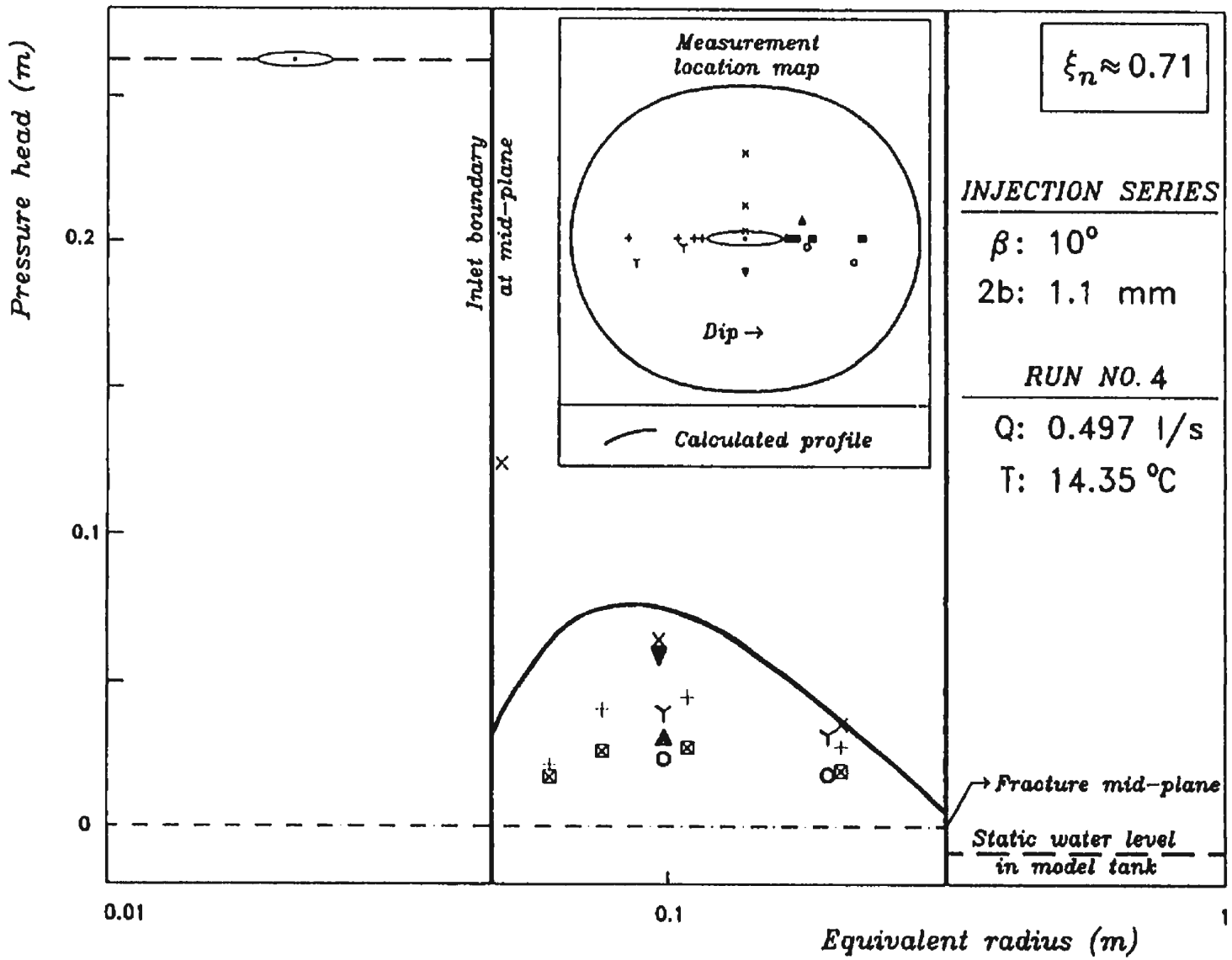

Figure 6.12. Injection pressure head vs. logarithm of equivalent radius: β=10°; 2b=1.1 mm; Run no. 4 (Table 5.1).

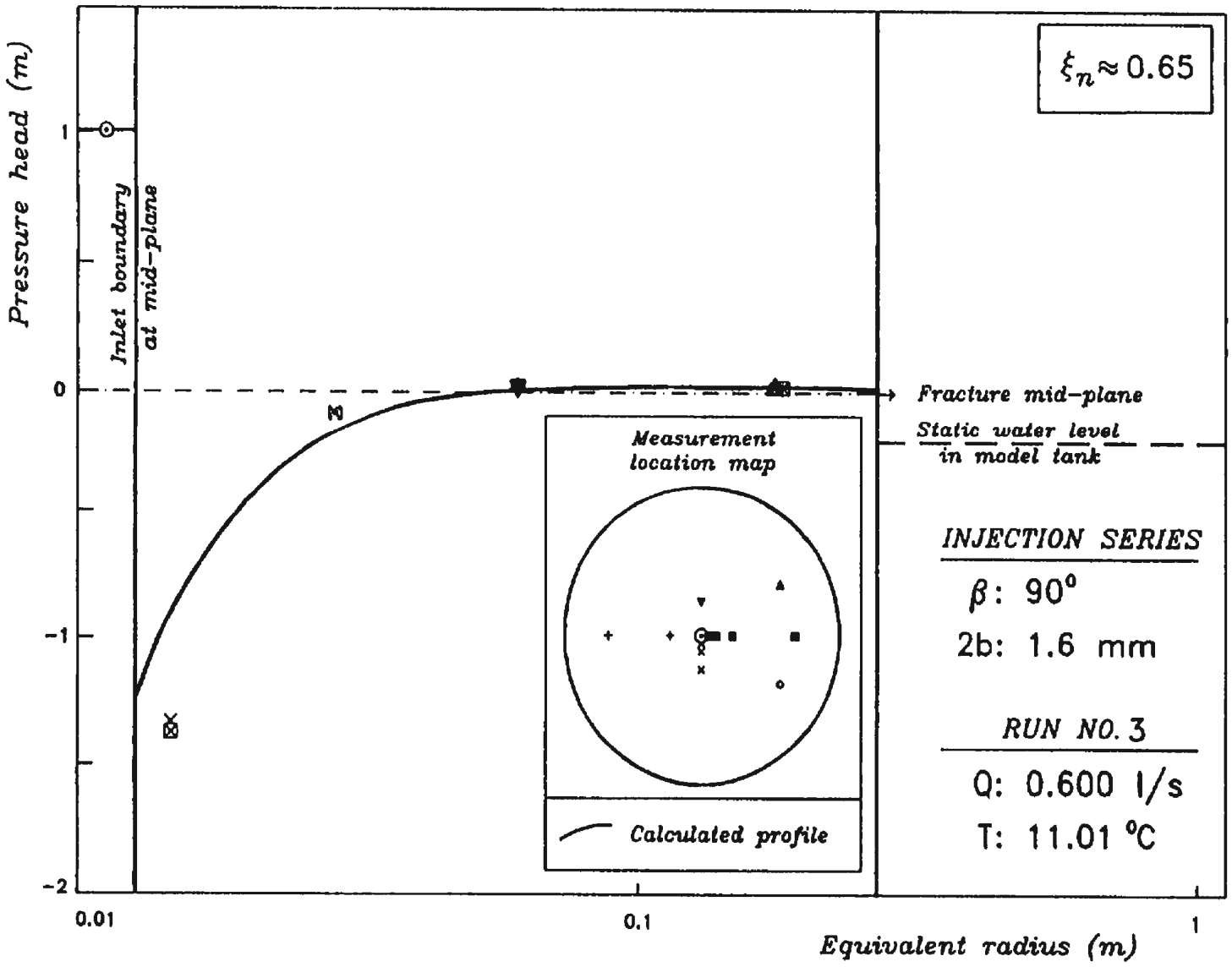

Figure 6.13. Injection pressure head vs. logarithm of equivalent radius: ß=90°; 2b=1.6 mm; Run no. 3 (Table 5.1).

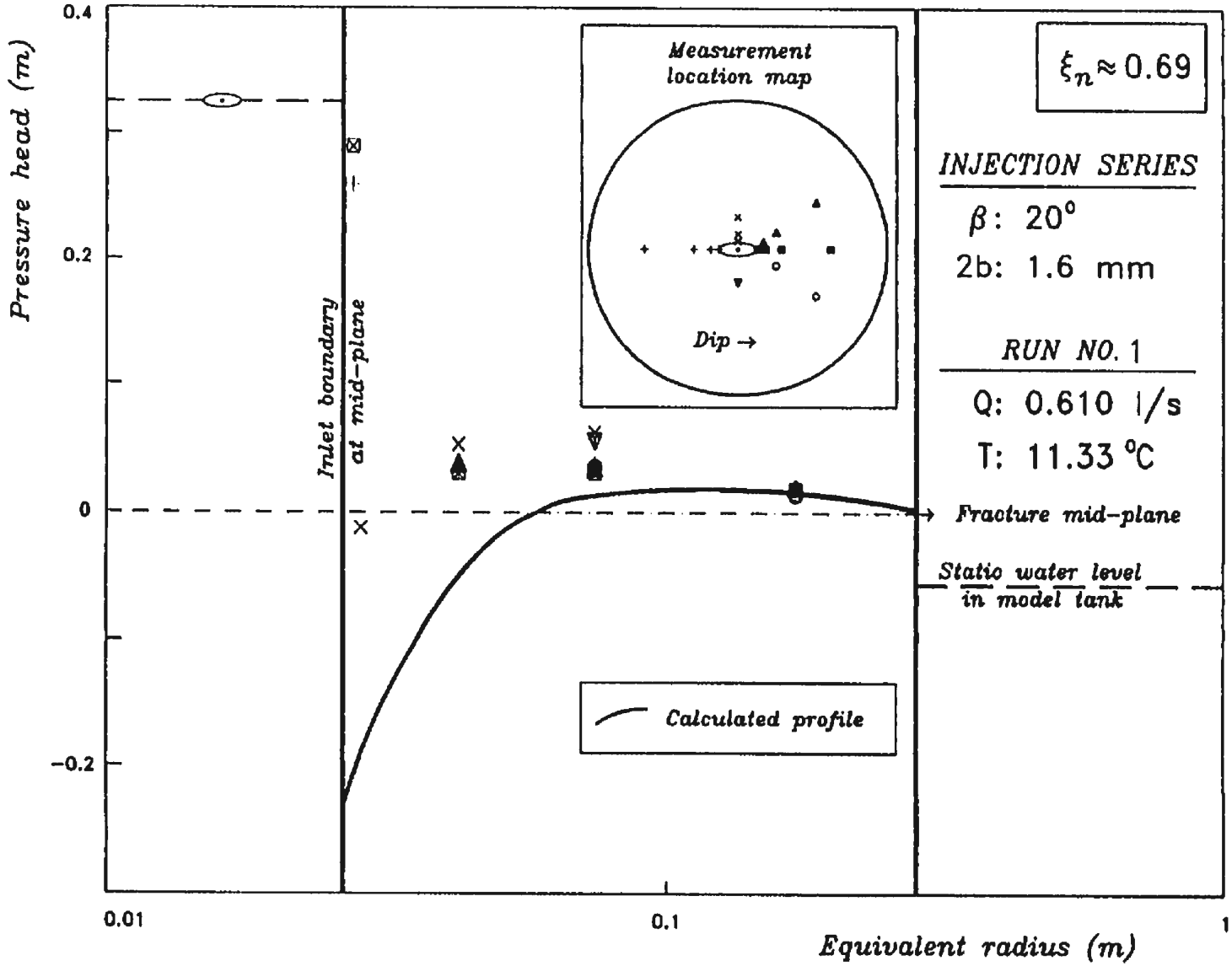

Figure 6.14. Injection pressure head vs. logarithm of equivalent radius: ß=20°; 2b=1.6 mm; Run no. 1 (Table 5.1).

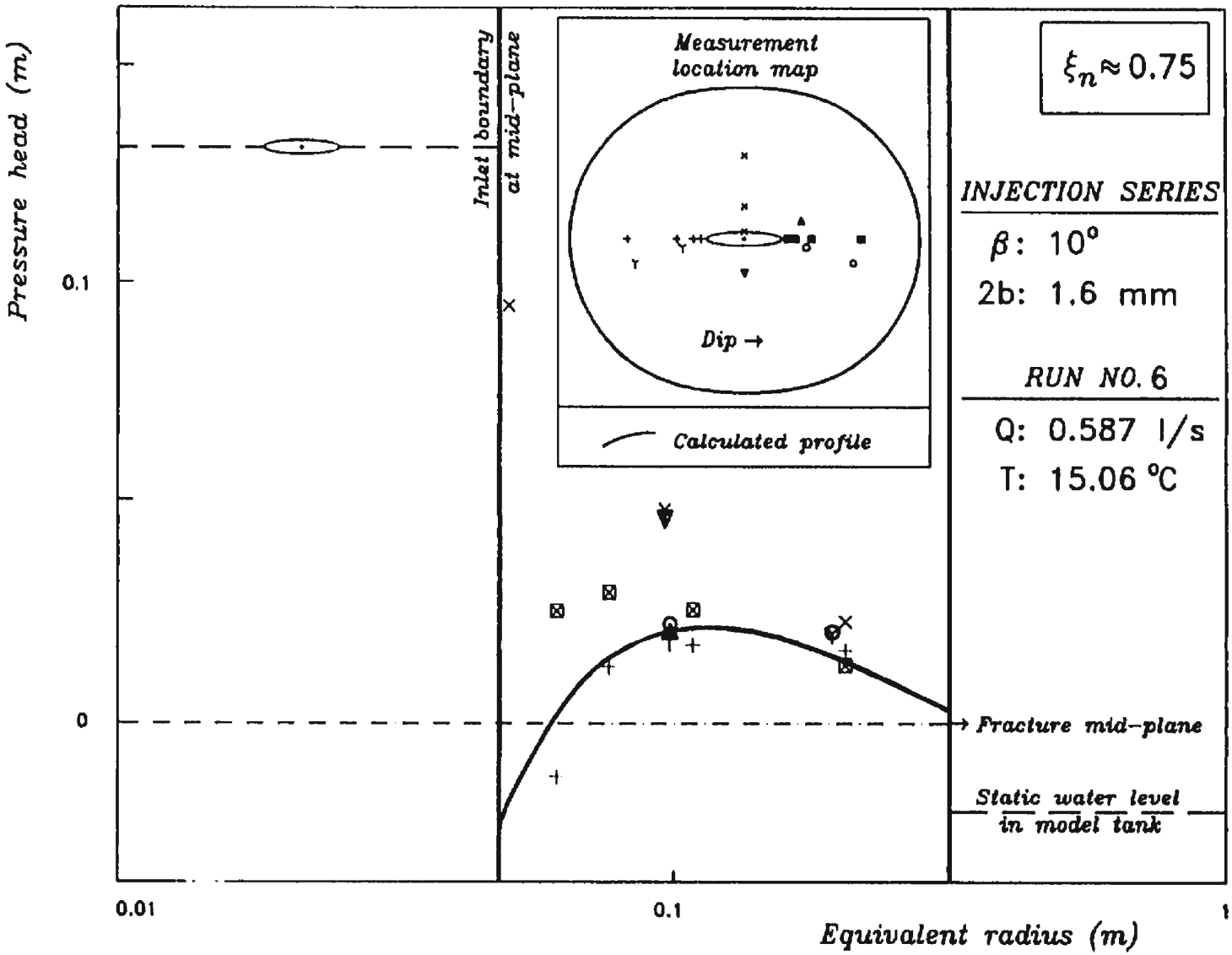

Figure 6.15. Injection pressure head vs. logarithm of equivalent radius: β=10°; 2b=1.6 mm; Run no. 6 (Table 5.1).

7 SUMMARY AND CONCLUSIONS

The problem of well test interpretation in acute systems has been investigated both theoretically and experimentally, and presented following a unifying and comprehensive approach. This investigation : a) establishes a basic understanding of the near wellbore flow mechanism in acute systems; b) formalizes the intersection angle dependent variations in the streamline pattern and hence in pressure distribution and observed response; and c) provides mathematical tools to predict these variations. In the following, the summary of the underlying work and the conclusions (including their implications and recommendations) are presented separately for each component.

The theoretical component of this study involved:

a) the derivation of the governing differential equation of flow in fractures of acute systems,

b) the introduction of analytical models for constant-flux tests under transient and steady-state conditions,

c) the formulation of the streamline-equipotential network created by the injection/pumping through acute systems under initially non-uniform heads, and

d) the development of a general, semi-analytical model accounting for the roughness, turbulence and intersection effects in interpreting single-well constant-flux tests.

The main conclusions are enumerated as follows:

1. The early period during which the system intersection angle dominates

the response is extended by a factor of $(e_\beta/e_{90})^2$ as this angle becomes smaller. Ignoring the intersection angle in the evaluation of data from the early period will therefore lead to an overestimate of transmissivity.

2. The zone of influence is essentially independent of the intersection angle. Thus, the biased response in reflecting the properties of the near wellbore area (due to logarithmic pressure distribution) is not further complicated due to non-orthogonality of the fracture-wellbore intersection. This implies that single-fracture permeability tests can be utilized in a network model without any reservations.

3. Interpretation of steady, single-well constant-flux tests by assuming an orthogonal system will produce overestimated aperture and hence hydraulic conductivity values.

4. In developing production strategies, it should be considered that: a) well losses can be minimized naturally by producing a system with the lowest possible intersection angle: and b) efficiency of and interference distance between producing wells largely depends on the intersection angle of the effective fracture(s) in the producing intervals.

5. A single wellbore may be adequate to obtain anisotropic point permeability in a fractured rock mass. This may result in a more homogenous sampling and/or substantial saving in drilling costs.

6. The predictions of any single-well test model based on an orthogonal system assumption can be refined by simply substituting the actual wellbore radius with the equivalent radius, e.

7. The single-fracture, constant-flux test models developed in this study can be readily extended to the interpretation of tests conducted in long wellbore intervals with multiple fractures by weighing the intersection angle of each subsystem with reference to the aperture distribution.

A considerable effort has been made to undertake a laboratory study: a) to verify the formation of the idealized streamline pattern and examine effects of likely interactions at the acute intersections particularly during injection tests; and b) to quantify the exit/entry loss coefficients as a function of the intersection angle. The original experimental set-up designed to carry out this investigation includes three distinct fracture-wellbore system models with 90°, 20° and 10° intersection angles. The laboratory programme involved testing these models for three different (i.e. fabrication, 2b=1.1 mm; closure, 2b=0.6 mm; opening, 2b=1.6 mm) apertures under steady, constant-flux, injection and pumping conditions.

The overall experimental set-up successfully simulated the conceptual testing environment which the mathematical model is expected to reproduce. It was therefore possible: a) to test the predicted pressure distribution and response; b) to interpret the deviations in terms of near wellbore flow mechanisms; and c) to derive the entry and exit loss

coefficients. The main conclusions reached are:

1. The mathematical models were successful in predicting the response observed in single-well, pumping tests and they are appropriate for interpreting the field test data. The quality of predictions are not influenced from the offset of the wellbore axis due to fracture closure.

2. The exit loss coefficient is virtually unchanged from unity and not affected by fracture closure.

3. The streamline pattern during injection tests, at both fabrication and opening apertures, however, does not form exactly as conceptualized. The reason for this is the dependence of the entry length, position and intensity of vena-contracta, and subsequently the distribution of the entry losses, on the streamline position with respect to intake section. Having recognized this limitation, the developed mathematical models still provide the best alternative in interpreting single-well injection tests in acute systems.

4. Entry loss coefficient is not very sensitive to the intersection angle and can be roughly taken as 0.65 for all angles, probably less than about 5°. In field applications, this coefficient may slightly change for different ratios of wellbore to inlet areas due to differences in wellbore radius and/or apertures.

REFERENCES

Atkinson, L.C. 1987. A laboratory and numerical investigation of steady-state, two regime, radial flow to a well from rough, horizontal, deformable fractures. Ph.D. Thesis, Memorial University of Newfoundland, St John's, NF.

Baker, W.J. 1955. Flow in fissured formations. In: Proc. 4th World Petroleum Congress, Rome, Vol. Section II/E, Paper 7, 379- 393.

Basak, P. 1978. Analytical solutions for two-regime well flow problems. Journal of Hydrology, 38, 147-159.

Bear, J. 1972. Dynamics of fluids in porous media. Elsevier, New York.

Bear, J. 1979. Hydraulics of groundwater. McGraw-Hill, New York.

Bianchi, L. and Snow, D. 1968. Permeability of crystalline rock interpreted from measured orientations and apertures of fractures. Annals of Arid Zone, 8, 1, 231-245.

Bredehoeft, J.D. and Papadopulos, S.S. 1980. A method for determining the hydraulic properties of tight formations. Water Resources Research, 16, 1, 233-238.

Bruin, J. and Hudson, H.E. 1955. Selected methods for pumping test analysis. Illinois State Water Survey, Report of Investigation 25.

Caldwell, I.A. 1972. The theoretical determination of the permeability tensor for jointed rocks. In: Proc. ISRM-IAEG Symp. on Percolation through Fissured Rock, Stuttgart, T1-C.

Carslaw, H.S. and Jaeger, J.C. 1959. Conduction of heat in solids, 2nd Edn., Oxford University Press, London.

Castillo, E. 1972. Mathematical model for two dimensional percolation through fissured rock. In: Proc. ISRM-IAEG Symp. on Percolation through Fissured Rock, Stuttgart, T1-D.

Cedergren, H.R. 1988. Seepage, drainage and flow nets. 2nd Edn., Wiley, New York.

Chernyshev, S.N. and Dearman, W.R. 1991. Rock fractures, Butterworth-Heinemann, London.

Cinco-Ley, H. 1974. Unsteady-state pressure distributions created by a slanted well, or a well with an inclined fracture. PhD Thesis, Stanford University, Stanford, CA.

Cooper, H. H., Bredehoeft, J.D. and Papadopulos, I.S. 1967. Response of a finite-diameter well to an instantaneous charge of water. Water Resources Research, 3, 1, 263-269.

Cooper, H.H. and Jacob, C.E. 1946. A generalized graphical method for evaluating formation constants and summarizing well-field history. Trans. Am. Geophys. Union, 27, 4, 527-534.

Cornet, F.H. 1992. In situ stress heterogeneity identification with the HTPF tool. In: Proc. 33rd U.S. Rock Mech. Symp., Santa Fe, 39-48.

Cornwell, D.K. and Murphy, H.D. 1985. Experiments with non-darcy flow in joints with large scale roughness. In: Proc. Int. Symp. on the Fundamentals of Rock Joints, Bjorkliden, 323-332.

De Marsily, C. 1985. Flow and transport in fractured rocks: connectivity and scale effect. In: Proc. Int. Congress on Hydrogeology of Rocks of Low Permeability, Memoirs of International Association of Hydrogeologists, Tucson, Vol. 17, 267-277.

Doe, T. and Remer, J. 1980. Analysis of constant-head well tests in nonporous fractured rock. In: Proc. 3rd Invitational Well Testing Symp., Lawrence Berkeley Lab. Report LBL-12076, Berkeley, CA, 84-89.

Doe, T.W., Long, J.C.S., Endo, H.K. and Wilson, C.R. 1982. Approaches to evaluating the permeability and porosity of fractured rock masses. In: Proc. 23rd U.S. Rock Mech. Symp., Berkeley, 30-38.

Doe, T.W. and Osnes, J.D. 1985. Interpretation of fracture geometry from well test. In: Proc. Int. Symp. on the Fundamentals of Rock Joints, Bjorkliden, 281-292.

Fried, E. and Idelchik, I.E. 1989. Flow resistance: a design guide for engineers. Hemisphere, New York.

Goldstein, R.J. (Ed.). 1983. Fluid mechanics measurements. Hemisphere, Washington.

Gringarten, A.C. 1982. Flow-test evaluation of fractured reservoirs. In: T.N. Narasimhan (Ed.), Recent Trends in Hydrogeology. Geological Society of America Special Paper, Vol. 189, 237-264.

Hannoura, A. and Barends, F.B.J. 1981. Non-Darcy flow; a state of the art. In: Proc. Euromech 143, Delft, 37-51.

Hantush, M.S. 1964. Hydraulics of wells. Advances in Hydroscience, Vol. 1, 281-433.

Hsieh, P.A. 1987. Characterizing the hydraulic properties of fractured rock masses: methodology and case histories. In: Proc. 28th U.S. Rock Mech. Symp., Tucson, 465-472.

Hubbert, M.K. 1940. The theory of ground-water motion. Journal of Geology, 48, 8, 785-944.

Hubbert, M.K. 1956. Darcy's law and the field equations of the flow of underground fluids. Trans. Am. Inst. Min. Metal. Eng., 207, 222-239.

Huitt, J.L. 1956. Fluid flow in simulated fractures. Am. Inst. Chem. Eng. Journal, 2, 2, 595-264.

Ingersoll, L.R., Adler, F.T., Plass, H.J. and Ingersoll, A.C. 1950. Theory of earth heat exchangers for the heat pump. Heating, Piping and Air Conditioning, 22, 113-122.

Iwai, K. 1976. Fundamental studies of fluid flow through a single fracture. Ph.D. Thesis, Univ. California, Berkeley, CA.

Jacob, C.E. 1940. On the flow of water in an elastic artesian aquifer. Trans. Am. Geophys. Union, 21, 574- 586.

Jacob, C.E. 1947. Drawdown test to determine effective radius of artesian well. Trans. Am. Soc. Civil Eng., 112, 1047-1070.

Jacob, C.E. and Lohman, S.W. 1952. Nonsteady flow to a well of constant drawdown in an extensive aquifer. Trans. Am. Geophys. Union, 33, 4, 559-569.

JSME (Japan Society of Mechanical Engineers). 1988. Visualized flow: fluid motion in basic and engineering situations revealed by flow visualization. Pergamon Press, Oxford.

Karasaki, K. 1987. Well test analysis in fractured media. Ph.D. Thesis, Univ. California, Berkeley, CA.

Kline, S.J. and McClintock, F.A. 1953. Describing uncertainties in single-sample experiments. Mechanical Engineering, 75, 3-8.

Kruseman, G.P. and Ridder, N.A. 1970. Analysis and evaluation of pumping

test data. International Institute for Land Reclamation and Improvement, Bulletin 11, Wageningen, Netherlands.

Lamb, H. 1945. Hydrodynamics. 6th Edn., Dover, New York.

Lennox, D.H. 1966. Analysis and application of step-drawdown test. Journal of the Hydraulic Div., Proc. Am. Soc. Civil Eng., HY6, 25-48.

Lohman, S.W. 1972. Ground-water hydraulics. U.S. Geological Survey Professional Paper, Vol. 708.

Long, J. C.S. and Witherspoon, P.A. 1985. The relationship of the degree of interconnection to permeability in fracture networks. Journal of Geophys. Research, 90, B4, 3087-3098.

Louis, C. and Maini, Y.N.T. 1970. Determination of in situ hydraulic parameters in jointed rock. In: Proc. 2nd Congress Int. Soc. Rock Mech., Belgrade, Vol. 1, 1-32.

Louis, C. 1974. Introduction a l'hydraulique des roches. Bull. BRGM, Vol. 2, Section III, No. 4, 283-356.

Maini, Y.N.T, Noorishad, J. and Sharp, J. 1972. Theoretical and field considerations on the determination of in situ hydraulic parameters in fractured rock. In: Proc. ISRM-IAEG Symp. on Percolation through Fissured Rock, Stuttgart, T1-E.

Marine, I.W. 1980. Determination of the location and connectivity of fractures in metamorphic rock with in-hole tracers. Ground Water, 18, 3, 252-261.

Matthews, C.S. and Russell, P.G. 1967. Pressure buildup and flow tests in wells. Soc. Pet. Eng., AIME Monograph, Vol. 1.

Murphy, H.D. 1979. Flow near the outlet of a geothermal energy reservoir. Ph.D. Thesis, Los Alamos National Lab., Report no. LA-7906, Los Alamos, NM.

Neuman, S.P. 1987. Stochastic continuum representation of fractured rock permeability as an alternative to the REV and fracture network concepts. In: Proc. 28th U.S. Rock Mech. Symp., Tucson, 533-561.

Nordqvist, A.W., Tsang, Y.W., Tsang, C.F., Dverstorp, B. and Andersson, J. 1992. A variable aperture fracture network model for flow and transport in fractured rocks. Water Resources Research, 28, 6, 1703-1713.

Parrish, D.R. 1963. Fluid flow in rough fractures. In: Proc. Production Research Symp. SPE Paper No 563, 9 (Preprint).

Parsons, R.W. 1966. Permeability of idealized fractured rock. Journal of Society of Petroleum Engineers, 126-136.

Pyrak-Nolte, L.J., Myer, L.R., Cook,N.G.W. and Witherspoon, P.A. 1987. Hydraulic and mechanical properties of natural fractures in low permeability rock. In: Proc. 6th Int. Congress on Rock Mech., 225-231.

Ramey, H.C. 1982. Well-loss function and the skin effect: a review. In: T.N. Narasimhan (Ed.), Recent Trends in Hydrogeology. Geological Society of America Special Paper, Vol. 189, 265-272.

Rissler, P. 1978. Determination of the water permeability of jointed rock. Ph.D. Thesis, The Inst. for Foundation Eng., Soil Mech. and Water Ways Construction, RWTH (University) Aachen, Germany, English Edition Series, Vol. 5.

Rorabough, M.I. 1953. Graphical and theoretical analysis of step-drawdown

test of artesian well. Proc. Am. Soc. Civil Eng., 79, Section 362.

Rouleau, A. 1988. A numerical simulator for flow and transport in stochastic discrete fracture networks. National Hydrology Research Inst. Paper No. 39, Environment Canada, Saskatoon.

Rouse, H. 1961. Fluid mechanics for hydraulic engineers. Dover, New York.

Schlichting, H. 1979. Boundary-layer theory. 7th Edn., McGraw- Hill, New York.

Schwartz, F.W. and Smith, L. 1985. An overview of the stochastic modeling of dispersion in fractured media. In: Proc. NATO Adv. Study Inst. on Fundamentals of Transport Phenomena in Porous Media, Newark, 728-750.

Sharp, J.C. and Maini, Y.N.T. 1972. Fundamental considerations on the hydraulic characteristics of joints in rocks. In: Proc. ISRM-IAEG Symp. on Percolation through Fissured Rock, Stuttgart, T1-F.

Silliman, S. and Robinson, R. 1989. Identifying fracture interconnections between boreholes using natural temperature profiling: I. conceptual basis. Ground Water, 27, 3, 393-402.

Smith, L. Mase, C.W. and Schwartz, F.W. 1987. Estimation of fracture aperture using hydraulic and tracer tests. In: Proc. 28th U.S. Rock Mech. Symp., Tucson, 453-463.

Snow, D.T. 1969. Anisotropic permeability of fractured media. Water Resources Research, 5, 6, 1273-1289.

Snow, D.T. 1970. The frequency and apertures of fractures in rock. Int. J. Rock Mech. and Min. Sci., 7, 1, 23-40.

Stearns, D.W. and Friedman, M. 1972. Reservoirs in fractured rocks. In: R.E. King (Ed.), Stratigraphic oil and gas fields: classification, exploration methods and case histories. AAPG Memoir 16 and SEG Special Publ. 10, 83-106.

Stehfest, H. 1970. Algorithm 368: Numerical inversion of Laplace transforms. Communications of ACM, 13, 1, 47-49.

Streltsova-Adams, T.D. 1978. Well hydraulics in heterogenous aquifer formations. Advances in Hydroscience, Vol. 11, 357- 423.

Sundaram, P.N. and Frink, D. 1983. Electrical analogy of hydraulic flow through rock fractures. Geotechnical Testing Journal, 6, 1, 3-9.

Theis, C.V. 1935. The relation between the lowering of the piezometric surface and the rate and duration of discharge of a well using ground-water storage. Trans. Am. Geophys. Union, 16, 519-524.

Tsang, C.F., Hufschmied, P. and Hale, F.V. 1990. Determination of fracture inflow parameters with a borehole fluid conductivity logging method. Water Resources Research, 26, 4, 561-578.

Tsang, Y.W. and Tsang, C.F. 1990. Hydrological characterization of variable-aperture fractures. In: Proc. Int. Symp. on Rock Joints, Loen, Norway, 423-431.

Tuma, J.J. 1987. Engineering mathematics handbook. 3rd Edn., McGraw-Hill, New York.

Uraiet, A.A. and Raghavan, R. 1980. Unsteady flow to a well producing at a constant pressure. Journal of Petroleum Technology, 1803-1812.

Van Everdingen, A.F. 1953. The skin effect and its influence on the productive capacity of a well. Trans. Am. Inst. Min. Metal. Eng.,

198, 171-176.

Vennard, J.K. and Street, R.L. 1982. Elementary fluid mechanics. 6th Edn., Wiley, New York.

Ward-Smith, A.J. 1980. Internal fluid flow: the fluid dynamics of flow pipes and ducts. Clarendon Press, Oxford.

Wilson, C.R., Doe, T.W., Long, C.S. and Witherspoon, P.A. 1979. Permeability characterization of nearly impermeable rock masses for nuclear waste repository siting. In: Proc. the Workshop on Low-flow, Low-permeability Measurements in Largely Impermeable Rocks, OECD, Paris, 13-27.

Wilson, C.R. and Witherspoon, P.A. 1976. Flow interference effects at fracture intersections. Water Resources Research, 12, 1, 102-104.

Wilson, C.R., Witherspoon, P.A., Long, J.C.S., Galbraith, R.M., DuBois, A.O. and McPherson, M.J. 1983. Large-scale hydraulic conductivity measurements in fractured granite. Int. J. Rock Mech. Min. Sci. and Geomech. Abstr., 20, 6, 269-276.

Woolley, D.R. 1982. Depth-yield relationships of bores in fractured rocks in N.S.W. In: Proc. Groundwater in Fractured Rock, Canberra, 283-292.

Zeigler, T.W. 1976. Determination of rock mass permeability. Tech. Rep. S-76-2, U.S. Army Eng. Waterways Exp. Stn., Vicksburg.

APPENDIX A

AN EXPRESSION FOR THE PERIMETER OF AN EQUIPOTENTIAL SURFACE IN A CONVERGENT/DIVERGENT FLOW FIELD COMPOSED OF STRAIGHT STREAMLINES NORMAL TO THE ELLIPTICAL INNER BOUNDARY

The parametric equations of an ellipse (Figure A.1) are

$$\begin{aligned} x_0 &= a\cos\theta \\ y_0 &= b\sin\theta \end{aligned} \tag{A.1}$$

where a: semi-major axis,

b: semi-minor axis, and

θ: position angle.

Equation A.1 defines the position vector $\vec{R}$ describing the ellipse by

$$\vec{R}(\theta) = \vec{I}\, a\cos\theta + \vec{J}\, b\sin\theta \tag{A.2}$$

Taking the derivative of the position vector $\vec{R}$ produces a vector $\vec{T}$ tangent to the ellipse,

$$\frac{d}{d\theta}\vec{R}(\theta) = \vec{T}(\theta) = -\vec{I}\, a\sin\theta + \vec{J}\, b\cos\theta \tag{A.3}$$

A vector $\vec{N}$ normal to this tangent vector $\vec{T}$ can be found from the orthogonality condition

$$\vec{N}\cdot\vec{T} = 0 \tag{A.4}$$

as

$$\vec{N}(\theta) = \vec{i}\, b \cos\theta + \vec{j}\, a \sin\theta \tag{A.5}$$

The normal vector $\vec{N}$ can be assigned any length l to obtain

$$\vec{L}(\theta) = \frac{l}{|\vec{N}(\theta)|} (\vec{i}\, b \cos\theta + \vec{j}\, a \sin\theta) \tag{A.6}$$

Hence, the position vector $\vec{P}$ for an equipotential surface at any normal distance l from the ellipse is defined by (Figure A.1)

$$\vec{P}(\theta) = \vec{R}(\theta) + \vec{L}(\theta) \tag{A.7}$$

which enables writing the parametric equations of an equipotential surface in the same plane as

$$x(\theta) = \left(a + \frac{l\, b}{|\vec{N}(\theta)|}\right)\cos\theta \tag{A.8}$$

$$y(\theta) = \left(b + \frac{l\, a}{|\vec{N}(\theta)|}\right)\sin\theta \tag{A.9}$$

Any expression for the perimeter Γ of such an equipotential surface needs to satisfy the general arc length equation for closed curves

$$\Gamma=4\int_0^{\pi/2}\sqrt{[x'(\theta)]^2+[y'(\theta)]^2}\,d\theta \qquad (A.10)$$

Differentiating Equations A.8 and A.9, and, substituting these in Equation A.10, the perimeter Γ expression is established as

$$\Gamma=4\int_0^{\pi/2}\left(1+\frac{l\,a\,b}{|\vec{N}(\theta)|^3}\right)|\vec{N}(\theta)|\,d\theta \qquad (A.11)$$

Referring to Equation A.10, the perimeter of an ellipse Γ_E is readily obtained as

$$\Gamma_E=4\int_0^{\pi/2}|\vec{N}(\theta)|\,d\theta \qquad \{|\vec{N}(\theta)|=|\vec{T}(\theta)| \qquad (A.12)$$

The expression for the perimeter Γ (Equation A.11) then reduces to

$$\Gamma=\Gamma_E+4\,l\,a\,b\int_0^{\pi/2}\left(\frac{1}{|\vec{N}(\theta)|^2}\right)d(\theta) \qquad (A.13)$$

Solving for the integral in the second term, Equation A.13 takes on a compact form

$$\Gamma=\Gamma_E+2\pi l \qquad (A.14)$$

Rearranging Equation A.14 results in a more familiar format, the perimeter expression for an equivalent circle,

$$\Gamma = 2\pi\,(e+1) \qquad \left\{ e = \frac{\Gamma_E}{2\pi} \right. \qquad \text{(A.15)}$$

where the term $(e+1)$ may be considered as the equivalent radius.

The perimeter of an ellipse Γ_E (Equation A.12) is usually given by

$$\Gamma_E = 4\,a\,E(\kappa, \pi/2) \qquad \left\{ \kappa = \sqrt{1-b^2/a^2} \right. \qquad \text{(A.16)}$$

where $E(\kappa, \pi/2)$ is the complete elliptical integral given by (Tuma, 1987)

$$E(\kappa, \pi/2) = \int_0^{\pi/2} \sqrt{1-\kappa^2 \sin^2\alpha}\, d\alpha \qquad \{ \alpha = 90 + \theta \qquad \text{(A.17)}$$

The values of this function are tabulated in most mathematical handbooks (e.g. Tuma, 1987).

An interesting point is that Equation A.16 is a general result, valid regardless of the geometry of the inner flow boundary. For applications with other geometries the term Γ_E should be replaced with the corresponding perimeter expression.

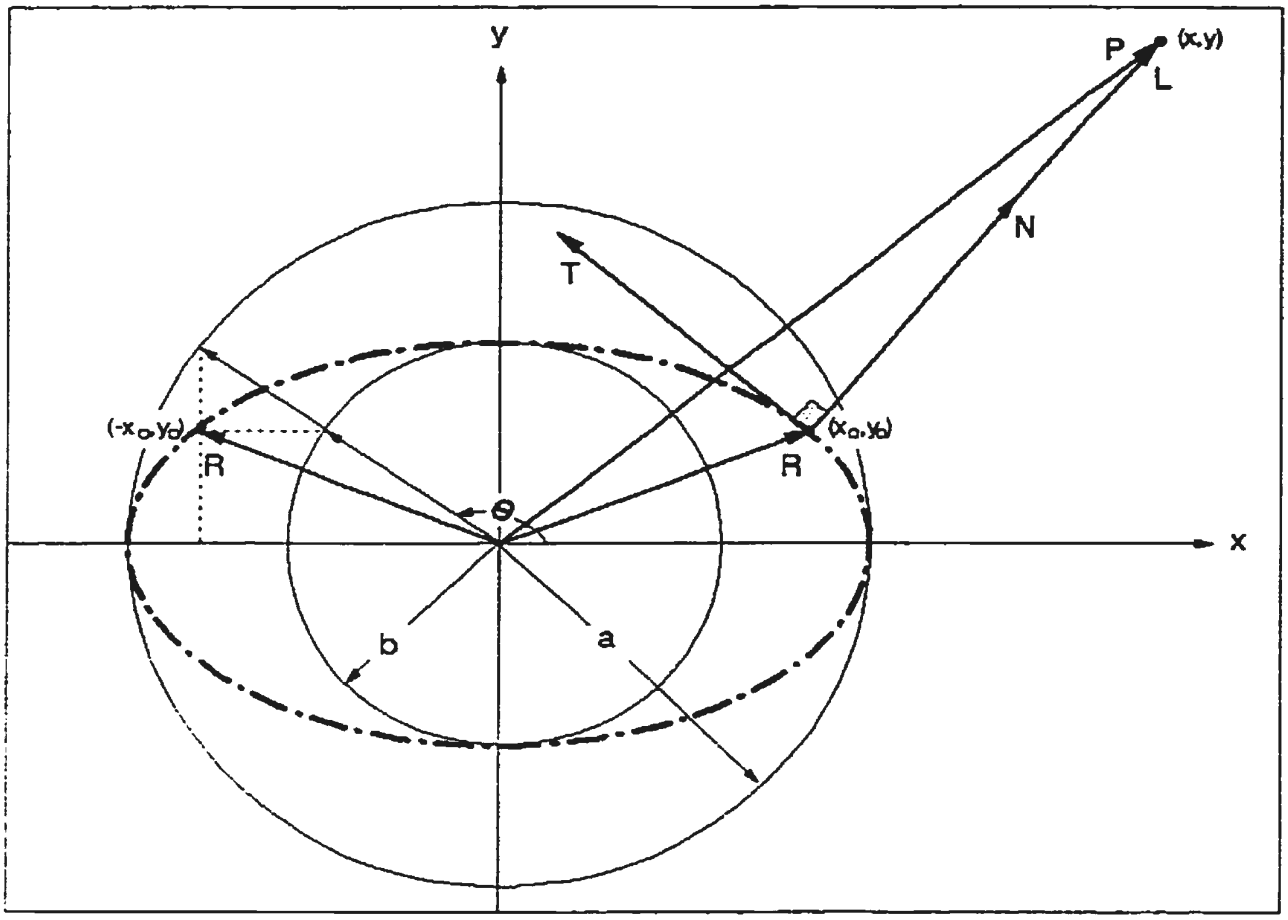

Figure A.1. Pictorial definition of the terms used in the derivation.

APPENDIX B

IN-FRACTURE PRESSURE HEAD MEASUREMENTS

1. The pumping and injection series are tabulated separately for 90°, 20° and 10° models.

2. All pressure head values are given in meters.

3. Measurement hole locations are illustrated in Figure B.1.

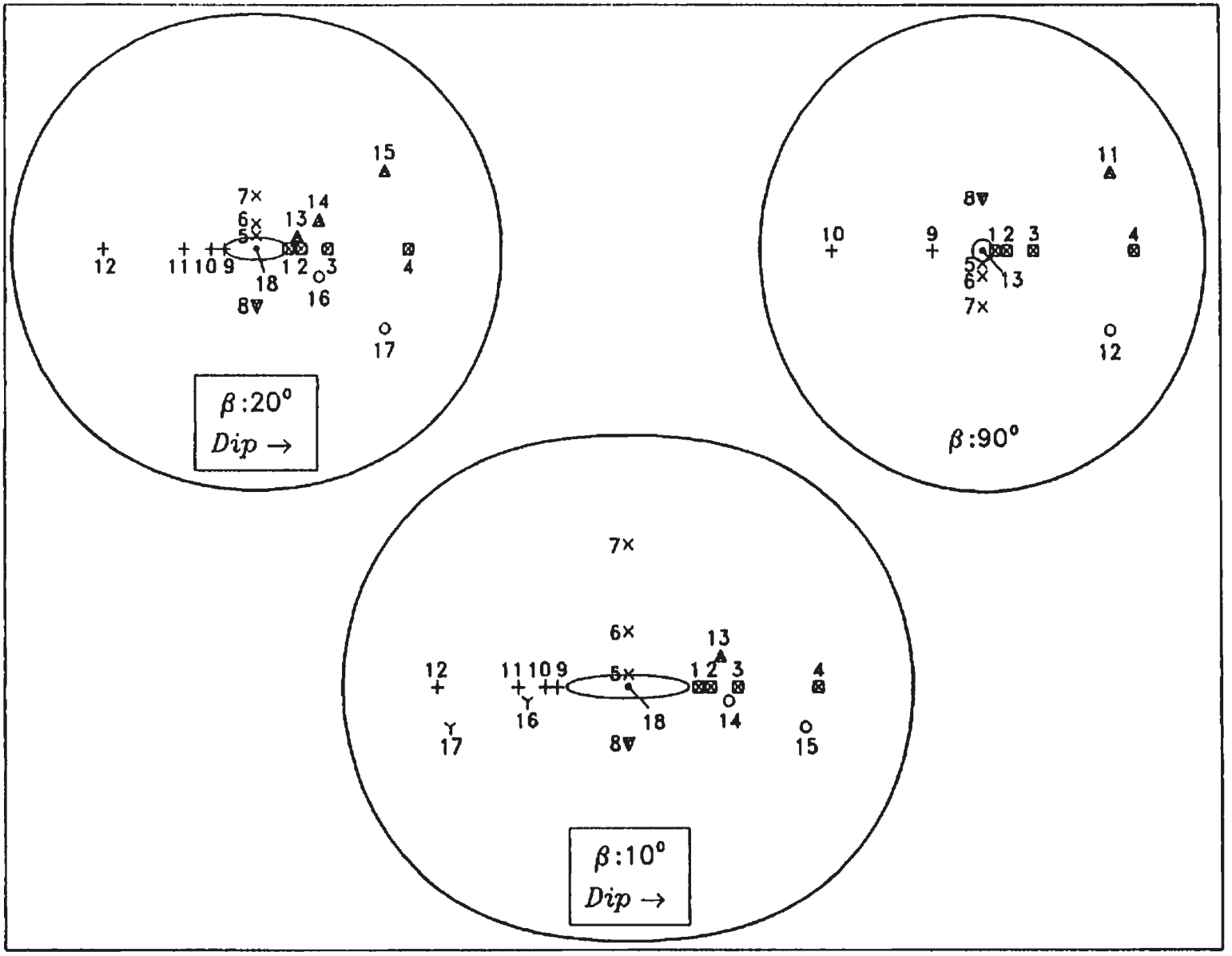

Figure B.1. Location map of the in-fracture pressure measurement holes.

PUMPING SERIES : β: 90° 2b: 1.1 mm

Run no.	1	2	3	4*	5	6
Hole no.*	Q: 0.292 l/s T: 15.67 °C	Q: 0.183 l/s T: 15.63 °C	Q: 0.395 l/s T: 15.61 °C	Q: 0.454 l/s T: 15.60 °C	Q: 0.481 l/s T: 15.59 °C	Q: 0.391 l/s T: 15.57 °C
1	−0.150	0.217	−0.636	−0.971	−1.137	−0.613
2	0.263	0.390	0.104	−0.003	−0.054	0.111
3	0.419	0.464	0.368	0.336	0.320	0.371
4	0.494	0.505	0.482	0.474	0.471	0.483
5	−0.128	0.232	−0.600	−0.927	−1.090	−0.578
6	0.280	0.401	0.131	0.031	−0.019	0.138
7	0.432	0.472	0.389	0.363	0.348	0.391
8	0.417	0.463	0.365	0.332	0.316	0.368
9	0.414	0.460	0.360	0.326	0.309	0.363
10	0.507	0.513	0.502	0.499	0.497	0.502
11	0.505	0.512	0.499	0.496	0.494	0.499
12	0.493	0.504	0.481	0.473	0.470	0.482
13	−0.322	0.151	−0.947	−1.382	−1.599	−0.918

PUMPING SERIES : β: 90° 2b: 0.6 mm

Run no.	1	2	3*	4	5	6
Hole no.	Q: 0.247 l/s T: 11.22 °C	Q: 0.304 l/s T: 11.21 °C	Q: 0.355 l/s T: 11.17 °C	Q: 0.151 l/s T: 11.16 °C	Q: 0.277 l/s T: 11.15 °C	Q: 0.176 l/s T: 11.14 °C
1	−1.513	−2.323	−3.168	−0.431	−1.926	−0.679
2	−0.337	−0.633	−0.928	0.071	−0.487	−0.026
3	0.036	−0.097	−0.224	0.242	−0.034	0.190
4	0.373	0.339	0.306	0.434	0.355	0.418
5	−1.501	−2.309	−3.152	−0.424	−1.913	−0.671
6	−0.440	−0.750	−1.061	0.011	−0.601	−0.098
7	0.025	−0.109	−0.238	0.235	−0.046	0.182
8	0.073	−0.055	−0.177	0.263	0.007	0.216
9	0.028	−0.106	−0.234	0.237	−0.042	0.184
10	0.363	0.327	0.292	0.428	0.343	0.411
11	0.352	0.314	0.276	0.421	0.331	0.403
12	0.332	0.291	0.250	0.409	0.308	0.389
13	−2.037	−3.077	−4.170	−0.650	−2.568	−0.966

*) For the hole locations, refer to Figure A.2.

*) For the pressure head vs. logarithmic distance graphs of the marked runs, refer to Figures 6.4 to 6.15

PUMPING SERIES : **δ: 20°** **2b: 1.1 mm**

Run no.	1	2	3	4	5	6*	7
Hole	Q: 0.810 l/s	Q: 0.757 l/s	Q: 0.681 l/s	Q: 0.182 l/s	Q: 0.288 l/s	Q: 0.443 l/s	Q: 0.202 l/s
no.	T: 14.58 °C	T: 14.35 °C	T: 14.59 °C	T: 13.57 °C	T: 12.84 °C	T: 13.68 °C	T: 14.10 °C
1	−0.887	−0.728	−0.514	0.395	0.269	0.020	0.376
2	−0.225	−0.149	−0.043	0.434	0.360	0.228	0.423
3	0.223	0.251	0.290	0.477	0.444	0.389	0.472
4	0.425	0.433	0.444	0.504	0.493	0.475	0.502
5	−0.817	−0.667	−0.465	0.398	0.277	0.041	0.380
6	−0.181	−0.107	−0.007	0.441	0.372	0.247	0.431
7	0.177	0.208	0.253	0.470	0.432	0.370	0.464
8	0.176	0.207	0.252	0.470	0.431	0.369	0.464
9	−0.866	−0.709	−0.497	0.399	0.274	0.029	0.379
10	−0.138	−0.067	0.028	0.448	0.384	0.265	0.438
11	0.228	0.256	0.294	0.478	0.446	0.392	0.473
12	0.436	0.444	0.454	0.506	0.496	0.480	0.504
13	−0.189	−0.115	−0.014	0.440	0.370	0.243	0.429
14	0.153	0.186	0.234	0.466	0.425	0.359	0.460
15	0.468	0.473	0.479	0.511	0.504	0.493	0.510
16	0.169	0.201	0.247	0.468	0.430	0.366	0.462
17	0.447	0.453	0.462	0.507	0.499	0.484	0.506
18	−0.931	−0.764	−0.541	0.397	0.269	0.012	0.377

PUMPING SERIES : **δ: 20°** **2b: 0.6 mm**

Run no.	1*	2
Hole	Q: 0.363 l/s	Q: 0.229 l/s
no.	T: 11.91 °C	T: 11.78 °C
1	−1.101	−0.333
2	−0.546	−0.082
3	−0.165	0.112
4	0.234	0.347
5	−0.973	−0.266
6	−0.562	−0.092
7	−0.147	0.123
8	−0.147	0.123
9	−1.153	−0.364
10	−0.578	−0.101
11	−0.167	0.111
12	0.243	0.352
13	−0.559	−0.090
14	−0.139	0.128
15	0.238	0.349
16	−0.145	0.124
17	0.221	0.339
18	−1.226	−0.395

PUMPING SERIES : β: 10° 2b: 1.1 mm

Run no.	1	2	3	4	5	6	7	8*
Hole	Q: 0.193 l/s	Q: 0.312 l/s	Q: 0.366 l/s	Q: 0.537 l/s	Q: 0.601 l/s	Q: 0.664 l/s	Q: 0.375 l/s	Q: 0.451 l/s
no.	T: 14.54 °C	T: 14.52 °C	T: 14.49 °C	T: 14.46 °C	T: 14.43 °C	T: 14.39 °C	T: 14.39 °C	T: 14.39 °C
1	0.421	0.368	0.340	0.240	0.197	0.152	0.336	0.293
2	0.434	0.395	0.374	0.300	0.268	0.236	0.370	0.338
3	0.450	0.424	0.410	0.364	0.344	0.325	0.408	0.388
4	0.470	0.458	0.452	0.432	0.425	0.416	0.451	0.443
5	0.414	0.352	0.318	0.193	0.136	0.079	0.313	0.258
6	0.442	0.409	0.393	0.336	0.312	0.287	0.390	0.365
7	0.468	0.454	0.448	0.427	0.419	0.409	0.447	0.438
8	0.443	0.410	0.394	0.338	0.314	0.289	0.391	0.367
9	0.423	0.373	0.346	0.249	0.206	0.162	0.342	0.299
10	0.439	0.405	0.385	0.316	0.285	0.256	0.382	0.351
11	0.451	0.427	0.414	0.369	0.349	0.331	0.412	0.392
12	0.469	0.456	0.450	0.429	0.421	0.412	0.449	0.440
13	0.451	0.426	0.412	0.364	0.343	0.323	0.410	0.388
14	0.449	0.423	0.408	0.359	0.337	0.316	0.406	0.384
15	0.467	0.452	0.446	0.423	0.414	0.404	0.445	0.435
16	0.446	0.417	0.402	0.349	0.327	0.305	0.399	0.376
17	0.469	0.456	0.450	0.429	0.421	0.412	0.449	0.440
18	0.409	0.342	0.306	0.171	0.111	0.049	0.300	0.242

PUMPING SERIES : β: 10° 2b: 0.6 mm

Run no.	1	2	3*
Hole	Q: 0.182 l/s	Q: 0.283 l/s	Q: 0.323 l/s
no.	T: 15.11 °C	T: 15.02 °C	T: 14.92 °C
1	0.116	−0.118	−0.222
2	0.189	0.002	−0.078
3	0.272	0.141	0.085
4	0.404	0.353	0.332
5	0.117	−0.148	−0.261
6	0.233	0.081	0.015
7	0.408	0.358	0.338
8	0.234	0.083	0.017
9	0.111	−0.124	−0.229
10	0.207	0.025	−0.051
11	0.276	0.146	0.092
12	0.409	0.360	0.340
13	0.280	0.143	0.088
14	0.277	0.139	0.084
15	0.408	0.355	0.335
16	0.266	0.125	0.067
17	0.405	0.351	0.330
18	0.090	−0.190	−0.312

INJECTION SERIES : β: 90° 2b: 1.1 mm

Run no.	1	2	3	4	5	6*
Hole	Q: 0.175 l/s	Q: 0.279 l/s	Q: 0.343 l/s	Q: 0.433 l/s	Q: 0.473 l/s	Q: 0.524 l/s
no.	T: 16.21 °C	T: 15.69 °C	T: 15.65 °C	T: 15.80 °C	T: 15.59 °C	T: 15.61 °C
1	−0.308	−0.744	−1.099	−1.653	−1.956	−2.370
2	0.061	0.051	0.013	−0.060	−0.070	−0.094
3	0.052	0.063	0.050	0.032	0.046	0.060
4	0.027	0.030	0.017	0.002	0.018	0.036
5	−0.301	−0.731	−1.082	−1.631	−1.930	−2.339
6	0.060	0.049	0.010	−0.063	−0.074	−0.098
7	0.052	0.062	0.049	0.031	0.046	0.060
8	0.052	0.063	0.050	0.032	0.047	0.061
9	0.051	0.061	0.048	0.030	0.044	0.057
10	0.027	0.031	0.017	0.003	0.019	0.038
11	0.048	0.054	0.039	0.018	0.030	0.041
12	0.047	0.054	0.039	0.017	0.029	0.040
13	0.263	0.560	0.782	1.167	1.390	1.694

INJECTION SERIES : β: 90° 2b: 1.6 mm

Run no.	1	2	3*	4	5
Hole	Q: 0.383 l/s	Q: 0.498 l/s	Q: 0.600 l/s	Q: 0.661 l/s	Q: 0.346 l/s
no.	T: 10.91 °C	T: 11.06 °C	T: 11.01 °C	T: 10.94 °C	T: 10.95 °C
1	−0.586	−0.936	−1.328	−1.608	−0.483
2	−0.004	−0.053	−0.095	−0.142	0.010
3	0.027	0.019	0.022	0.007	0.031
4	0.012	0.008	0.016	0.005	0.016
5	−0.611	−0.970	−1.373	−1.660	−0.505
6	0.002	−0.044	−0.083	−0.128	0.016
7	0.026	0.018	0.021	0.006	0.031
8	0.026	0.018	0.020	0.005	0.030
9	0.023	0.014	0.015	−0.001	0.028
10	0.011	0.005	0.013	0.001	0.015
11	0.023	0.013	0.014	−0.002	0.027
12	0.024	0.015	0.017	0.001	0.029
13	0.439	0.701	1.004	1.192	0.369

INJECTION SERIES : **δ: 20°** **2b: 1.1 mm**

Run no.	1	2	3	4	5*	6	7
Hole	Q: 0.423 l/s	Q: 0.281 l/s	Q: 0.215 l/s	Q: 0.170 l/s	Q: 0.515 l/s	Q: 0.758 l/s	Q: 0.639 l/s
no.	T: 11.47 °C	T: 11.47 °C	T: 11.54 °C	T: 11.57 °C	T: 11.54 °C	T: 11.35 °C	T: 11.35 °C
1	0.349	0.159	0.127	0.103	0.464	0.763	0.721
2	0.067	0.069	0.058	0.049	0.049	−0.035	0.012
3	0.053	0.049	0.038	0.031	0.049	0.045	0.049
4	0.028	0.024	0.016	0.012	0.029	0.050	0.038
5	0.038	0.069	0.069	0.062	−0.020	−0.183	−0.142
6	0.095	0.082	0.068	0.057	0.085	0.021	0.056
7	0.091	0.068	0.051	0.041	0.099	0.123	0.111
8	0.085	0.065	0.049	0.039	0.091	0.111	0.101
9	0.314	0.131	0.125	0.093	0.418	0.700	0.674
10	0.069	0.069	0.059	0.050	0.051	−0.032	0.014
11	0.062	0.053	0.041	0.033	0.061	0.063	0.063
12	0.024	0.022	0.014	0.011	0.023	0.042	0.032
13	0.074	0.072	0.061	0.051	0.058	−0.021	0.023
14	0.056	0.050	0.039	0.032	0.053	0.051	0.054
15	0.028	0.024	0.016	0.012	0.028	0.050	0.038
16	0.059	0.052	0.040	0.032	0.057	0.057	0.058
17	0.024	0.022	0.014	0.011	0.023	0.040	0.031
18	0.417	0.229	0.154	0.111	0.564	1.075	0.803

INJECTION SERIES : **δ: 20°** **2b: 1.6 mm**

Run no.	1*	2	3	4
Hole	Q: 0.610 l/s	Q: 0.777 l/s	Q: 0.408 l/s	Q: 0.287 l/s
no.	T: 11.33 °C	T: 11.29 °C	T: 11.32 °C	T: 11.34 °C
1	0.290	0.383	0.147	0.083
2	0.031	−0.006	0.035	0.035
3	0.031	0.025	0.027	0.022
4	0.018	0.021	0.014	0.009
5	−0.012	−0.086	0.024	0.043
6	0.053	0.022	0.046	0.043
7	0.062	0.064	0.042	0.033
8	0.057	0.058	0.040	0.031
9	0.261	0.337	0.132	0.078
10	0.032	−0.004	0.035	0.036
11	0.038	0.034	0.030	0.024
12	0.015	0.017	0.012	0.008
13	0.036	0.001	0.038	0.037
14	0.033	0.028	0.028	0.023
15	0.018	0.020	0.013	0.009
16	0.035	0.031	0.029	0.023
17	0.014	0.016	0.012	0.008
18	0.315	0.479	0.161	0.092

INJECTION SERIES : **δ: 10°** **2b: 1.1 mm**

Run no.	1	2	3	4°	5	6	7	8
Hole	Q: 0.371 l/s	Q: 0.583 l/s	Q: 0.676 l/s	Q: 0.497 l/s	Q: 0.175 l/s	Q: 0.220 l/s	Q: 0.298 l/s	Q: 0.392 l/s
no.	T: 14.35 °C	T: 14.37 °C	T: 14.36 °C	T: 14.35 °C	T: 14.37 °C	T: 14.38 °C	T: 14.42 °C	T: 14.43 °C
1	0.039	0.004	−0.024	0.017	0.032	0.030	0.036	0.037
2	0.041	0.021	0.004	0.026	0.028	0.027	0.035	0.040
3	0.036	0.028	0.019	0.028	0.022	0.021	0.029	0.036
4	0.023	0.021	0.018	0.019	0.012	0.010	0.015	0.023
5	0.111	0.117	0.108	0.124	0.065	0.076	0.093	0.114
6	0.060	0.068	0.066	0.064	0.033	0.036	0.048	0.062
7	0.033	0.040	0.042	0.036	0.016	0.016	0.023	0.035
8	0.058	0.063	0.060	0.060	0.032	0.034	0.046	0.059
9	0.042	0.009	−0.018	0.021	0.033	0.032	0.038	0.040
10	0.050	0.037	0.024	0.041	0.032	0.032	0.042	0.050
11	0.047	0.048	0.044	0.045	0.027	0.027	0.037	0.048
12	0.028	0.031	0.031	0.028	0.014	0.013	0.020	0.029
13	0.039	0.030	0.020	0.030	0.024	0.024	0.032	0.039
14	0.045	0.041	0.034	0.040	0.027	0.027	0.036	0.046
15	0.032	0.036	0.036	0.032	0.016	0.015	0.022	0.033
16	0.035	0.022	0.010	0.023	0.023	0.021	0.028	0.034
17	0.023	0.019	0.016	0.018	0.012	0.010	0.016	0.023
18	0.183	0.327	0.401	0.262	0.072	0.091	0.134	0.196

INJECTION SERIES : **δ: 10°** **2b: 1.6 mm**

Run no.	1	2	3	4	5	6°
Hole	Q: 0.378 l/s	Q: 0.285 l/s	Q: 0.204 l/s	Q: 0.546 l/s	Q: 0.731 l/s	Q: 0.587 l/s
no.	T: 15.29 °C	T: 15.12 °C	T: 15.13 °C	T: 15.14 °C	T: 15.10 °C	T: 15.06 °C
1	0.031	0.019	0.017	0.030	0.007	0.025
2	0.030	0.018	0.015	0.033	0.019	0.030
3	0.025	0.012	0.011	0.028	0.021	0.026
4	0.015	0.003	0.004	0.015	0.010	0.013
5	0.059	0.039	0.028	0.096	0.077	0.095
6	0.037	0.021	0.017	0.048	0.043	0.047
7	0.020	0.007	0.007	0.025	0.021	0.023
8	0.037	0.022	0.017	0.049	0.045	0.048
9	0.012	0.005	0.008	−0.005	−0.036	−0.013
10	0.022	0.011	0.011	0.017	0.000	0.013
11	0.021	0.009	0.009	0.021	0.012	0.018
12	0.017	0.005	0.005	0.018	0.013	0.016
13	0.023	0.011	0.010	0.023	0.013	0.020
14	0.022	0.010	0.010	0.022	0.012	0.019
15	0.019	0.006	0.006	0.022	0.018	0.020
16	0.024	0.012	0.011	0.025	0.016	0.022
17	0.019	0.007	0.006	0.022	0.018	0.020
18	0.075	0.043	0.029	0.121	0.179	0.132